THE UNIVERSITY OF CALGARY

Detailed Marine Gravity Field Determination by Combination of Heterogeneous Data

by

Jinwen Li

A THESIS

SUBMITTED TO THE FACULTY OF GRADUATE STUDIES IN PARTIAL FULFILLMENT OF THE REQUIREMENT FOR THE DEGREE OF MASTER OF SCIENCE IN GEOMATICS ENGINEERING

DEPARTMENT OF GEOMATICS ENGINEERING

CALGARY, ALBERTA

August, 1996

ABSTRACT

For the optimal combination of heterogeneous data, three methods, namely, space domain least-squares collocations (LSC), frequency domain input output system theory (IOST) and least-squares adjustment in the frequency domain (LSAFD), are theoretically and numerically compared. Numerical computations show that results obtained by using only a single data set deviate from those obtained by combining two types of data, which suggest that adding a second data type to the input gives a strong control condition to the solutions of the problem.

The accuracies of the results obtained by both IOST and LSC methods are very close but the first method has much higher efficiency than the second one. Non-isotropic PSD functions can be easily used by the IOST but the LSC requires isotropic covariance functions. Based on numerical results, this study shows that using non-isotropic PSDs gives better results than using isotropic ones. The LSAFD method requires less a priori information than the other two methods, but it only improves the accuracy of the data type that has poorer accuracy (geoid height in our case). Results from the real data processing show that after optimal combination of altimeter and shipborne data, about 50% of the input noise level can be suppressed.

ACKNOWLEDGMENTS

I would like to express my sincere thanks to my supervisor, Dr. Michael G. Sideris, for his continuous support and help throughout my M.Sc. program. His guidance and advice were essential for the completion of this thesis.

I wish to express my thanks to my interim supervisor, Dr. J. A. R. Blais, for his guidance and help during the period of Dr. Sideris' sabbatical absence, as well as for the beneficial discussions we had about this research. Shipborne data for the Labrador Sea area provided by him were essential for the completion of this thesis.

Special thanks go to Professor I. N. Tziavos of the University of Thessaloniki, Greece, for providing me with the altimeter and shipborne data in the Central Mediterranean area.

Thanks also go to Dr. Changyou Zhang and Mr. Y. C. Li, for providing me with some computer programs as well as for the beneficial discussions we had.

The financial support for this research has been provided by a Natural Sciences and Engineering Research Council of Canada research grant to Dr. M. G. Sideris.

TABLE OF CONTENTS

LIST OF TABLES

LIST OF FIGURES

CHAPTER ONE
INTRODUCTION AND RESEARCH BACKGROUND

1.1 Research Background

Detailed knowledge of the fine structure of the marine gravity field has potential applications in marine geodesy, geophysics, oceanography, marine resources, navigation, etc. The traditional method of acquisition of gravity data is by gravity measurements. Offshore gravity measurements have been carried out on board of ships and have been used for local marine gravity field determination. This is, however, a slow and costly process. In most cases, offshore gravity measurement is a by-product of seismic reflection profiling. The precision of this type of marine gravity survey usually falls between 2.0 and 5.0 mgal. If a survey is especially designed for gravity, precision of marine gravity measurements better than 1.0 mgal can be obtained (Hayling, 1994). To date, shipborne gravity measurements are still far from covering all offshore areas because of their excessive workload and high cost. Therefore, their distribution is very inhomogeneous. On the other hand, as a by-product of seismic profiling, the accuracies of many marine gravity measurements are not sufficient for geophysical prospecting.

Satellite altimetry gives observations of sea surface heights that are approximately equivalent to geoid heights and are very useful in mapping the ocean geoid and thus for studying the marine gravity field. It generated a new data set with unprecedented spatial and temporal coverage of the global oceans. The altimetric measurements have improved both the horizontal resolution of the oceanic geoid and its accuracy. The precision of altimeter measurements ranges from 20 cm (GEOS-3) to 2.4 cm (TOPEX/POSEIDON). The accuracies of altimetry observations range from about 65 cm (Seasat) to 14 cm

(TOPEX/POSEIDON). The densest ground track separation of the satellite altimeter is about 2 - 3 km at 60° latitude, which was achieved during the GEOSAT Geodetic Mission (GM) phase (Seeber, 1993). The new data sets acquired from satellite altimetry have led to extensive studies on the determination of detailed marine gravity field for more than two decades and has led to great new understanding of the Earth's gravity field; e.g., see Koch (1970), Kahn and Bryan (1972), Rapp (1985), Balmino et al. (1987), Hwang (1989), Basic and Rapp (1992), Sandwell (1992), Zhang and Blais (1993) and Zhang and Sideris (1995). In nearly all the previous studies of using satellite altimetry data to derive the gravity field, shipborne gravity was used only as an independent source for checking the quality of the computed gravity anomalies rather than as an additional data set.

The computation of marine gravity anomalies from shipborne gravity measurements is simple and straightforward while the computation of the geoid height from gravity data is somewhat complicated. Gravity anomaly (or disturbance) can be computed from the gravity observation by subtracting the corresponding normal gravity, which is produced by a previously selected normal reference field. For the computation of the local geoid height, Stokes' integral (or Hotine's integral) or the least-squares collocation method are usually employed. Because the satellite altimetry gives observations of sea surface heights that are approximately equivalent to geoid heights, the computation of marine geoid heights from altimetry observations is straightforward. The determination of gravity anomalies from the satellite altimetry, which is categorized as an inverse problem in physical geodesy, can be done by the inverse Stokes integral (or the inverse Hotine integral) or by the least-squares collocation method. This inverse problem is an improperly posed problem (Moritz, 1980) and with unstable solutions. Efforts should therefore be put to the regularization of this improperly posed problem when altimeter data are used to compute gravity anomalies.

Discussions on regularization techniques in physical geodesy can be found in, e.g., Neyman (1985), Rauhut (1992) and Moritz (1980).

The computation of the marine gravity anomalies from altimeter data using the inverse Stokes operator method has been done by, e.g., Balmino et al. (1987). The derivation of marine gravity disturbances from altimeter data using the inverse Hotine approach has been done by, e.g., Zhang and Blais (1993, 1995), and Zhang and Sideris (1995). The Hotine kernel is much simpler and has certain numerical advantages compared to the Stokes kernel (Zhang and Blais, 1993; Jekeli, 1979). Three ways of modifying the inverse Hotine kernel using FFT techniques are discussed in Zhang and Blais (1993). These modified inverse Hotine formulas have high efficiency in computations because they are based on FFT techniques. The accuracies of the recovered gravity disturbances using inverse Hotine methods will depend on the noise levels of the altimeter data, the errors in the reference field, modelling errors and numerical techniques, etc. Zhang and Blais (1995) has shown that a precision of about 8 mgal was obtained for the recovered gravity disturbances in the Labrador Sea area by inverting one year averaged GEOSAT data using the inverse Hotine approach.

The alongtrack vertical deflections can be computed by differentiating the altimeter sea surface height (Sandwell, 1984 and 1992; Sandwell and McAdoo, 1990). After averaging vertical deflections of individual alongtrack profiles, averaged geoid height and gravity anomaly can be derived from these averaged vertical deflections. In using this differentiation procedure, the derivative operator acts as a high-pass filter that suppresses the long-wavelength orbital errors and other long-wavelength errors. Therefore, no cross-over adjustment is needed if the differentiation procedure is employed.

In areas where altimetry data and shipborne gravity anomalies are available, these two types of data (heterogeneous data) could be combined to determine the gravity field quantities (geoid height and gravity anomaly). The combination of different types of data can be hopefully used to improve the accuracies of the determined quantities of the gravity field. Simulation studies have confirmed that this combination can usually produce estimates with high accuracies (Li and Sideris, 1995). Two papers on combining altimeter and shipborne data for practical determination of the local marine gravity field have been written by Arabelos and Tziavos (1990a) and Hwang and Parsons (1995). In their computations, they employed the least-squares collocation technique. In this study, we will explore different methods for such tasks.

Several numerical methods for gravity field determination using heterogeneous data have been investigated by many authors. Among these methods, least-squares collocation, frequency domain adjustment and input-output system theory are well recognized (e.g., Moritz, 1980; Barzaghi et al., 1993; Vassiliou, 1986; Schwarz et al., 1990; Sideris, 1996; Sansò and Sideris, 1995).

Least-squares collocation (LSC) is an optimal estimation method that offers many theoretical advantages and has been widely used in physical geodesy. The application of conventional (space domain) LSC in physical geodesy was discussed in detail by Moritz (1980). Its practical applications in gravity field modeling can be found in, e.g., Tscherning (1974), Rapp (1985), Knudsen (1987a, 1991) and Basic and Rapp (1992). The advantage of conventional LSC is that optimal use is made of the available data (homogenous data type or heterogeneous data types) without gridding in advance. A fast (frequency domain) LSC method, which is aiming to overcome the computational difficulties with conventional LSC, was studied by, e.g., Eren (1980) and Bottoni and

Barzaghi (1993). The fast LSC solution requires that the input data be gridded. Consequently, the corresponding covariance matrices take the form of Toeplitz matrices. The advantage of using fast LSC method is that a considerable gain in computation time and storage is obtained in comparison with conventional LSC. Yet, the fast LSC is suffering from edge effects in comparison with conventional LSC, and requires that the data be gridded.

In practice, least-squares collocation is quite accommodating with data types allowed and estimated quantities but relies on a-priori information about the field (normally an isotropic covariance function). The use of LSC in gravity field determination by combination of heterogeneous data needs the auto- and cross-covariances of the signals as well as the noise variances of the observations. Theoretically, the covariance functions for different quantities of the gravity field should be self-consistent (Jordan, 1972). Here 'self-consistent' means that the signal covariance functions for different quantities of the field should be derived from a single covariance function (e. g., the covariance function of the disturbing potential) by rigorous covariance propagation. The practical covariance functions could be computed empirically using observations. If covariance functions for different quantities are all computed independently by employing the observed data, then the covariance functions may not be strictly self-consistent. Since there usually are not enough data available for all empirical covariance computations -- for example, we may have enough altimetry data for geoid height covariance computation, but not enough gravity data for gravity anomaly covariance and geoid-gravity anomaly cross-covariance computation -- we need to derive some covariance and cross-covariance functions from an empirical one. In this later case, self-consistent covariance functions (or analytical models) should be used. Some self-consistent covariance functions that could be used for local gravity field modelling were presented by Jordan (1972). Some global gravity field covariance models,

which can be adjusted according the local empirical covariance values to fit the local applications, were presented by Tscherning and Rapp (1974).

Spectral techniques have been widely applied in processing of large data sets in physical geodesy for decades. Previous work on using spectral technique for gravity field determination provided no error estimates of the results (Zhang, 1993; Olgiati, 1995). Sideris (1996) showed that error prediction in spectral methods is possible provided that the input signals and their errors are stochastic variables with known power spectral densities (PSDs).

A frequency domain adjustment method, hereafter termed least-squares adjustment in the frequency domain (LSAFD), was studied by Barzaghi et al. (1993) for gravity field determination using heterogeneous data. The frequency domain adjustment method needs the observation spectra and noise PSDs of the data (Barzaghi et al., 1993; Sideris, 1996). The observation spectra can be obtained easily from the observations using FFT. The theoretical foundation embedded in the frequency domain adjustment technique is that all data types contributing to this adjustment should satisfy some condition equations or, in another words, should be self-consistent.

Input-output system theory (IOST) has been investigated for its physical geodesy applications by several authors, e.g. Sansò and Sideris (1995), Sideris (1996), Li and Sideris (1995) and Wu and Sideris (1995). Detailed discussions on IOST could be found in Bendat and Piersol (1980, 1986). The use of input-output system theory in local gravity field determination assumes that signal and noise PSDs of the data are known. Sideris (1996) and Sansò and Sideris (1995) showed that the input-output system theory is formally equivalent to least-squares collocation. In practical applications, the covariance

functions used by the least-squares collocation method have an isotropic structure, yet, the PSDs used by input-output system theory can be 2-D anisotropic functions. This difference between least-squares collocation and input-output system theory introduces some approximation errors to the least- squares collocation method.

The combination of altimeter data from different missions for gravity field recovery using LSC has been done by many authors, e.g. Rapp (1985), Basic and Rapp (1992) and Arabelos and Tziavos (1995). LSAFD and IOST can also be used for the combination of these altimetry data. Error estimates of the predicted geoid heights by combination of altimeter data from different missions using either space domain or frequency domain methods can be obtained. Geoid heights obtained by combination of different altimeter missions could further be combined with shipborne gravity anomalies using the methods mentioned above to improve the accuracies of geoid height and gravity anomaly predictions. The use of the LSC method in the combination of altimeter data from different missions has the advantage that it uses directly all the available data despite the differences in resolution of different altimetry missions. Yet, the use of LSAFD and IOST for the combination of data from different altimeter missions requires that all the data be reduced to the same resolution (gridded with the same spacing). Numerical experiments and comparisons of these three methods by combining data from different altimeter missions should be carried out.

Some simulation computations have been done to intercompare the conventional LSC, IOST and LSAFD methods (Li and Sideris, 1995). Further simulations and the application of these three methods to real observations remain to be done in this thesis. While in simulation studies we were able to use exact signal and noise PSDs, in real applications this is not possible because we can not obtain exact signal and noise PSDs from observations.

The main problem in real applications is therefore how to effectively estimate the signal and noise PSDs from real data. Sailor (1994) discussed methods for altimetry data spectral analysis and signal and noise PSDs estimation in profile analysis. How 2-D signal and noise PSDs of the altimetry data can be estimated remain a problem to be investigated and tested.

1.2 Thesis Objective

The main objective of this research is to study methods used in the determination of local marine gravity field using heterogeneous data. Tests are made with geoid heights and gravity anomalies, using simulated observations and real data. Different methods, i.e., input-output system theory, least-squares collocation and frequency domain adjustment will be employed and explored in this study. Theoretical comparison of these three methods will be carried out. Results obtained using the different methods with simulation data and real data will be intercompared. The results obtained by combining heterogeneous data will also be compared to those obtained by methods using a single input data type.

1.3 Outline of the Thesis

The thesis consists of seven chapters. The basic contents of each chapter are outlined below.

Chapter 2 discusses briefly the altimetry data records, marine gravity data records and the techniques for preprocessing of altimetry and shipborne data. Preprocessing is an essential step for further handling of the data. The preprocessing of the altimetry data includes

editing of the data from original data records, along track data interpolation, data stacking (averaging), crossover adjustment and gridding.

Chapter 3 outlines the theoretical foundations and mathematical formulas used for the combination of heterogeneous data. These models include the single-input single-output system, the multiple-input multiple-output (or single-output) system, least-squares collocation and frequency domain adjustment. Theoretical discussions of these three methods will be given.

Chapter 4 describes the techniques for the estimation of signal and noise power spectral densities and covariance functions. The estimation of the signal PSDs and covariances is essential for the adjustment results. Two methods for the computation of PSDs and covariances are presented. The modeling of the local gravity field (residual field) is discussed in detail.

Chapter 5 gives the results of simulation studies. Simulated observations corrupted with uniform distributed and Gaussian noises are used for this study. Results are intercompared using different methods in each case. Internal accuracies and external accuracies are investigated and compared.

Chapter 6 presents the results obtained using real data from two test areas. The first test area is the Central Mediterranean area with 60 x 60 data points that are on a 5' x 5' grid. Altimetry data used in this test area is from the ERS-1 mission. The second test area is in the Labrador Sea area with 30 x 30 data points that are given on a 10' x 10' grid. The altimetry data used in this area are from the GEOSAT Exact Repeat Mission (ERM). Results obtained using IOST, LSC and LSAFD are compared. The geoid height predictions

obtained by combination of heterogeneous data are also compared with those obtained by single input data type (i.e., the results computed by gravity anomaly).

Chapter 7 summarizes the findings of this study and gives the main conclusions and recommendations for further research.

CHAPTER TWO

PREPROCESSING OF ALTIMETRY AND SHIPBORNE DATA

Original altimeter raw data are distributed in the form of GDR (Geophysical Data Record) or OPR (Ocean Product Record) which are stored on CD-ROMs. Due to acquisition or recording problems such as excessive noise, signal dropout, losses of signal due to transducer malfunction, etc., spurious and/or degraded data signals might exist in the record. In a preprocessing stage, to derive geoid height observations from the GDRs or OPRs, altimetry data have to be (a) edited to reject spurious and/or degraded data and land data, (b) corrected for environmental and geophysical effects, (c) stacked to produce mean tracks to suppress time-dependent errors, (d) corrected for stationary sea surface (SST) effects, and (e) crossover adjusted to remove (or suppress) the radial orbital errors. Finally, to meet the requirements of the spectral method, the altimetry derived data also have to be gridded.

The shipborne data are subjected to errors such as navigation errors, Eotvos effects, mislevelling of the platform, datum errors, system calibration errors, scale factor inaccuracies, coordinate errors, as well as vibration and thermal stress noise (Zhang, 1993). For combination of the altimeter and shipborne data, the reference system used in both data sets should be consistent. For those points with repeated observations, the averaged values will be used.

This chapter will discuss these preprocessing problems of the altimeter and shipborne data.

2.1 Altimetry Data

2.1.1 GEOSAT, ERS and TOPEX/POSEIDON Altimetry Missions

The GEOSAT altimeter mission, which consists of a Geodetic Mission (GM) phase and an Exact Repeat Mission (ERM) phase, was launched in 1985 (Cheney, et al., 1991). In the GM phase GEOSAT accumulated hundreds of millions of observations of the sea level with an average cross-track spacing of approximately 4 kilometers that are of significance for marine gravity field studies. Because of the military significance of the GM, most of the sea level data (especially those of the northern hemisphere) collected during the GM phase are classified. The ERM of GEOSAT covered 62 complete 17-day repeat cycles. The ERM data have been distributed for scientific studies to the scientific community (Cheney et al., 1991). The following are some characteristics of the GEOSAT GM and ERM data (Cheney et al., 1991; Seeber, 1993):

Precision: 3 cm

Accuracy: 50 cm

Along-track ground separation

GM phase: 10 km

ERM phase: 10 km

Equatorial cross-track ground separation

GM phase: 4 km

ERM phase: 164 km

In this context, precision is the ability to determine changes in sea level over a distance limited by the along-track resolution. The accuracy is the uncertainty of the geoid or sea level

measurement when expressed in geocentric coordinates (1 standard deviation).

The ERS missions (Battric, 1993; Seeber, 1993) are a series of remote sensing satellites launched in the 1990's, in order to investigate the environment and improve the marine gravity field in global and local applications, and to ensure long-term continuity of the data. The ERS-1 was launched in 1991 and the ERS-2 satellite was successfully launched in 1995. The ERS-1 mission consists of a 3-day repeat cycle, a 35-day repeat cycle and a 168-day repeat cycle. The main drawback of a 3-day cycle in geodetic applications is the wide separation of the radar altimeter tracks. The majority of the ERS missions are performed in a 35-day repeat cycle (multidisciplinary phase). The 168-day repeat cycle (Geodetic Phase) of the ERS-1 mission offers a high density of altimeter ground tracks and is thus favored for the measurement of mean-sea levels and the ocean geoid. Some characteristics of the ERS-1 mission are as follows (Battric, 1993; Seeber, 1993):

Precision: 10 cm (10 cm is the designed precision, actually 4-cm precision is obtained)

Accuracy: 25 cm

Along-track separation

3-day repeat cycle: 10 km

35-day repeat cycle: 10 km

168-day repeat cycle: 10 km

Equatorial cross-track separation

3-day repeat cycle: 900 km

35-day repeat cycle: 84 km

168-day repeat cycle: 18 km

The TOPEX/POSEIDON mission is dedicated to space oceanography and was launched in 1992 into a 10-day repeat orbit to make precise and accurate observations of the sea level for several years using satellite altimetry. It carries a GPS receiver for precise orbit determination. Some characteristics, which are of interest in this study, of the TOPEX/POSEIDON mission are as follows (AVISO, 1994; Seeber, 1993):

Precision: 2.4 cm
Accuracy: 14 cm
Along-track separation: <10 km
Equatorial cross-track separation: 314 km

2.1.2 Editing and Stacking of Altimetry Data

Data editing refers to those pre-analysis procedures that are designed to detect and eliminate spurious and/or degraded data signals that might have resulted from acquisition and recording problems such as excessive noise, signal dropout, loss of signal due to transducer malfunctions, etc.

Satellite altimetry measures the distance from the satellite to the ocean surface. These measurements offer an exciting possibility for the determination of the gravity field both on global and local scales. The sea surface height (SSH), which does not, in general, deviate from the geoid undulation by more than a few meters, can be obtained by differencing the ellipsoid height of the satellite and the altimetry range measurements. The altimeter range measurements recorded in GDRs or OPRs were corrected only for instrumental effects by the altimeter data processing center (AVISO, 1994; Battric, 1993; Cheney et al., 1991). They should be also corrected for environmental, geophysical and sea state bias effects by

the users for using them for further studies. Preprocessing, in this context, is to prepare altimeter and shipborne data that will readily act as the input of the combination techniques described in chapter 3. Therefore, the preprocessing of altimeter data includes extracting altimeter data for a given area of interest; removing land, spurious and degraded data from GDR or OPR records; correcting for environmental, geophysical and sea state bias effects such as wet and dry troposphere, ionosphere, oceanic and body tide, etc.; suppressing the time-dependent component of SST and removing its stationary part from the altimeter record; removing or suppressing radial errors; and finally gridding.

In editing altimetry GDRs or OPRs, some criteria have been selected for rejecting spurious data (Tables 2.1 - 2.3). The value for each correction that should be made to the altimeter range measurement has already been given in the GDRs or OPRs. Some correction terms have more than one value available. In this case, which value to use depends on the user's choice. To obtain altimeter sea surface height, we applied the corrections for wet and dry troposphere, ionosphere, solid tide, oceanic tide and electromagnetic bias to the altimeter range measurements. For those correction terms with multiple values available, the value based on insitu measurements are first considered. If the value based on the insitu measurement is not available, some other values will be used.

After applying the above corrections to the altimeter range measurements, we can obtain the sea surface height (SSH). The SSH consists of geoid height, the time -dependent and time - independent sea surface topography, the radial orbit errors, the errors due to improper environmental, geophysical corrections, and measurement noise. In order to enhance the signal-to-noise ratio and remove data gaps from one-per-second sea surface heights derived from altimeter range measurements, the sea surface heights from individual profiles have been stacked (averaged).

We will describe briefly the altimeter products of the three altimetry missions, i.e., GEOSAT GDRs, ERS OPRs and TOPEX/POSEIDON GDRs, because of their relatively high measurement accuracies and wide availability compared to earlier altimetry missions such as Seasat.

The GEOSAT T2-GDR data set for each measurement consists of 34 fields (Cheney et al., 1991). The OPR data set for each measurement of ERS-1 consists of 49 fields (Dumont and Stum, 1993). The TOPEX/POSEIDON GDR data set for each measurement consists of 132 fields (AVISO, 1994). All these data sets are time records and consist of the following groups of elements (Cheney et al., 1991; Dumont and Stum, 1993; AVISO, 1994):

1) Time
2) Location
3) Altitude
4) Attitude
5) Altimeter range
6) Environmental correction (such as tropospheric corrections, ionospheric corrections, etc.)
7) Significant wave height (SWH)
8) Backscatter coefficient and Automatic Gain Control (AGC)
9) Geophysical quantity (such as mean sea level, geoid height, tidal effects, etc.)
10) Brightness temperature
11) Flags.

For more details of the elements included in each group, see AVISO (1994), Cheney et al. (1991) and Battric (1993).

Table 2.1 Data Editing Criteria For GEOSAT T2-GDR

Land data are rejected
-100 m < sea surface height (H) < 100 m
0 < standard deviation of H < 0.1 m
-10 m < H-Geoid < 10 m
Off-nadir angle (Attitude) < 1.3 deg.
0.25 dB < Automatic Gain Control (AGC) < 25 dB

Table 2.2: Data Editing Criteria for ERS-1 OPR

Land data are rejected
745 000 < altitude < 825 000 m
standard deviation of altitude < 40 cm
6 dB < backscattering coefficient < 30 dB
-130 m < sea surface height < 100 m
-5 m < ocean tide < 5 m
-1 m < body tide < 1m
-0.5 m < tidal loading < 0.5 m
-2 500 mm < dry tropospheric correction < -1 900 mm
-500 mm < wet tropospheric correction < -1 mm
-400 mm < ionospheric correction < - 1 mm
-500 mm < electronic bias correction < 0 mm
0 mm < significance wave height < 15 000 mm

Table 2.3: Data Editing Criteria for TOPEX/POSEIDON GDR

TOPEX	POSEIDON
Nval_H_Alt > 5 (10 Hz heights)	Nval_H_Alt > 15 (20 Hz heights)
RMS_H_ Alt < 100 mm (10 Hz heights)	RMS_H_Alt < 175 mm (20 Hz heights)
check ocean/land and ice distribution conditions (bit number 2 and 3 of Geo_Bad_1 flag) to retain only ocean data	
-130 000 mm < CNES one per second satellite altitude (HP_Sat) - One per second altimeter range (H_Alt) < 10 000 mm	
-2 500 mm < dry troposphere correction (Dry_Cor) < -1 900 mm	
-500 mm < wet troposphere correction (Wet_Corr, Wet_H_Rad) < -1 mm	
-400 mm < Doris ionosphere correction (Iono_Dor) < 0 mm	
-4 00 mm < Topex ionosphere correction (Iono_Cor) < 40 mm	
-5 000 mm < ocean tide (H_Eot_CR, H_Eot_Sch) < 5 000 mm	
-500 mm < loading tide (H_Lt_CR, H_Lt_Sch) < 500 mm	
-1 000 mm < solid earth tide (H_Set) < 1 000 mm	
-15 000 mm < polar tide (H_Pol) < 15 000 mm	
-500 mm < sea state bias correction (EM_Bias_Corr_K1, EM_Bias_Corr_K2) < 0 mm	
0 mm < significant wave height (SWH_K) < 11 000 mm	
7 dB < Ku band sigma naught (Sigma0_K) < 25 dB	
0 deg < waveform attitude (Att_Wvf) < 0.3 deg	

Note: Nval_H_Alt is the number of valid points used to compute the range over one second; RMS_H_Alt is the root mean square of difference for ten per second altimeter range from H_Alt.

Data editing criteria are usually selected according to experiences and personal preferences. Different criteria are applied for editing altimeter from different missions. Tables 2.1, 2.2 and 2.3 give for each parameter of GEOSAT GDR, ERS-1 OPR and TOPEX/POSEIDON GDR respectively, the lower and upper boundary of the range out of which an altimeter measurement is to be removed. These criteria can be found in Wang and Rapp (1992), Demmou et al. (1995) and AVISO (1994). For more detailed explanation of each term given in the above tables, the altimeter data manuals, i.e., AVISO (1994), Battric (1993) and Cheney et al. (1991), should be referred to.

For GDRs and OPRs, several values may have been provided for some elements of the environmental correction. Generally, which value to use depends on the user's decision. It is recommended that the value that has been computed based on in situ satellite observations be used (Cheney et al., 1991). When the value based on in situ observations is not available, other values will be used.

The stacking of altimeter data means that the altimeter derived SSHs are averaged over some chosen repeat cycles. Because the repeat profile measurements are not given on exactly the same points, an interpolation procedure is needed. To do this, we first select for each track a cycle that has the most measurements as the reference cycle. Then, interpolation is carried out for each other repeat cycle, respectively, to obtain the corresponding observations at the reference points for each other repeat cycle. In this study, a cubic spline interpolation algorithm is employed. After interpolation, all cycles for each track are simply averaged to obtain stacked SSH. The standard deviations of the stacked SSH are also computed simultaneously in the averaging process.

2.1.3 Radial Orbit Error and Crossover Adjustment

The range measurement of the satellite altimeter consists of signal, systematic errors and random noise. Among the error sources, the radial orbit error is the largest part of the altimeter error budget (Houry et al., 1994), and has its dominant energy at zero frequency (the bias), and at a frequency of one cycle per revolution with wavelength of approximately 40 000 km (Sandwell, 1984).

While a rather sophisticated model of the radial orbit error is required for global evaluation of altimetry data (Moore and Ehlers, 1993; Schrama, 1989; Knudsen, 1993; Houry et al., 1994), a simple p-parametric polynomial model is sufficient in regional applications. Commonly used, such regional models include the bias model, the bias-tilt model and the quadratic model (Lenk et al., 1995). We used the bias-tilt model (p=2) to describe the radial orbit error in this study. The bias-tilt model can be written as:

$$\Delta r = a + b\mu \qquad (2.1)$$

where Δr is the radial orbit error, μ is the longitude or time difference between the running point and a reference point of the cycle, and a and b are unknown parameters to be determined. These parameters can be determined from the discrepancies of the sea surface heights at the crossovers of ascending and descending tracks.

In local areas, a cross-over adjustment has been used to determine the parameters in the radial orbit error model and then to remove the orbital error from altimetry sea surface heights (Knudsen, 1987a and 1987b).

At a cross-over point, the cross-over discrepancy (north going track minus south going track) is then

$$h_i - h_j = \Delta r_i - \Delta r_j + v_{ij} = (a_i + b_i\mu_j) - (a_j + b_j\mu_i) + v_{ij} \qquad (2.2)$$

where h_i-h_j is a cross-over difference; a_i, b_i, a_j and b_j are the unknown bias and tilt parameters; μ_i and μ_j are the coordinates along i-th and j-th track of cross-over points, respectively (Knudsen, 1992). More details on cross-over adjustment can be found in, e.g., Knudsen (1987a and 1987b), Tai (1988), Vermeer (1993), Schrama (1989), Fukuda (1990) and Wunsch (1991).

Relative longitudes or relative time can all be used as coordinates μ_j in eq. (2.2). We used relative longitudes as the coordinates in the cross-over adjustment. Cross-over discrepancies are computed for stacked sea-surface heights. By cross-over adjustment, the bias and tilt parameters are determined for each track. Then, the stacked altimeter data are corrected using the bias and tilt parameters. Thus the track related radial orbital errors are significantly reduced. But the adjusted altimeter data still include the effects of the stationary SST, which should be removed if the altimeter data are used as geoid height observations.

2.1.4 Effect of Sea Surface Topography

Satellite altimeter data contain information about both the geoid and the sea surface topography (SST). For the purpose of gravity field recovery using altimeter data, the SST must be removed from the altimeter data. SST consists of a time-dependent component and a time-independent component (stationary part). The effect of the time-dependent component on the altimeter measurement can be substantially suppressed by stacking of repeat tracks,

while that of the stationary part cannot. The time-independent component of the SST, which is about 2 m in magnitude, is modeled by a spherical harmonic series as follows (Engelis, 1987; Denker and Rapp, 1990; Knudson, 1993):

$$SST(\phi,\lambda) = \sum_{i=1}^{\infty}\sum_{j=0}^{i}(\bar{C}_{ij}^{SST}\cos j\lambda + \bar{S}_{ij}^{SST}\sin j\lambda)\bar{P}_{ij}(\sin\phi) \qquad (2.3)$$

where $\bar{C}_{ij}^{SST}$ and $\bar{S}_{ij}^{SST}$ are fully normalized SST spherical harmonic coefficients; ϕ and λ are the spherical coordinates of the point at which the SST is to be computed; $\bar{P}_{ij}(\cos\phi)$ is a fully normalized Legendre function.

Several such harmonic expansion models for the stationary SST are currently available (e.g., Engelis, 1987; Denker and Rapp, 1990). In this study, the stationary SST is computed using the Denker and Rapp model that has a maximum degree and order of 10. The value of the stationary SST is then subtracted from the altimeter data to obtain the altimeter geoid observation.

2.2 Shipborne Data

The shipborne data in the Labrador Sea area used in this study are from the same files as used in Zhang (1993). The shipborne data records include coordinates and their accuracies of the observation points, observed value of the gravity referred to IGSN71 and their accuracies, terrain corrections and their accuracies, free air anomaly and Bouguer anomaly referred to GRS67. The values of the observed gravity given in the data records were referred to IGSN71 and have already been corrected for solid tide errors, oceanic tide errors and Eotvos effects. For more details on the format of these marine gravity data records, see Zhang (1993).

Since the altimeter data are referred to the GRS80 system, we use the following formulas to reduce the values of the free air anomaly referred to GRS67 to those referred to GRS80:

$$\Delta g_{GRS80} = \Delta g_{GRS67} + \gamma_{GRS67} - \gamma_{GRS80} \tag{2.4}$$

$$\gamma_{GRS67} = 978031.8(1 + 0.0053024\sin^2\varphi - 0.0000059\sin^2(2\varphi)) \text{ mgal} \tag{2.5}$$

$$\gamma_{GRS80} = 978032.7(1 + 0.0053024\sin^2\varphi - 0.0000058\sin^2(2\varphi)) \text{ mgal} \tag{2.6}$$

where φ is latitude. For some points, repeat gravity measurements are available, but for some other points no repeat measurement is available. For those points with repeat observations, we averaged all the repeat measurements.

2.3 Gridding of Altimetry and Shipborne Data

Crossover adjusted altimetry sea surface heights are given at approximately equally spaced intervals along the altimeter subsatellite tracks. The intervals of the data between tracks are much larger than those of the data along tracks. The shipborne gravity anomalies are usually given at irregularly distributed points. For our studies, we need regularly distributed data to use spectral methods. Thus one of the important aspects of preprocessing of the altimetry and shipborne data is the gridding of the data. Gridding is a procedure whereby point values of sea surface heights and gravity anomalies are predicted at the nodes of a grid using irregular observations.

A dedicated study on gridding of altimetry data was done by Cruz (1983), and several gridding methods were studied and compared there. We chose the least-squares collocation method for data gridding, because it has the advantages of taking into account the data accuracy estimates and providing accuracy estimates of the predicted values (Cruz, 1983).

The covariances used in the least squares collocation gridding procedure were derived by linear interpolation from a table of covariances that were computed empirically from the real irregular data. Only neighbouring data around the prediction grid are used in the gridding process. Figures 2-1 and 2-2 show the empirical functions used to grid altimeter and shipborne data in the Labrador Sea area.

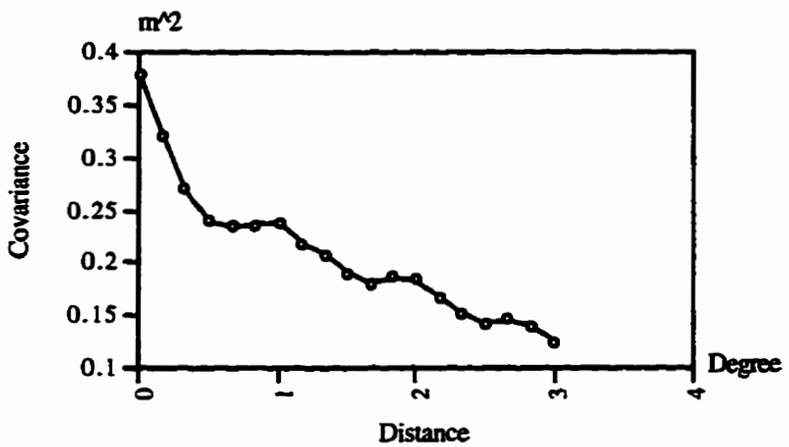

Fig. 2-1: Empirical covariance function of altimeter data used for gridding in the Labrador Sea area

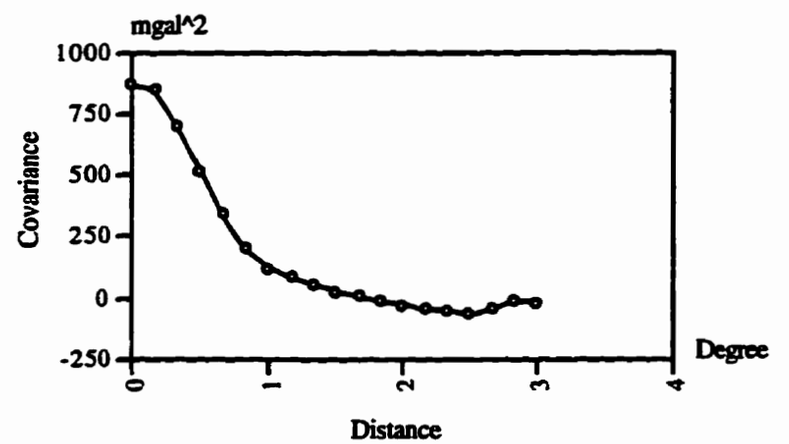

Fig. 2-2: Empirical covariance function of gravity data used for gridding in the Labrador Sea area

CHAPTER THREE
DISCUSSION OF OPTIMAL COMBINATION TECHNIQUES

This chapter discusses optimal combination techniques used for gravity field recovery by combination of heterogeneous data. In the first two sections, the single-input single-output and the double-input double-output systems are discussed. Section 3.3 discusses the least-squares collocation technique and section 3.4 presents the frequency domain adjustment method.

3.1 Single-input Single-output System

Input-output system theory has been widely used in science and engineering applications; detailed discussions can be found in, e.g., Bendat and Piersol (1971). An ideal (noise free) single-input single-output system in the space domain can be illustrated as in Fig. 3-1.

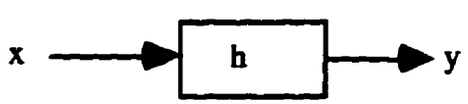

Fig. 3-1: An ideal single-input single-output system, x is the noise free input, h is the system response, y is the system output.

In convolution form, the system in Fig. 3-1 is

$$y = x * h \tag{3.1}$$

where $*$ denotes the convolution operator. This convolution can be efficiently evaluated in the frequency domain, where eq. (3.1) takes the form

$$F\{y\}=F\{x\}F\{h\} \tag{3.2}$$

Here F denotes the Fourier transform operator.

Examples of single-input single-output systems in physical geodesy are the computation of geoid undulations from gravity anomalies (or disturbances) by Stokes' (or Hotine's) integral, the computation of gravity anomalies (or disturbances) by the inverse-Stokes (or inverse-Hotine) integral, the computation of the components of the deflections of the vertical by Vening Meinesz' formula, the computation of gravity anomaly by inverse-Vening Meinesz' formulas, etc. Two examples of single-input linear systems used in physical geodesy are shown in Fig. 3-2.

Fig. 3-2: Two examples of single-input single-output systems: Stokes' and inverse-Stokes' integrals, N is the geoid height, Δg is the gravity anomaly, S and S^{-1} are Stokes' and inverse-Stokes' kernels, respectively.

In convolution form, the systems shown in Fig. 3-2 can be written as

$$N=\Delta g * S \tag{3.3}$$

$$\Delta g=N * S^{-1} \tag{3.4}$$

The corresponding frequency domain expressions of eqs. (3.3) and (3.4) are

$$F\{N\}=F\{\Delta g\}F\{S\} \tag{3.5}$$

$$F\{\Delta g\}=F\{N\}F\{S^{-1}\} \tag{3.6}$$

The FFT technique can be used for evaluation of these convolutions with great efficiency. Such discussions have been presented by Strang van Hees (1990) where the forward Stokes' formula was evaluated by FFT techniques, and by Zhang and Blais (1993) where the inverse problem was tackled using FFT techniques.

Until recently, spectral methods provided no error estimates of the output (Zhang, 1993; Olgiati, 1995). The problem of error estimation associated with spectral methods was discussed in Sideris (1987) and Schwarz et al. (1990) and was recently tackled by Sideris (1996). In the later paper, it is clearly shown that error estimates can be derived for the results using spectral methods, provided that the input signals and their errors are stochastic variables with known PSDs. Fig. 3-3 shows a single input-output system with input and output noise.

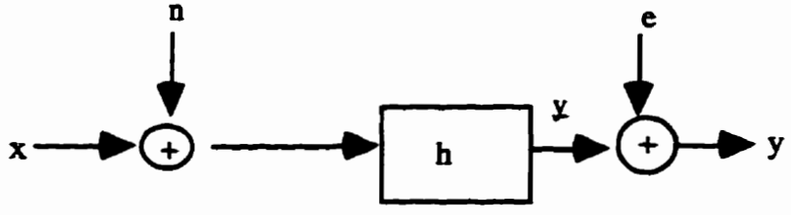

Fig. 3-3: A single-input single-output system with noise; x is the input signal, n is the input noise, y is the system output, n is the output error and y is the noise free output.

In convolution form, the system shown in Fig. 3-3 can be written as

$$y = (x+n)*h + e \tag{3.7}$$

The corresponding frequency domain expression of eq. (3.7) is

$$F\{y\} = F\{x+n\}F\{h\} + F\{e\} \tag{3.8}$$

Leaving aside the derivations and following Sideris (1996), taking into account the data noise, we can represent Stokes' formula in spectral form by the input output system theory with noise as follows:

$$F\{\hat{N}\} = P_{N\Delta g}(P_{\Delta g\Delta g} + P_{n_{\Delta g}n_{\Delta g}})^{-1}F\{\Delta g\} \tag{3.9}$$

$$P_{ee}(\hat{N}) = P_{NN} - P_{N\Delta g}(P_{\Delta g\Delta g} + P_{n_{\Delta g}n_{\Delta g}})^{-1}P_{\Delta gN} \tag{3.10}$$

where $\hat{N}$ is the estimate of geoid undulation; P_{NN} and $P_{\Delta g\Delta g}$ are the auto-signal PSDs of geoid undulation and gravity anomaly, respectively; $P_{n_{\Delta g}n_{\Delta g}}$ is the PSD of the Δg-noise; $P_{N\Delta g} = P^{*}_{\Delta gN}$ is the cross-signal PSD between geoid undulation and gravity anomaly; $P_{ee}(\hat{N})$ is the error PSD of the estimated $\hat{N}$; superscript * denotes complex conjugate. This solution has been obtained by minimizing P_{ee} in the same manner as in Section 3.2.

Similarly, we have the following expressions for the "inverse-Stokes formula":

$$F\{\Delta\hat{g}\} = P_{\Delta gN}(P_{NN} + P_{n_hn_h})^{-1}F\{N\} \tag{3.11}$$

$$P_{ee}(\Delta\hat{g}) = P_{\Delta g\Delta g} - P_{\Delta gN}(P_{NN} + P_{n_hn_h})^{-1}P_{N\Delta g} \tag{3.12}$$

Here $P_{ee}(\Delta\hat{g})$ is the error PSD of the estimated gravity anomaly and $P_{n_hn_h}$ is the PSD of the N-noise.

3.2 Double-input Single-output System

The double-input linear system has been described in detail by Bendat and Piersol (1986). A noise free double-input single-output linear system is shown in Fig. 3-4.

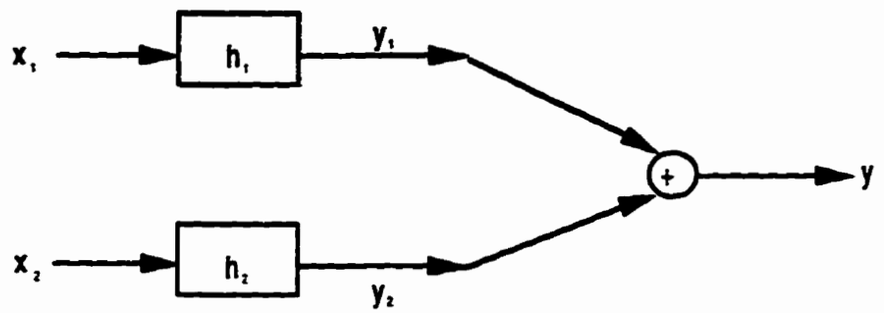

Fig. 3-4: An ideal double-input single-output system

In this study, we are actually interested in double-input single-output systems with noise, which take the geoid height and gravity anomaly observations as noise-corrupted input signals and their estimations as the output. These double-input single-output linear systems with noise are shown in Fig. 3-5 and Fig. 3-6.

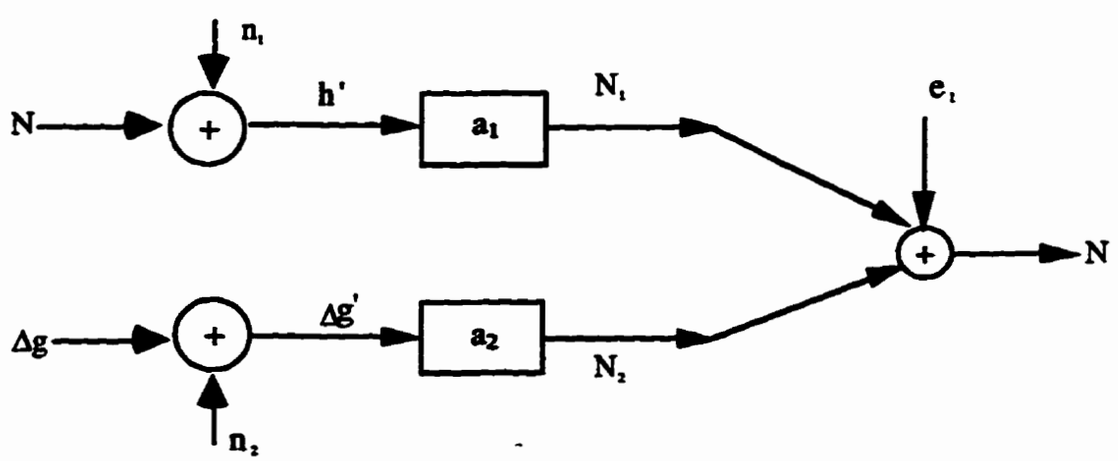

Fig. 3-5: Double-input single-output system representation for computation of geoid height by combination of altimeter and shipborne gravity data; h' and Δg' are geoid height and gravity anomaly observations, respectively.

In convolution form, the system shown in Figure 3-5 is

$$N = (N+n_1) * a_1 + (\Delta g+n_2) * a_2 + e_1 \qquad (3.13)$$

The corresponding frequency domain expression for eq. (3.13) is

$$F\{N\} = F\{N+n_1\}F\{a_1\} + F\{\Delta g+ n_2\}F\{a_2\} + F\{e_1\} \qquad (3.14)$$

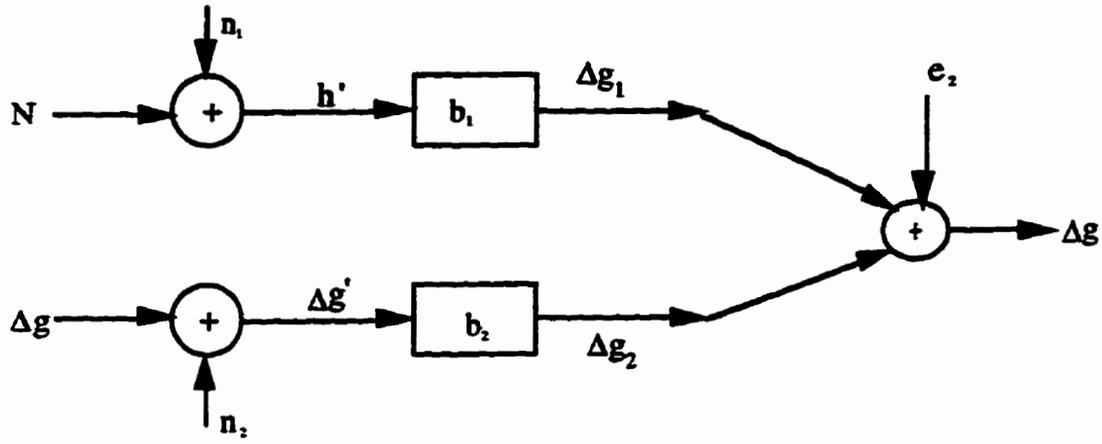

Fig. 3-6: Double-input single-output system representation for computation of the gravity anomaly by combination of the altimeter and shipborne data.

In convolution form, the system shown in Figure 3-6 is

$$\Delta g = (N+n_1) * b_1 + (\Delta g+n_2) * b_2 + e_2 \qquad (3.15)$$

In the frequency domain, eq. (3.15) takes the form

$$F\{\Delta g\} = F\{N+n_1\}F\{b_1\} + F\{\Delta g+ n_2\}F\{b_2\} + F\{e_2\} \qquad (3.16)$$

In general, eqs. (3.13) and (3.15) can be written as

$$y = h' * b_1 + \Delta g' * b_2 + e \tag{3.17}$$

where y can be either N or Δg.

Let the capital letters denote frequency domain values and the small case letters denote the spatial domain quantities. In the frequency domain, (3.17) takes the form

$$Y = H'B_1 + \Delta G'B_2 + E \tag{3.18}$$

It can be rewritten as

$$E = Y - (H'B_1 + \Delta G'B_2) \tag{3.19}$$

By multiplying E by E* and taking the expectation, the system output noise PSD is

$$\begin{aligned} P_{ee}(Y) = {} & P_{yy} - B_1 P_{h'y} - B_2 P_{\Delta g'y} - B_1^* P_{yh'} + B_1^* B_1 P_{h'h'} + B_1^* B_2 P_{\Delta g'h'} \\ & - B_2^* P_{y\Delta g'} + B_1 B_2^* P_{h'\Delta g'} + B_2^* B_2 P_{\Delta g'\Delta g'} \end{aligned} \tag{3.20}$$

By minimizing $P_{ee}(Y)$ over all possible choices of B_1 and B_2, we obtain the optimal transfer functions. These optimal transfer functions yield optimum linear least-squares prediction of Y from noisy data h' and $\Delta g'$ (Bendat and Piersol, 1986; Wu and Sideris, 1996). The optimal transfer functions B_1 and B_2 can be obtained by setting the following partial derivatives equal to zero:

$$\frac{\partial P_{ee}(Y)}{\partial B_1^*} = 0 \tag{3.21}$$

$$\frac{\partial P_{ee}(Y)}{\partial B_2^*} = 0 \tag{3.22}$$

Assuming that the input noises n_1 and n_2 are uncorrelated and that signal and noise are uncorrelated and solving the above equations, we obtain the following optimal estimates:

$$\hat{Y} = B_1 H' + B_2 \Delta G' \tag{3.23}$$

$$B_1 = \frac{(P_{\Delta g\Delta g} + P_{n_{\Delta g} n_{\Delta g}})P_{yh} - P_{\Delta gh}P_{y\Delta g}}{(P_{hh} + P_{n_h n_h})(P_{\Delta g\Delta g} + P_{n_{\Delta g} n_{\Delta g}}) - |P_{h\Delta g}|^2} \tag{3.24}$$

$$B_2 = \frac{(P_{hh} + P_{n_h n_h})P_{y\Delta g} - P_{h\Delta g}P_{yh}}{(P_{hh} + P_{n_h n_h})(P_{\Delta g\Delta g} + P_{n_{\Delta g} n_{\Delta g}}) - |P_{h\Delta g}|^2} \tag{3.25}$$

$$P_{ee}(Y) = P_{yy} - |B_1|^2(P_{hh} + P_{n_h n_h}) + B_1^* B_2 P_{\Delta gh} + B_2^* B_1 P_{h\Delta g} - |B_2|^2(P_{\Delta g\Delta g} + P_{n_{\Delta g} n_{\Delta g}}) \tag{3.26}$$

$$P_{\hat{y}\hat{y}} = |B_1|^2(P_{hh} + P_{n_h n_h}) - B_1^* B_2 P_{\Delta gh} - B_2^* B_1 P_{h\Delta g} + |B_2|^2(P_{\Delta g\Delta g} + P_{n_{\Delta g} n_{\Delta g}}) \tag{3.27}$$

$$P_{\Delta\hat{g}\hat{N}} = B_1^* B_2 P_{\Delta gh} \tag{3.28}$$

where $\hat{Y}$ is the estimate of the spectra of y, which can be either h (i.e. N) or Δg; P_{hh}, $P_{\Delta g\Delta g}$ are the auto-power spectral densities of h and Δg, respectively; $P_{h\Delta g} = P^*_{\Delta gh}$ is the cross-power spectral density between h and Δg; P_{yh}, $P_{y\Delta g}$ are the cross- power spectral densities between y and h, and y and Δg, respectively; $P_{n_h n_h}$ and $P_{n_{\Delta g} n_{\Delta g}}$ are the noise PSDs of h and Δg, respectively; $P_{ee}(Y)$ is the prediction error PSD of Y; $P_{\hat{y}\hat{y}}$ is the estimate of auto-PSD of y and

$P_{\Delta\hat{g}\hat{N}} = P^{*}_{\hat{N}\Delta\hat{g}}$ is the estimate of the cross-PSD between Δg and N. It is clear that the IOST solution depends on the signal-to-noise ratios.

For detailed derivation of the above equations, see Sideris (1996) and Wu and Sideris (1996).

The above expressions can also be written in an equivalent stepwise form (Sideris, 1996):

$$\hat{Y}_h = P_{yh}P_{hh}^{-1}H^{'} \tag{3.29}$$

$$\hat{Y} = \hat{Y}_h + \bar{P}_{\Delta g}\bar{P}^{-1}_{\Delta g\Delta g}(\Delta G^{'} - P_{\Delta gh}P_{hh}^{-1}H^{'}) \tag{3.30}$$

$$\bar{P}_{\Delta g} = P_{y\Delta g} - P_{yh}P_{hh}^{-1}P_{h\Delta g} \tag{3.31}$$

$$\bar{P}_{\Delta g\Delta g} = P_{\Delta g\Delta g} - P_{\Delta gh}P_{hh}^{-1}P_{h\Delta g} \tag{3.32}$$

$$P_{ee}(Y) = P_{yy} - P_{yh}P_{hh}^{-1}P^{*}_{yh} - \bar{P}_{\Delta g}\bar{P}^{-1}_{\Delta g\Delta g}\bar{P}^{*}_{\Delta g} = P_{ee_h} - \bar{P}_{\Delta g}\bar{P}^{-1}_{\Delta g\Delta g}\bar{P}^{*}_{\Delta g} \tag{3.33}$$

$$P_{\hat{y}\hat{y}} = P_{yh}P_{hh}^{-1}P^{*}_{yh} - \bar{P}_{\Delta g}\bar{P}^{-1}_{\Delta g\Delta g}\bar{P}^{*}_{\Delta g} = P_{\hat{y}_h\hat{y}_h} - \bar{P}_{\Delta g}\bar{P}^{-1}_{\Delta g\Delta g}\bar{P}^{*}_{\Delta g}P \tag{3.34}$$

$$P_{\Delta\hat{g}_h\hat{N}_h} = P_{\Delta gh}P_{hh}^{-1}P_{h\Delta g} \tag{3.35}$$

$$P_{\Delta\hat{g}\hat{N}} = P_{\Delta g\Delta g}\bar{P}^{-1}_{\Delta g\Delta g}P_{\Delta\hat{g}_h\hat{N}_h} \tag{3.36}$$

In this form, the contribution of each input can be computed sequentially in the same manner as in sequential LSC in the space domain. We see that when noise is present at the input and output stage, the frequency domain solution of the IOST is formally equivalent to LSC. More

details on IOST in physical geodesy can be found in Sideris (1996), Schwarz et al. (1990) and Sansò and Sideris (1995).

3.3 Least-squares Collocation

The application of conventional (space domain) LSC in physical geodesy has been discussed in detail by Moritz (1980). Its practical applications in gravity field modeling can be found in, e.g., Tscherning (1974), Rapp (1985) and Basic and Rapp (1992). A fast (frequency domain) LSC method was studied by Eren (1980) and Bottoni and Barzaghi (1993). The advantage of using fast LSC method is that a considerable gain in computation time and storage is obtained in comparison with conventional LSC when gridded data are available. We will use conventional LSC in this study.

Assuming that the Earth's gravity field is a stochastic process and that signal and noise are not correlated, we have the mathematical model of conventional LSC for gravity field modeling using altimetry-derived geoid heights h' and shipborne gravity anomalies $\Delta g'$ as

$$\begin{Bmatrix} h \\ \Delta g \end{Bmatrix} = \begin{bmatrix} C_{hh'} & C_{h\Delta g'} \\ C_{\Delta gh'} & C_{\Delta g\Delta g'} \end{bmatrix} \left\{ \begin{bmatrix} C_{hh} & C_{h\Delta g} \\ C_{\Delta gh} & C_{\Delta g\Delta g} \end{bmatrix} + \begin{bmatrix} D_{hh} & 0 \\ 0 & D_{\Delta g\Delta g} \end{bmatrix} \right\}^{-1} \begin{Bmatrix} h' \\ \Delta g' \end{Bmatrix} \tag{3.37}$$

$$C_{ee}(N) = C_{NN} - \begin{bmatrix} C_{Nh'} & C_{N\Delta g'} \end{bmatrix} \left(\begin{bmatrix} C_{hh} & C_{h\Delta g} \\ C_{\Delta gh} & C_{\Delta g\Delta g} \end{bmatrix} + \begin{bmatrix} D_{hh} & 0 \\ 0 & D_{\Delta g\Delta g} \end{bmatrix} \right)^{-1} \begin{bmatrix} C_{h'N} \\ C_{\Delta g'N} \end{bmatrix} \tag{3.38}$$

$$C_{ee}(\Delta g) = C_{\Delta g\Delta g} - \begin{bmatrix} C_{\Delta gh'} & C_{\Delta g\Delta g'} \end{bmatrix} \left(\begin{bmatrix} C_{hh} & C_{h\Delta g} \\ C_{\Delta gh} & C_{\Delta g\Delta g} \end{bmatrix} + \begin{bmatrix} D_{hh} & 0 \\ 0 & D_{\Delta g\Delta g} \end{bmatrix} \right)^{-1} \begin{bmatrix} C_{h'\Delta g} \\ C_{\Delta g'\Delta g} \end{bmatrix} \tag{3.39}$$

where $C_{ee}(N)$ and $C_{ee}(\Delta g)$ are the predicted error covariance matrices of N and Δg, respectively;

C_{NN}, $C_{\Delta g\Delta g}$ are auto-covariance functions of geoid height and gravity anomaly, respectively; $C_{N\Delta g} = C_{\Delta gN}$ is the cross-covariance function between geoid height and gravity anomaly; $C_{Nh'} = C_{h'N}$ and $C_{\Delta gh'} = C_{h'\Delta g}$ are covariance functions between signals (N and Δg, respectively) and geoid height observations; $C_{N\Delta g'} = C_{\Delta g'N}$ and $C_{\Delta g\Delta g'} = C_{\Delta g'\Delta g}$ are covariance functions between signal and gravity anomaly observations; D_{hh} and $D_{\Delta g\Delta g}$ denote the auto-covariance matrices for the geoid height and gravity anomaly observation errors, respectively.

LSC gives optimal estimates, i.e. having minimum error variances, in the sense of satisfying the minimum condition

$$\underline{v}^T C^{-1} \underline{v} = \min \tag{3.40}$$

where vector $\underline{v}$ consists of the estimated signals and the measuring noises and C is the covariance matrix of $\underline{v}$. For more details on LSC, Moritz (1980) should be consulted.

3.4. Least-squares adjustment in the frequency domain

Let H', $\Delta G'$, Y, N_h and $N_{\Delta g}$ represent again the spectra of h', $\Delta g'$, y, n_h and $n_{\Delta g}$, respectively. For each frequency component, we may write the following observation equations in the frequency domain:

$$\begin{Bmatrix} H' \\ \Delta G' \end{Bmatrix} = \begin{Bmatrix} B_1^{-1} \\ B_2^{-1} \end{Bmatrix} Y + \begin{Bmatrix} N_h \\ N_{\Delta g} \end{Bmatrix} = \begin{Bmatrix} H \\ \Delta G \end{Bmatrix} + \begin{Bmatrix} N_h \\ N_{\Delta g} \end{Bmatrix} \tag{3.41}$$

where

$$\left.\begin{aligned} B_1^{-1} &= 1 \\ B_2^{-1} &= 2\pi\gamma\sqrt{u^2+v^2} \end{aligned}\right\}, \quad \text{if } Y=H \tag{3.42}$$

$$\left.\begin{aligned} B_1^{-1} &= \frac{1}{2\pi\gamma\sqrt{u^2+v^2}} \\ B_2^{-1} &= 1 \end{aligned}\right\}, \quad \text{if } Y=\Delta G \tag{3.43}$$

B_1^{-1} and B_2^{-1} are perfectly known transfer functions; H and ΔG are the spectra of the signals of the observations h' and $\Delta g'$, respectively; and u and v are the frequencies in two directions corresponding to x and y, respectively.

Assuming that the input signals are completely deterministic and the input noises are stochastic variables, we have the optimum solution for each frequency, which is obtained by requiring that the frequency domain least-squares principle

$$N_h^T C_{N_h N_h}^{-1} N_h + N_{\Delta g}^T C_{N_{\Delta g} N_{\Delta g}}^{-1} N_{\Delta g} = \min$$

is fulfilled, as follows:

$$\begin{aligned} \hat{Y} &= \frac{P_{n_{\Delta g} n_{\Delta g}} B_1^{-2}}{B_1^{-2} P_{n_{\Delta g} n_{\Delta g}} + B_2^{-2} P_{n_h n_h}} B_1 H' + \frac{P_{n_h n_h} B_2^{-2}}{B_1^{-2} P_{n_{\Delta g} n_{\Delta g}} + B_2^{-2} P_{n_h n_h}} B_2 \Delta G' \\ &= \left(1+\frac{B_1^2 P_{n_h n_h}}{B_2^2 P_{n_{\Delta g} n_{\Delta g}}}\right)^{-1} B_1 H' + \left(1+\frac{B_2^2 P_{n_{\Delta g} n_{\Delta g}}}{B_1^2 P_{n_h n_h}}\right)^{-1} B_2 \Delta G' \end{aligned} \tag{3.44}$$

$$P_{ee}(Y) = \left(\frac{1}{B_1^2 P_{n_h n_h}} + \frac{1}{B_2^2 P_{n_{\Delta g} n_{\Delta g}}}\right)^{-1} = \left(\frac{1}{P_{e:n_h, e:n_h}} + \frac{1}{P_{e:n_{\Delta g}, e:n_{\Delta g}}}\right) \tag{3.45}$$

where $P_{n_h n_h}$ and $P_{n_{\Delta g} n_{\Delta g}}$ are the noise PSDs of h' and $\Delta g'$, respectively; $P_{ee}(Y)$ is the prediction

error PSD of Y; $P_{e:n_h,e:n_h}$ and $P_{e:n_{\Delta g},e:n_{\Delta g}}$ are the corresponding contributions to the output noise PSDs from the input noise PSDs of geoid height and gravity anomaly, respectively. More details on the LSAFD can be found in Barzaghi et al. (1993) and also in Sideris (1996).

3.5 Discussion

The LSC is an optimal estimator that offers many advantages and is quite accommodating in terms of the data types and estimated quantities. The assumption for the LSC method is that the mean values of both observations are equal to zero. Thus, the data should be centred before using LSC. The data can be either gridded or irregularly distributed. The use of LSC requires a priori information about the field, i.e., the isotropic covariance functions. The estimate relies on the a priori information as well as the noise covariances of the input data. Thus, the estimation of signal and noise covariances is a prerequisite of the LSC method. How these covariance functions can be obtained will be addressed in Chapter 4.

Assumptions for the IOST method are the same as for collocation, i.e., that both signal and their errors are random variables with known PSDs, which are the Fourier transforms of the covariance functions. The solution of IOST depends on this a priori information. Signal PSDs can be obtained, as described in the next chapter, from the corresponding covariance functions using the FFT method or can be computed directly from the data. A theoretical comparison of LSC and IOST was done by Sansò and Sideris (1995). The multiple-IOST solution is formally equivalent to stepwise LSC solution. Therefore, the multiple-IOST solution can be computed in a stepwise manner. The biggest disadvantage of LSC is that it requires matrix inversion, which is very slow and memory eating when a large data set is dealt with. The frequency solution of the IOST requires no such inversion, however. There is similarity between the LSC and the IOST in that both methods depend, to some extend, on the same a priori information (the PSD

is the Fourier transform of the covariance function).

Two differences should be mentioned here. First, the dimensions of the covariance matrices used in the methods are not the same. The dimension of the covariance matrix used in LSC is bigger than that used in IOST (for computing the PSD). Second, the IOST method can use non-isotropic PSDs without any difficulty in the practical computations, but, LSC usually requires isotropic covariances. Using non-isotropic covariances in LSC will make LSC even more difficult to implement. The estimation of signal and error PSDs will be discussed in the next chapter.

The covariance (or PSD) functions used in LSC (or IOST) are usually derived from observations and may have been adjusted to fit some analytical covariance (or PSD) function models. If the analytical models do not represent the reality, then using model derived covariance (or PSD) functions may lead to worse results be obtained.

LSAFD assumes that only the input noises are random variables; no a-priori stochastic information about the signal is needed. The LSAFD method employs the noise PSDs and assumes the transfer functions are perfectly known (Sideris, 1996). The noise PSDs are used to adjust the observation spectra and to weight the contributions of each data set. The differences between IOST and LSAFD are mainly that the IOST method has two functions, one is to filter input signals and the other is to combine them optimally, while the LSAFD method only conducts the weighted averaging (Wu, 1996). In this sense, better results can be expected with IOST method due to its filtering function.

CHAPER FOUR

POWER SPECTRAL DENSITY AND COVARIANCE ESTIMATION

An important issue in using the LSC, IOST and LSAFD methods is the determination of the a-priori information, i.e., the estimation of the signal and noise covariance and associated PSD functions. This chapter discusses the estimation method employed for such tasks. The first section highlights the basic concepts of covariance, correlation and power spectral density and their relations. Section 4.2 presents empirical covariance function estimation and modelling. Section 4.3 presents the techniques for PSD estimation. Finally, section 4.4 describes the error PSD estimations.

4.1 Concepts of Correlation, Covariance and Power Spectral Density

This section highlights some concepts related to correlation, covariance and power spectral density functions, as well as their relations. For more details, Bendat and Piersol (1980, 1986) and Sideris (1984) should be consulted.

The two dimensional correlation function of two ergodic stationary functions $f_1(x,y)$ and $f_2(x,y)$ is defined as

$$K_{1,2}(x',y') = E\{f_1(x,y)f_2(x+x',y+y')\} \tag{4.1}$$

where $E\{\}$ is the mathematical expectation operator. If $f_1(x,y)=f_2(x,y)$, then $K_{1,2}(x',y') = K_{1,1}(x',y')$ and it is called the auto-correlation function. Otherwise, $K_{1,2}(x',y')$ is the cross -correlation function. If $K_{1,2}(x',y') = K_{1,2}(\sqrt{x'^2+y'^2})$, the random functions $f_1(x,y)$ and $f_2(x,y)$ are said to be isotropic functions.

For discrete data, the corresponding discrete correlation function is defined as

$$K_{1,2}(k,l) = E\{f_1(i,j)f_2(k+i,l+j)\} = \lim_{\substack{M\to\infty \\ N\to\infty}} \frac{1}{M}\frac{1}{N}\sum_{i=0}^{M-1}\sum_{j=0}^{N-1} f_1(i,j)f_2(i,j) \qquad (4.2)$$

where M and N are the number of data points along x and y directions, respectively and k and l are wave numbers along x and y directions, respectively.

The covariance function of $f_1(x,y)$ and $f_2(x,y)$ is defined as

$$C_{1,2}(x',y') = E\{[f_1(x,y)-\bar{f}_1][f_2(x+x',y+y')-\bar{f}_2]\} \qquad (4.3)$$

where $\bar{f}_1$ and $\bar{f}_2$ are the mathematical expectations of $f_1(x,y)$ and $f_2(x,y)$, respectively. If $f_1(x,y)=f_2(x,y)$, then $C_{1,2}(x',y') = C_{1,1}(x',y')$ and it is called the auto-covariance function of $f_1(x,y)$. Otherwise, it is called the cross-covariance function. If $\bar{f}_1 = \bar{f}_2 = 0$, we call $f_1(x,y)$ and $f_2(x,y)$ centred functions. For centred functions, their covariance function and correlation function are identical, i.e.,

$$C_{1,2}(x',y') = K_{1,2}(x',y').$$

For discrete data, we have

$$\begin{aligned} C_{1,2}(k,l) &= E\{[f_1(i,j)-\bar{f}_1][f_2(i,j)-\bar{f}_2]\} \\ &= \lim_{\substack{M\to\infty \\ N\to\infty}} \frac{1}{M}\frac{1}{N}\sum_{i=0}^{M-1}\sum_{j=0}^{N-1} [f_1(i,j)-\bar{f}_1][f_2(k+i,l+j)-\bar{f}_2] \end{aligned} \qquad (4.4)$$

The power spectral density is defined as the frequency domain equivalent of the correlation

function. The power spectral density function of a random function describes the general composition of the data in terms of the mean square values of its power spectrum. The power spectral density function $P_{1,2}(u,v)$ of two random functions $f_1(x,y)$ and $f_2(x,y)$ is the Fourier transform of the corresponding correlation function $K_{1,2}(x',y')$ (Bendat and Piersol, 1980, 1986; Sideris, 1984):

$$P_{1,2}(u,v) = \int_{-\infty}^{+\infty}\int_{-\infty}^{+\infty} K_{1,2}(x,y)e^{-2i\pi(ux+vy)}dxdy \qquad (4.5)$$

For discrete data,

$$P_{1,2}(m,n) = \lim_{\substack{T_x\to\infty \\ T_y\to\infty}} \frac{1}{T_x}\frac{1}{T_y} F_1^*(m,n)F_2(m,n) \qquad (4.6)$$

where T_x and T_y are the data lengths along the x and y directions, respectively.

For centred random functions, the power spectral density function can also be written as

$$P_{1,2}(u,v) = \int_{-\infty}^{+\infty}\int_{-\infty}^{+\infty} C_{1,2}(x,y)e^{-2i\pi(ux+vy)}dxdy \qquad (4.7)$$

Again, $P_{1,2}(u,v)$ is called the auto-power spectral density function if $f_1(x,y)=f_2(x,y)$, and the cross-power spectral density if $f_1(x,y)$ and $f_2(x,y)$ are different.

Equations (4.5) and (4.7) are useful if PSD functions are to be computed from known correlation or covariance functions.

4.2 Estimation of Signal Covariance Functions

The successful use of LSC relies on reliable estimation of the signal and error covariances. This section discusses the estimation and modelling of the covariance function. Some analytical global covariance models for gravity field quantities were developed by Tscherning and Rapp (1974). We termed these models as Tscherning/Rapp models. Tscherning/Rapp models will be used in this study. Some self-consistent local covariance function models were discussed by Jordan (1972). In local applications, a long-wavelength field (e.g., the OSU91A model field) is usually removed from the observations and the residual field is dealt with. The removed field is afterwards added back to the adjusted quantities. This technique is called the remove-restore technique. Goad et al. (1984) discussed the computation of the local empirical gravity anomaly covariance function. The estimation of the local empirical covariance function using altimetry and gravity anomaly data was discussed by Knudsen (1987a).

4.2.1 Computation of Empirical Covariances

4.2.1.1 Direct Method

This method is used to compute the empirical covariance directly from the data. Formulas presented in the previous section can be applied in cases where given functions $f_1(x,y)$ and $f_2(x,y)$ are analytical continuous functions or discrete values of these functions are known on the infinite x-y plane. In real world applications, we usually only have discrete sampled data within a finite area. Therefore, we should rewrite the above formulas so that they are suitable for real world applications. Assuming that discrete grid values of $f_1(x,y)$ and $f_2(x,y)$ are given in a rectangular area of the size of $T_x T_y$ with grid spacings of Δx and Δy along x and y

directions respectively, and that $f_1(x,y)$ and $f_2(x,y)$ are centred, we could write the following covariance estimator

$$\hat{C}_{1,2}(k,l) = \hat{K}_{1,2}(k,l) = \frac{1}{M-k}\frac{1}{N-l}\sum_{i=0}^{M-l-k}\sum_{j=0}^{N-l-l} f_1(i,j)f_2(i+k,j+l) \qquad (4.8)$$

where $M=T_x/\Delta x$, $N=T_y/\Delta y$. If we substitute geoid height observations for $f_1(i,j)$ and $f_2(i,j)$, we get the empirical covariance estimator for the geoid height. If gravity anomaly observations are substituted for $f_1(i,j)$ and $f_2(i,j)$, we have the gravity anomaly empirical covariance estimator. If we substituted the observation values of geoid height for $f_1(i,j)$ and gravity anomaly for $f_2(i,j)$, we have the estimator for the empirical cross-covariance of the geoid height and the gravity anomaly.

4.2.1.2 Indirect Method

Because the covariance function and the power spectral density of a zero mean field are a pair of direct and inverse Fourier transforms, the covariance function can be computed simply from the known PSD through the following expression:

$$\hat{C}_{1,2}(k,l) = F^{-1}\{\hat{P}_{1,2}(u,v)\} \qquad (4.9)$$

4.2.2 Models for Covariance Functions of the Gravity Field

In this subsection, we discuss the modeling of the covariance functions for the gravity field. In covariance function modeling, analytical covariance functions are determined from empirical values. Various covariance function models for gravity field modeling, such as second and third order Markov models (Jordan, 1972), the logarithmic model, the Poisson

model, the Hirvonen model (Moritz, 1980) and the Tscherning/Rapp model (Tscherning and Rapp, 1974), have been proposed. Among these models, the Tscherning/Rapp model is the most widely used one.

We work with the residual gravity field, which is obtained by subtracting quantities produced by some reference field from the corresponding observations. Further more, we centralize the residual field by subtracting from the residual observations the corresponding mean value. The reference field can be any one of the known geopotential-model-produced fields. We use the OSU91 geopotential model field as the reference field. Thus, the residual observations for gravity anomaly and geoid height are

$$\begin{aligned}\Delta g &= \Delta g_{obs} - \Delta g_{ref} \\ &= \Delta g_{obs} - \frac{GM}{R^2}\sum_{n=2}^{360}(n-1)\left(\frac{a}{R}\right)^n \sum_{m=0}^{n}(\bar{C}_{nm}\cos m\lambda + \bar{S}_{nm}\sin m\lambda)\bar{P}_{nm}(\cos\theta)\end{aligned} \tag{4.10}$$

$$\begin{aligned}h &= h_{obs} - h_{ref} \\ &= h_{obs} - \frac{GM}{R\gamma}\sum_{n=2}^{360}\left(\frac{a}{R}\right)^n \sum_{m=0}^{n}(\bar{C}_{nm}\cos m\lambda + \bar{S}_{nm}\sin m\lambda)\bar{P}_{nm}(\cos\theta)\end{aligned} \tag{4.11}$$

where a=6378137 m, GM=3.9860044 x 10^{14} m^3s^{-2}, and γ is the normal gravity. The other symbols in the above expressions are well known and will not be explained in more detail.

We use the Tscherning/Rapp model in this study. The corresponding covariance function between two points separated by distance $\Delta\rho$ for the residual field can be represented as:

$$C(\Delta\rho) = C_{em}(\Delta\rho) + C_{T/R}(\Delta\rho) \tag{4.12}$$

where $C_{em}(\Delta\rho)$ is the covariance function associated with errors of the spherical coefficients

of the reference model, and $C_{T/R}(\Delta\rho)$ is the covariance function associated the Tscherning/Rapp model of the reference field. More specifically, the three covariance functions used by LSC for our task at hand can be written as:

$$C_{hh}(P,Q) = \sum_{n=2}^{360}\varepsilon_n(h,h)S^{n+1}P_n(\cos\psi) + \sum_{n=361}^{\infty}\sigma_n(h,h)S^{n+1}P_n(\cos\psi) \tag{4.13}$$

$$C_{\Delta g\Delta g}(P,Q) = \sum_{n=2}^{360}\varepsilon_n(\Delta g,\Delta g)S^{n+2}P_n(\cos\psi) + \sum_{n=361}^{\infty}\sigma_n(\Delta g,\Delta g)S^{n+2}P_n(\cos\psi) \tag{4.14}$$

$$C_{\Delta gh}(P,Q) = \sum_{n=2}^{360}\varepsilon_n(\Delta g,h)S^{n+1}P_n(\cos\psi) + \sum_{n=361}^{\infty}\sigma_n(\Delta g,h)S^{n+1}P_n(\cos\psi) \tag{4.15}$$

where $\varepsilon_n(h,h)$, $\varepsilon_n(\Delta g,\Delta g)$ and $\varepsilon_n(\Delta g,h)$ are degree variances associated with errors of the reference field, and $\sigma_n(h,h)$, $\sigma_n(\Delta g,\Delta g)$ and $\sigma_n(\Delta g,\Delta g)$ are signal degree variance computed using the Tscherning/Rapp model. The error degree variances associated with the reference field can be computed using the following expressions:

$$\varepsilon_n(h,h) = \frac{1}{\gamma^2}\varepsilon_n(T,T) \tag{4.16}$$

$$\varepsilon_n(\Delta g,\Delta g) = \frac{(n-1)^2}{R^2}\varepsilon_n(T,T) \tag{4.17}$$

$$\varepsilon_n(\Delta g,h) = \frac{n-1}{\gamma R}\varepsilon_n(T,T) \tag{4.18}$$

$$\varepsilon_n(T,T) = \left(\frac{GM}{R}\right)^2\sum_{m=0}^{n}(\bar{e}_{cnm}^2 + \bar{e}_{snm}^2) \tag{4.19}$$

where $\bar{e}_{cnm}$ and $\bar{e}_{snm}$ are the standard deviations of the fully normalized potential coefficients

$\bar{C}_{nm}$ and $\bar{S}_{nm}$, respectively.

The signal degree variances associated with the residual field can be obtained by the following formulas:

$$\sigma_n(h,h) = \frac{1}{\gamma^2}\sigma_n(T,T) \tag{4.20}$$

$$\sigma_n(\Delta g,\Delta g) = \frac{(n-1)^2}{R^2}\sigma_n(T,T) \tag{4.21}$$

$$\sigma_n(\Delta g,h) = \frac{n-1}{\gamma R}\sigma_n(T,T) \tag{4.22}$$

$$\sigma_n(T,T) = \frac{A}{(n-1)(n-2)(n+24)} \tag{4.23}$$

here A is a global parameter with a value of 425.28 mgal^2

The covariance functions expressed by eq.(4.10) through (4.23) are global. In local gravity field computation, these global functions are usually adjusted to fit the local characteristics of the field. A method for such adjustment was discussed by Knudsen (1987a). The adjustment of the global model is done by estimating the values of three parameters and then using these three parameters in the model. These three parameters are the Bjerhamar radius R_B, local variance (or covariance) value A and a scaling factor α. The estimation of the three parameters is done by fitting the global model to the empirical covariance values for the local area. The α parameter is used to scale the error degree variance of the reference field (i.e. the OSU91A model in this study) so that they represent the quality of the approximated potential coefficients set in the local area. For more details on the adjustment of the local covariance

function model, cf. Knudsen (1987a, b).

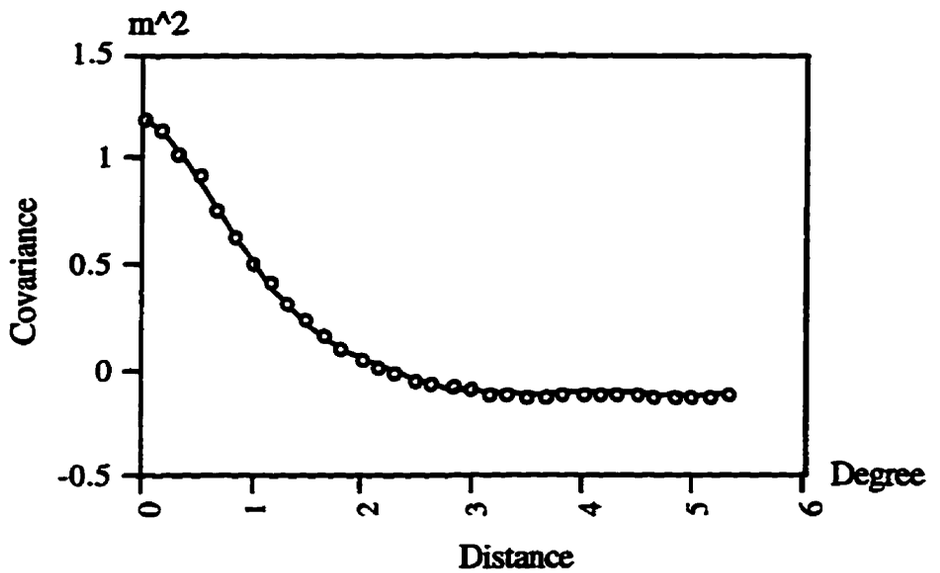

Fig. 4-1: Covariance function of residual geoid height for simulated data

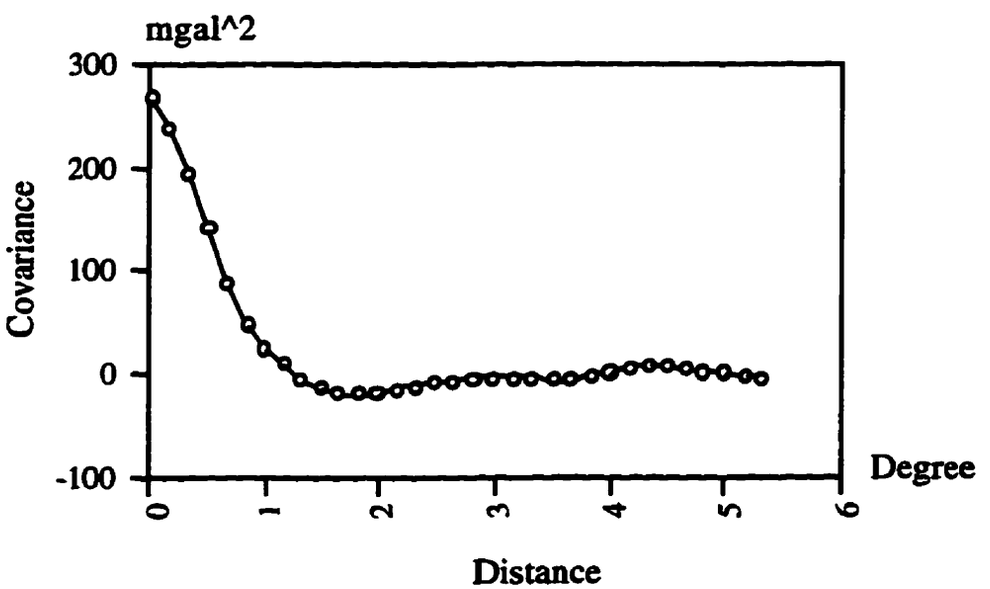

Fig. 4-2: Covariance function of residual gravity anomaly for simulated data

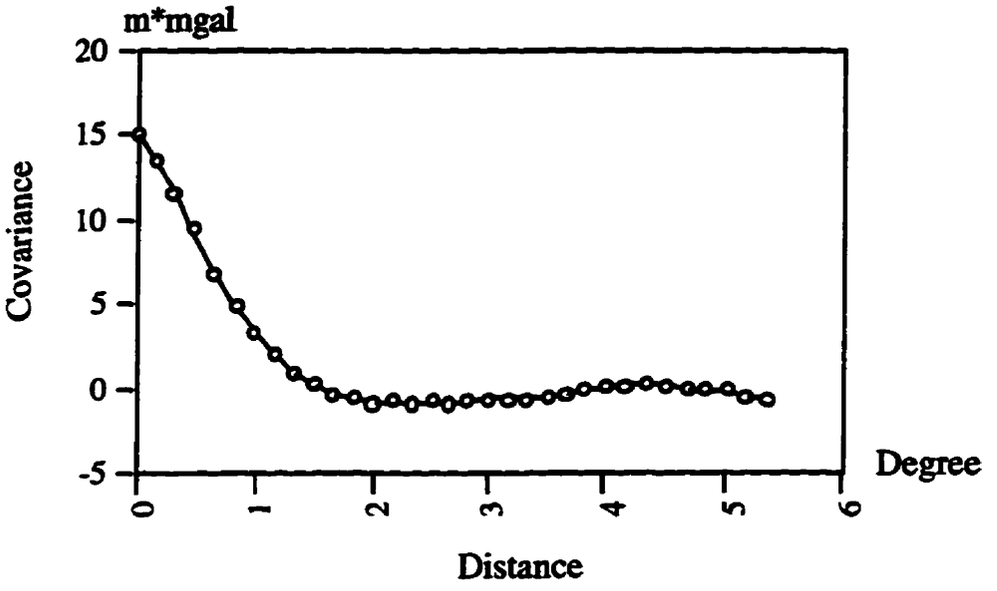

Fig. 4-3: Cross-covariance function between residual geoid and residual gravity for simulated data

In the simulation studies, we computed the covariance functions by Fourier transforming the isotropic PSD functions. The isotropic PSDs were computed by averaging the FFT-derived PSDs (i.e., PSDs computed by the direct method discussed in the following section) over all azimuths. Figures 4-1 to 4-3 show the signal covariance functions of the simulation data.

For our two test areas with real data, we used in the Central Mediterranean area strictly self-consistent (or analytical) covariance functions and in the Labrador Sea area pure empirical covariance functions. More specifically, in the Central Mediterranean area, the covariance functions were computed by fitting the empirical covariance functions to the Tscherning/Rapp model and thus they are self-consistent. In the Labrador Sea area, the covariances functions were computed from FFT-derived PSDs, without fitting them to analytical models. These covariance functions for different quantities may not satisfy the mathematical relationships

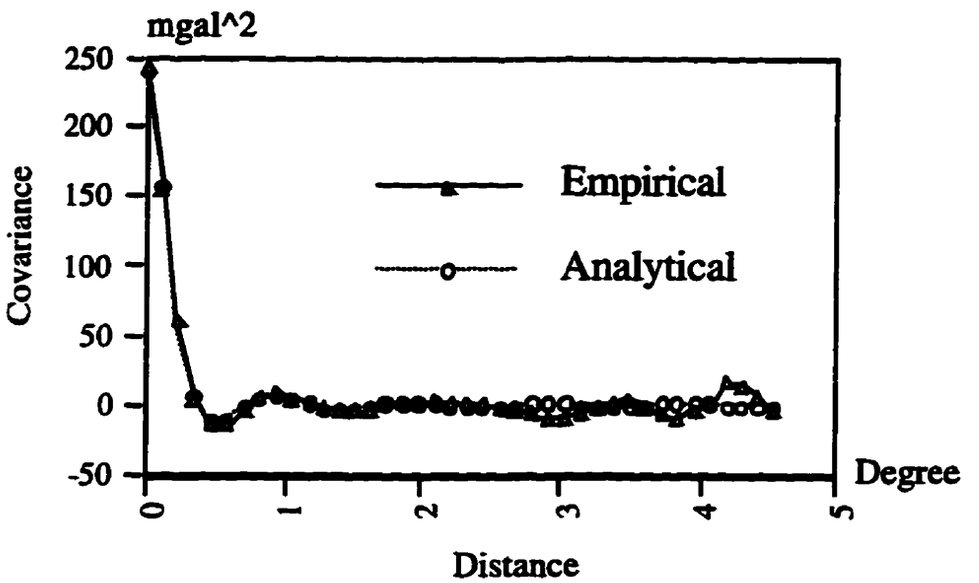

Fig. 4-4: Empirical and analytical covariance functions for gravity anomaly in the Central Mediterranean area

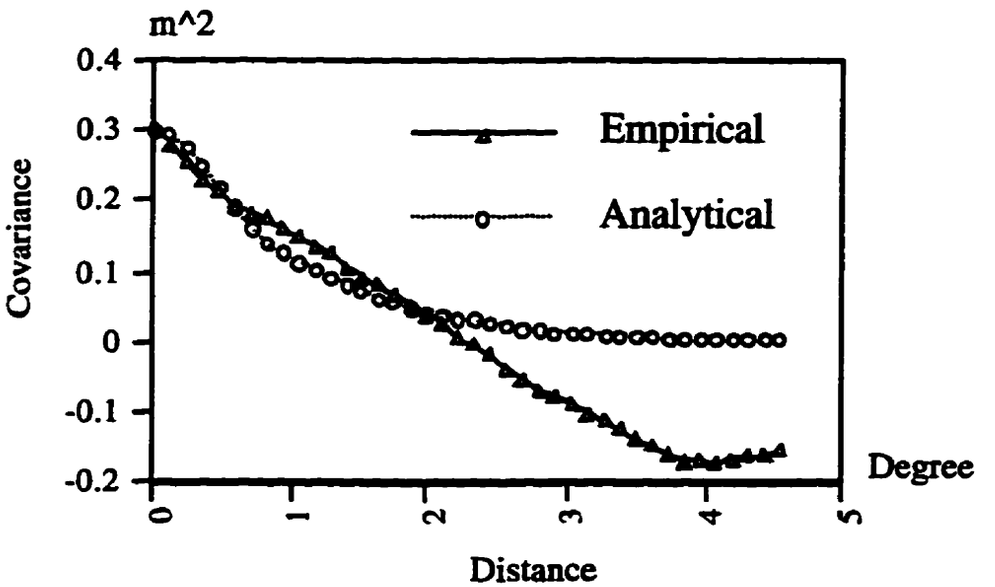

Fig. 4-5: Empirical and analytical covariance functions for geoid height in the Central Mediterranean area

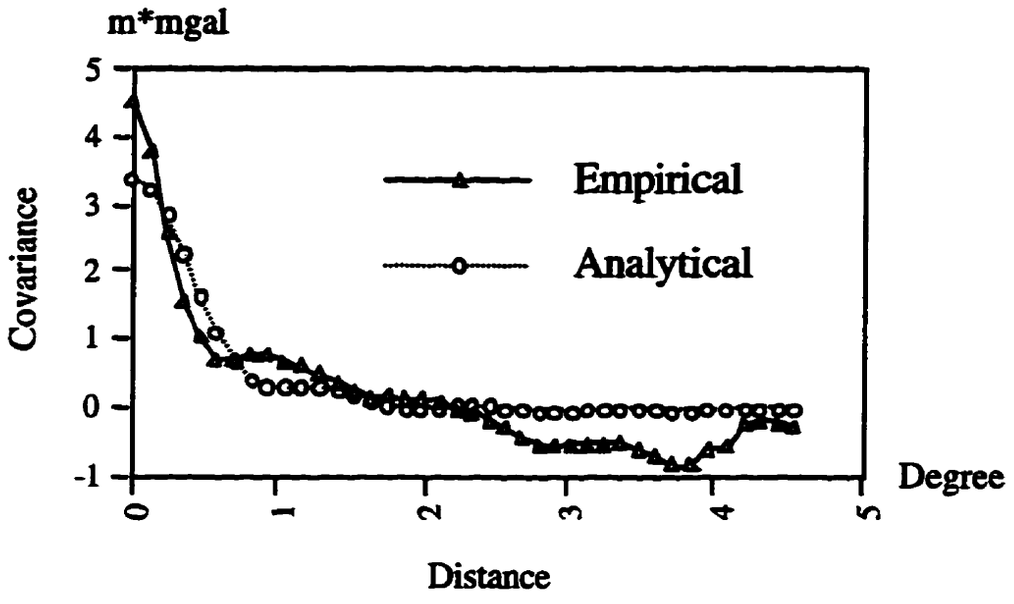

Fig. 4-6: Empirical and analytical covariance functions between gravity anomaly and geoid height in the Central Mediterranean area

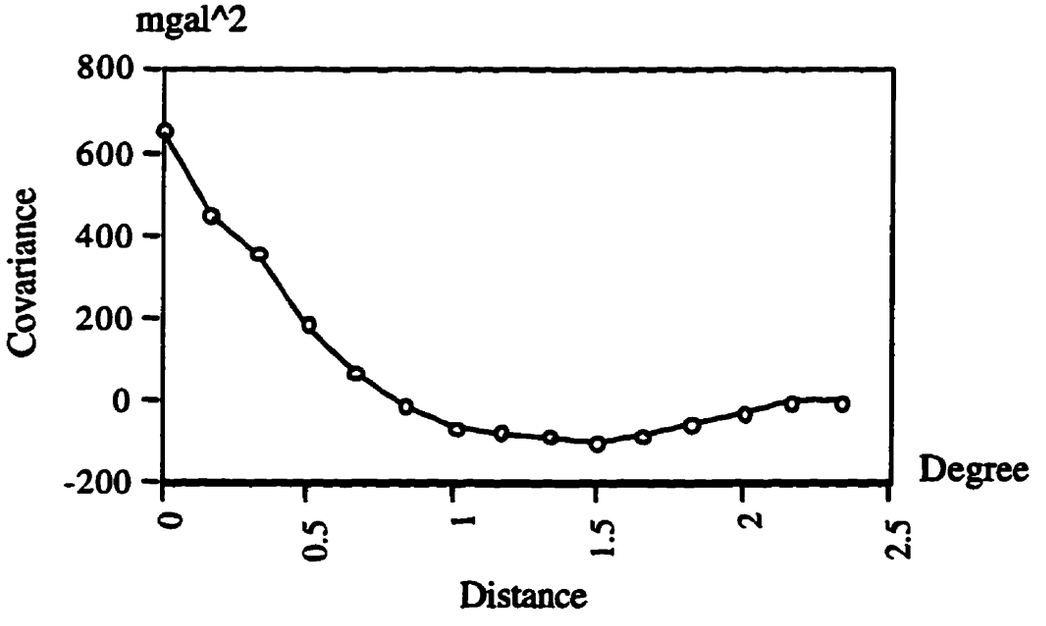

Fig. 4-7: Covariance function of gravity anomaly in the Labrador Sea area

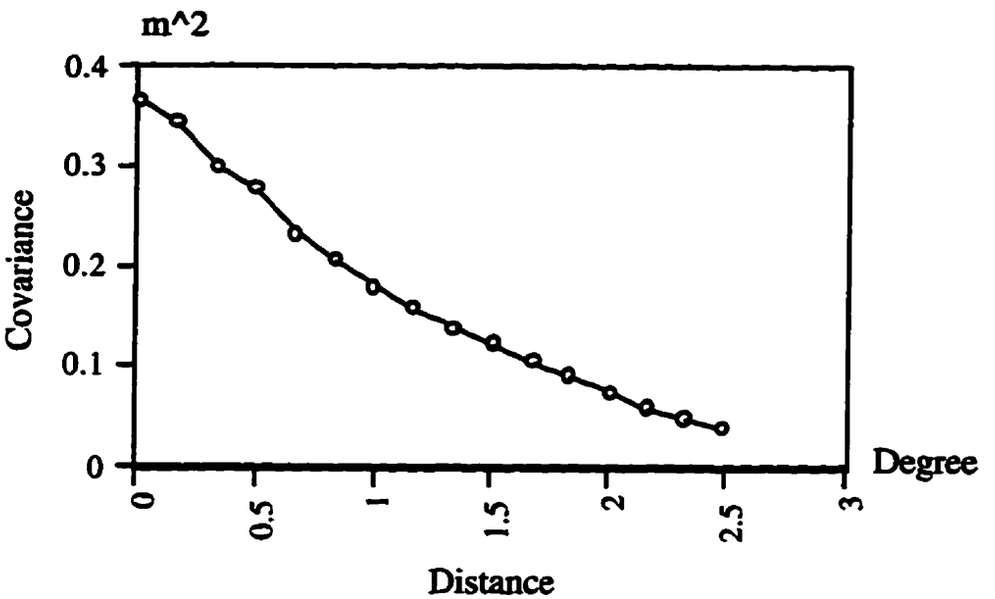

Fig. 4-8: Covariance function of geoid height in the Labrador Sea area

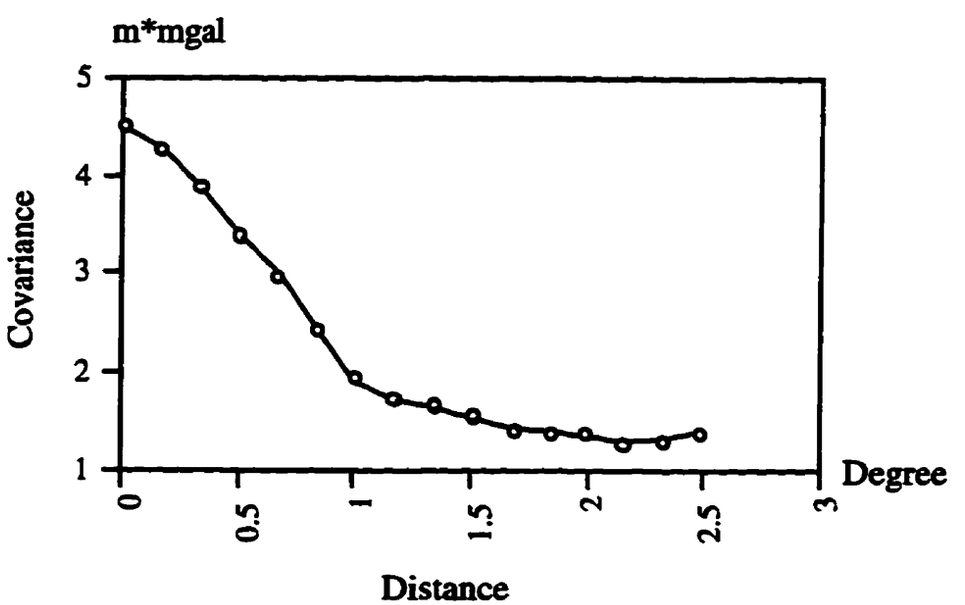

Fig. 4-9: Covariance function between geoid height and gravity anomaly in the Labrador Sea area

between different quantities, thus they may not be self-consistent. Figures 4-4 through 4-6 show the empirical and analytical covariance functions in the Central Mediterranean area. The empirical functions have been computed directly from the data. The analytical ones have been computed through the Tscherning/Rapp model described above.

Figures 4-8 through 4-9 show the covariance functions in the Labrador Sea area. These covariance functions have been computed from the corresponding PSD functions. No model fitting was carried out for these covariance functions.

4.3 Estimation of Signal Power Spectral Densities

This section briefly describes the PSD estimations. Like covariance estimations, there are basically two types of PSD estimation methods. One operates directly on the data set to yield a PSD estimate and is called the direct method. The other, Fourier-transforms the correlation or covariance function to obtain the PSD function and is called the indirect method.

4.3.1 Direct Method

The direct approach, also termed the periodogram method (Marple, 1987), yields the PSD estimate by taking the squared magnitude of the Fourier transform of the finite data set. This method can be formulated as

$$\hat{P}_{1,2}(m,n) = \frac{1}{T_x}\frac{1}{T_y}\{F_1^*(m,n)F_2(m,n)\} \qquad (4.24)$$

where $F_1(m,n)$ and $F_2(m,n)$ are discrete Fourier transform of $f_1(x,y)$ and $f_2(x,y)$, and * is the complex conjugate operator.

4.3.2 Indirect Method

An alternative method of the PSD estimation is first to make an estimation of the correlation (or covariance), and then perform a Fourier transform to obtain the PSD estimate. This method is also termed correlogram method. This method can be formulated as

$$\hat{P}_{1,2}(m,n) = F\{\hat{K}_{1,2}(k,l)\} \tag{4.25}$$

To control the effects of sidelobes in the spectral estimator, windows should be used. Thus, the most general form of the correlogaram method takes the form

$$\hat{P}_{1,2}(m,n) = F\{\hat{K}_{1,2}(k,l)w(k,l)\} \tag{4.26}$$

where w(k,l) is an appropriate window function (Marple, 1987; Sideris, 1984).

The two methods presented in this section have similar behavior and similar gross appearance, although some visual differences in the fine detail of the spectral shape will be apparent (Marple, 1987). Because they yield similar statistical characteristics, often the method selected is the one that may be computed most efficiently.

Both non-isotropic and isotropic signal PSDs will be used in the real data processing and the corresponding results will be compared. Figures 4-10 through 4-15 show the PSD functions used in the two test areas. The non-isotropical PSD functions are computed by the direct method and the isotropical ones are computed by the indirect method.

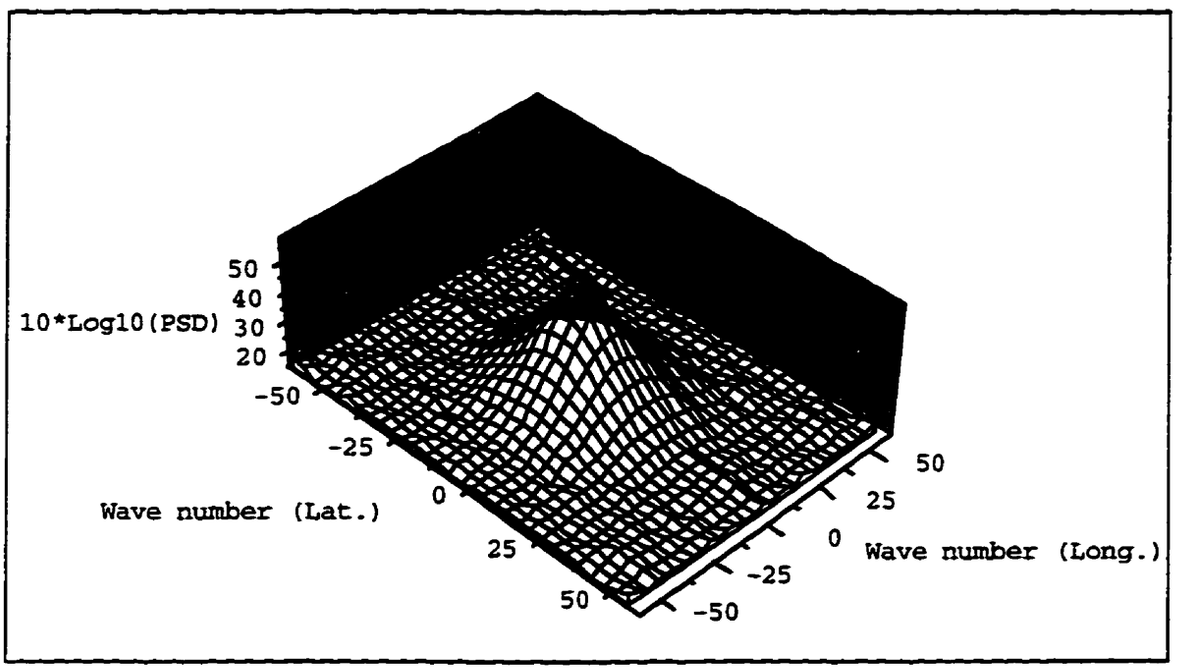

Fig. 4-10: Isotropic PSD function of geoid height for the Central Mediterranean area

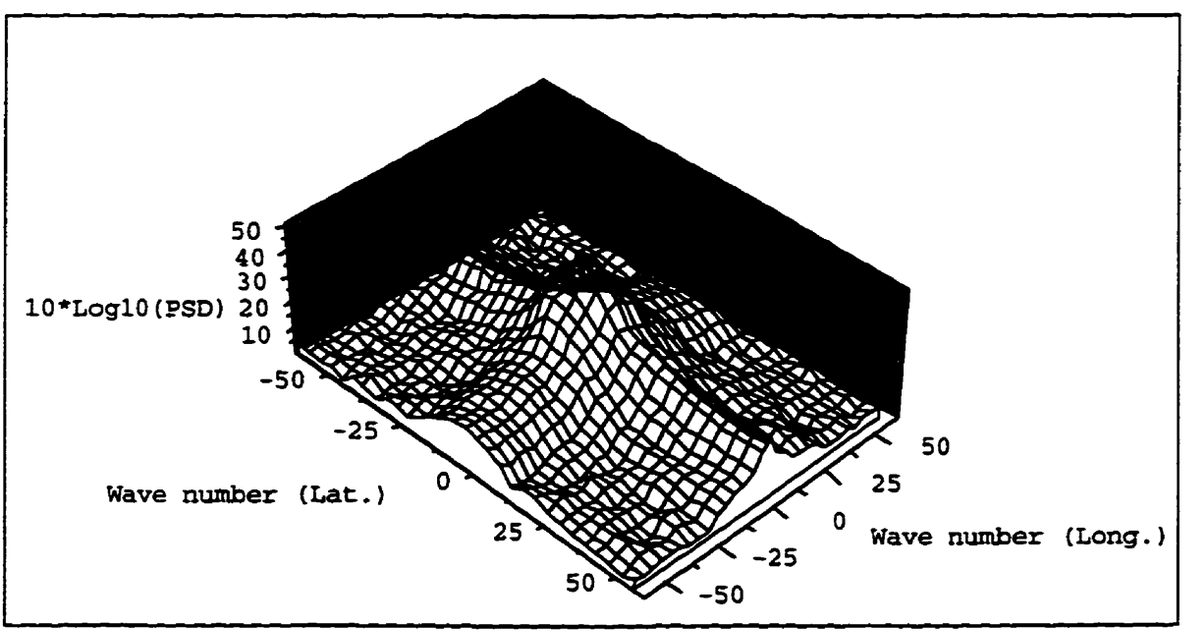

Fig. 4-11: Non-isotropic PSD function of geoid height for the Central Mediterranean area

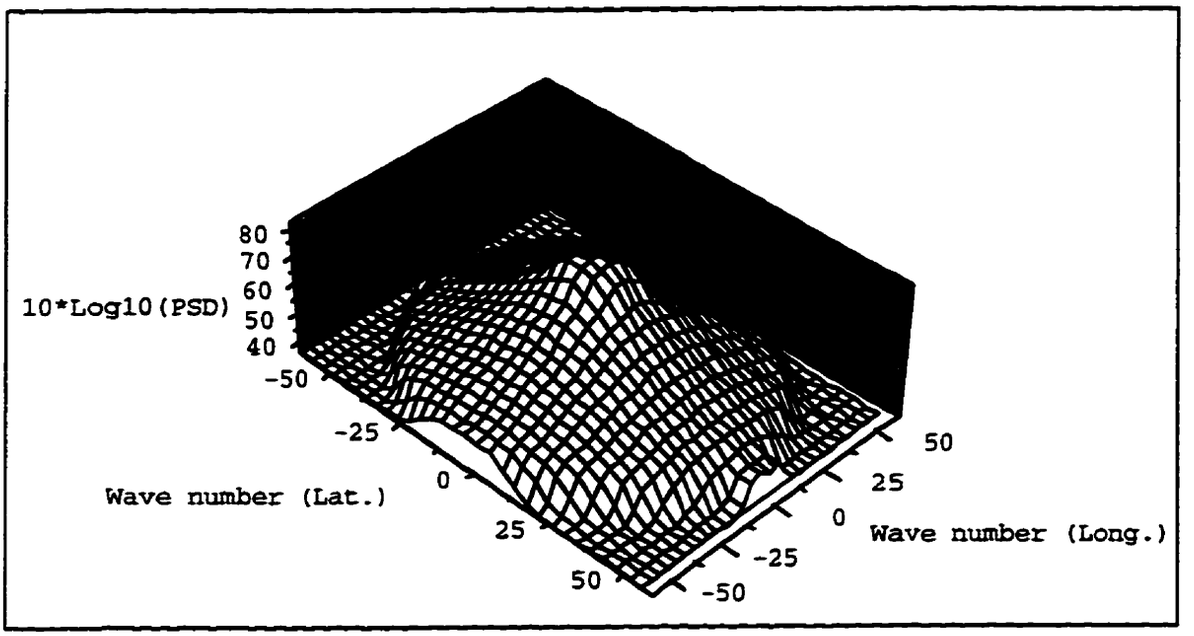

Fig. 4-12: Isotropic PSD function of gravity anomaly for the Central Mediterranean area

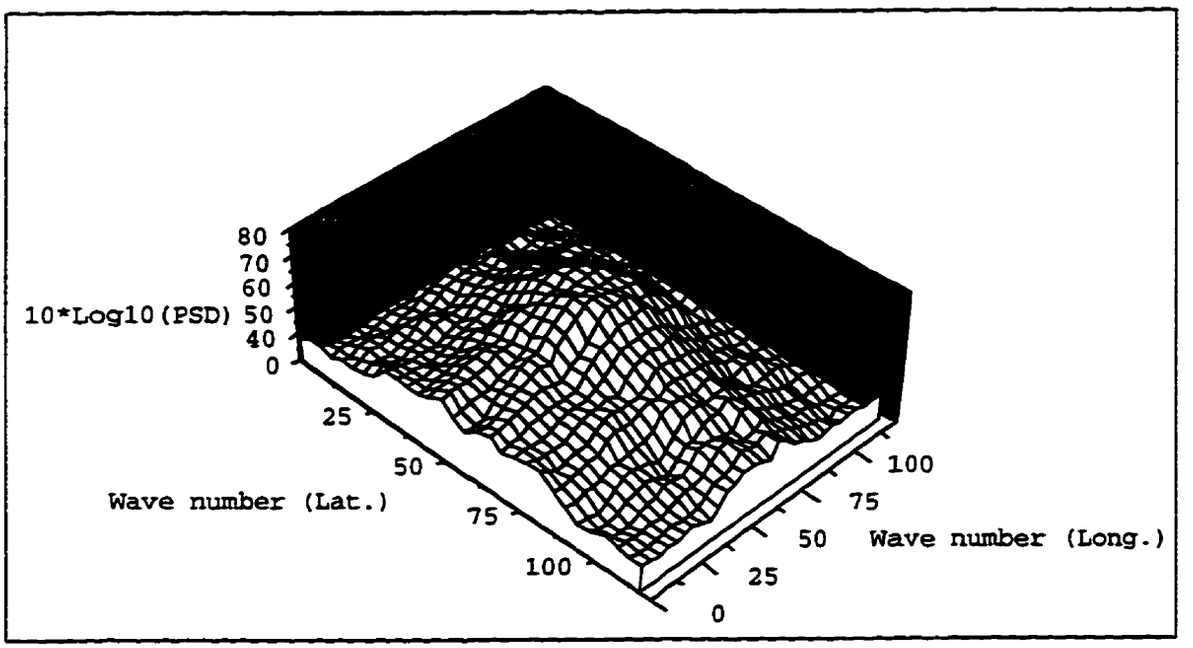

Fig. 4-13: Non-isotropic PSD function of gravity anomaly for the Central Mediterranean area

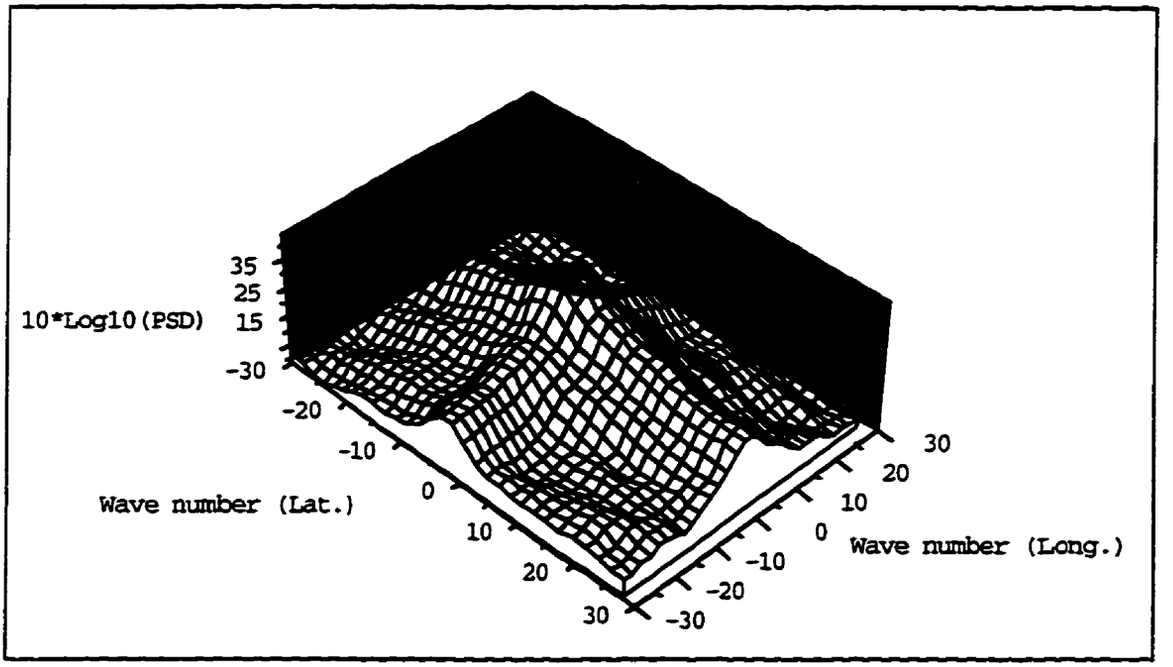

Fig. 4-14: Non-isotropic PSD function of geoid height for the Labrador Sea area

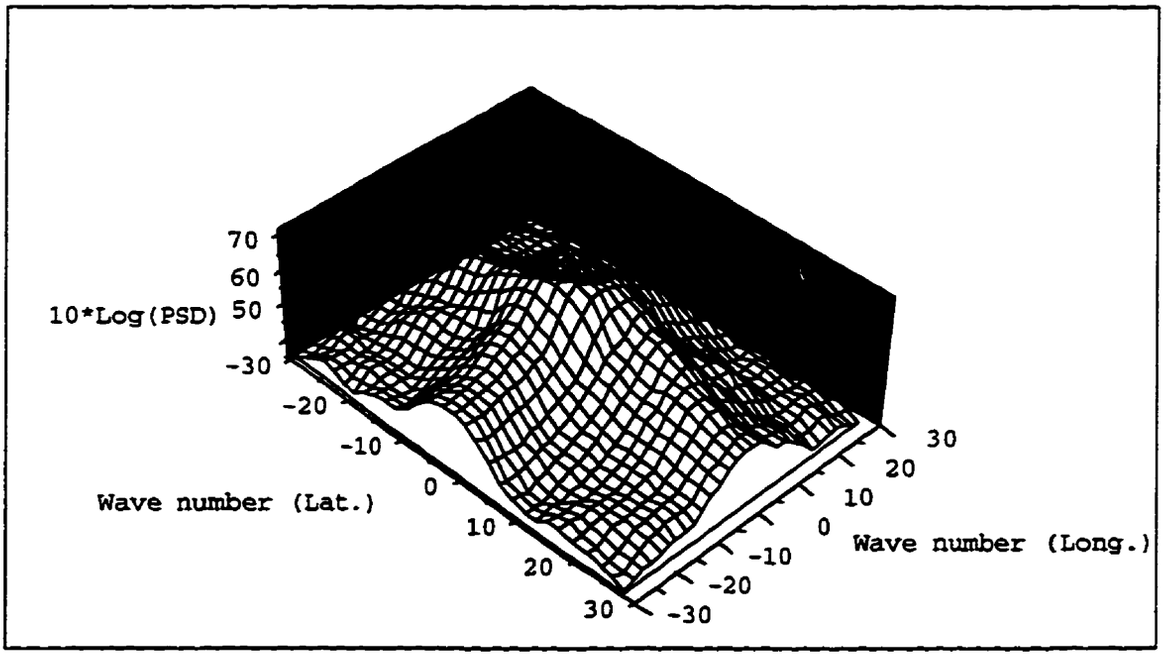

Fig. 4-15: Non-isotropic PSD function of gravity anomaly for the Labrador Sea area

4.4 Error Covariance and Error PSD

As stated in chapter two, in the application of LSC one needs to know the error covariances of geoid height and gravity anomaly observations, and in the use of IOST and LSAFD one needs to know the error PSDs of the observations. Usually observation errors are assumed to be white noise, and the variance of the white noise error can be approximately obtained from the observation accuracies. The corresponding error PSDs can be computed from the error covariances. For a white noise model with a given noise variance, the error covariance matrix is a constant diagonal matrix. The corresponding PSD function matrix is also a constant diagonal matrix.

When repeat observations like altimeter data are available, we can take advantage of the repeat observations to estimate the error PSDs following some more strict mathematical calculations, as discussed by Sailor (1994). Sailor presented one dimensional error PSD formulas for altimetry profile analysis. These one dimensional formulas can be easily extended to two dimensions.

If the observed sea surface height for two repeat tracks is $h_k(i,j)$ and $h_l(i,j)$ (corrupted by white noise) then the observation can be represented as

$$h_k(i,j) = N(i,j) + n_k(i,j) \tag{4.27}$$

$$h_l(i,j) = N(i,j) + n_l(i,j) \tag{4.28}$$

where $N(i,j)$ is the common geoid height signal which does not vary with time (or repeat tracks), $n_l(i,j)$ and $n_k(i,j)$ are independent realizations of the white noise process, which is assumed to be statistically independent of $N(i,j)$. If we subtract eqs. (4.28) from (4.27), we

get differential sea surface height observations of repeat track k and l

$$h_{diff}(i,j) = h_k(i,j) - h_l(i,j) = n_k(i,j) - n_l(i,j) \tag{4.29}$$

The noise PSD can be computed through the PSD of the differential sea surface as

$$\hat{P}_{n_k}(u,v) = \hat{P}_{n_l}(u,v) = \hat{P}_n(u,v) = \frac{1}{2}\hat{P}_{h_k - h_l}(u,v) \tag{4.30}$$

If $\bar{h}(i,j)$ is the value of M repeat ERMs, then

$$\bar{h}(i,j) = \frac{1}{M}\sum_{k=1}^{M} h_k(i,j) = N(i,j) + \frac{1}{M}\sum_{k=1}^{M} n_k(i,j) \tag{4.31}$$

Thus, the PSD of the mean value can be expressed as

$$\hat{P}_{\bar{h}}(u,v) = \hat{P}_N(u,v) + \frac{1}{M}\hat{P}_n(u,v) = \hat{P}_N(u,v) + \hat{P}_{\bar{n}}(u,v) \tag{4.32}$$

where $\hat{P}_N(u,v)$ and $P_{\bar{n}}(u,v)$ are the signal geoid height PSD and the noise PSD of the averaged observations, respectively.

For the altimetry sea surface height observations, these formulas can be used for error PSD estimation. As for gravity anomaly observations, we do not have repeat observations, but only data with error variances. An effective but non-rigorous way of estimating noise PSDs in practice is to approximate the noise PSDs by simple stationary models (Sideris, 1996).

In simulation studies, we used uniform distribution and Gaussian distribution noise models to generate two sets of noise-corrupted data to compare the effects of different noise character on

the results. We used white noise models in the real data processing, both for altimeter and shipborne data. We were unable to use the method discussed above in this section to compute directly the noise PSDs of the altimeter, because no original repeated track data were used since gridded data were already available in the test area.

CHAPTER FIVE
SIMULATION STUDIES

This chapter describes the simulation studies and presents their results. The LSC, IOST and LSAFD methods are intercompared using simulated observations. The purpose of the simulation study is to investigate the estimates obtained using each of the three methods with data with different noises. Simulation computations also allow us to compare the internal and external accuracies of the estimates.

5.1 Generation of Simulation Observations

For simulation studies, we first computed a set of gridded geoid heights using the coefficients of degree 37 to 360 of the OSU91A model. The corresponding spectra of these simulated sets of geoid heights were obtained using the 2D FFT method. The gravity anomalies on the same grids were computed by employing the geoid spectra so that the simulated geoid heights and gravity anomalies be self-consistent. To simulate noisy observations, uniform distributed and Gaussian noises were generated and added to the calculated geoid height and gravity anomaly signals, respectively, to simulate observations. Using these simulated observations, the three techniques discussed above were employed to determine the gravity field quantities.

For our simulation study, geoid height signals on 66 x 66 points in an area of 11° x 11° with grid spacings of 10' x 10' were generated. Gravity anomalies were also generated on the same grid as the geoid heights. For each of the two types of noises, noise levels with

variances of 0.01 m^2, 0.25 m^2 and 1.0 m^2 were assumed for geoid height, and noise levels with variances of 9 $mgal^2$, 36 $mgal^2$ and 100 $mgal^2$ were assumed for gravity anomalies. The

corresponding noise covariance and the noise PSD functions are diagonal matrices of constant elements, respectively. Thus we generated three sets of observations for geoid height and gravity anomaly, for each type of noise assumption. Using different estimation techniques on these simulated data, it enabled us to: a) numerically intercompare the results obtained by different methods; b) investigate the responses of each methods to the input noise level; c) compare the response of the estimates to different types of input noises; d) compare internal and external estimation errors.

Table 5.1 gives the statistics of the simulated field. Figures 5-1 through 5-3 give 3D graphs of simulated geoid heights and gravity anomalies, input uniform distribution noises added to the geoid heights and gravity anomalies, and the corresponding simulated noisy observations, respectively. Figures 5-4 and 5-5 give 3D graphs of Gaussian distribution input noises added to the geoid heights and gravity anomalies, and the corresponding simulated noisy observations, respectively.

Table 5.1 Statistics of the simulated field

	Max.	Min.	Mean	S.D.
Geoid (m)	3.44	-2.44	0.00	1.09
Gravity (mgal)	68.66	-48.21	0.00	16.42

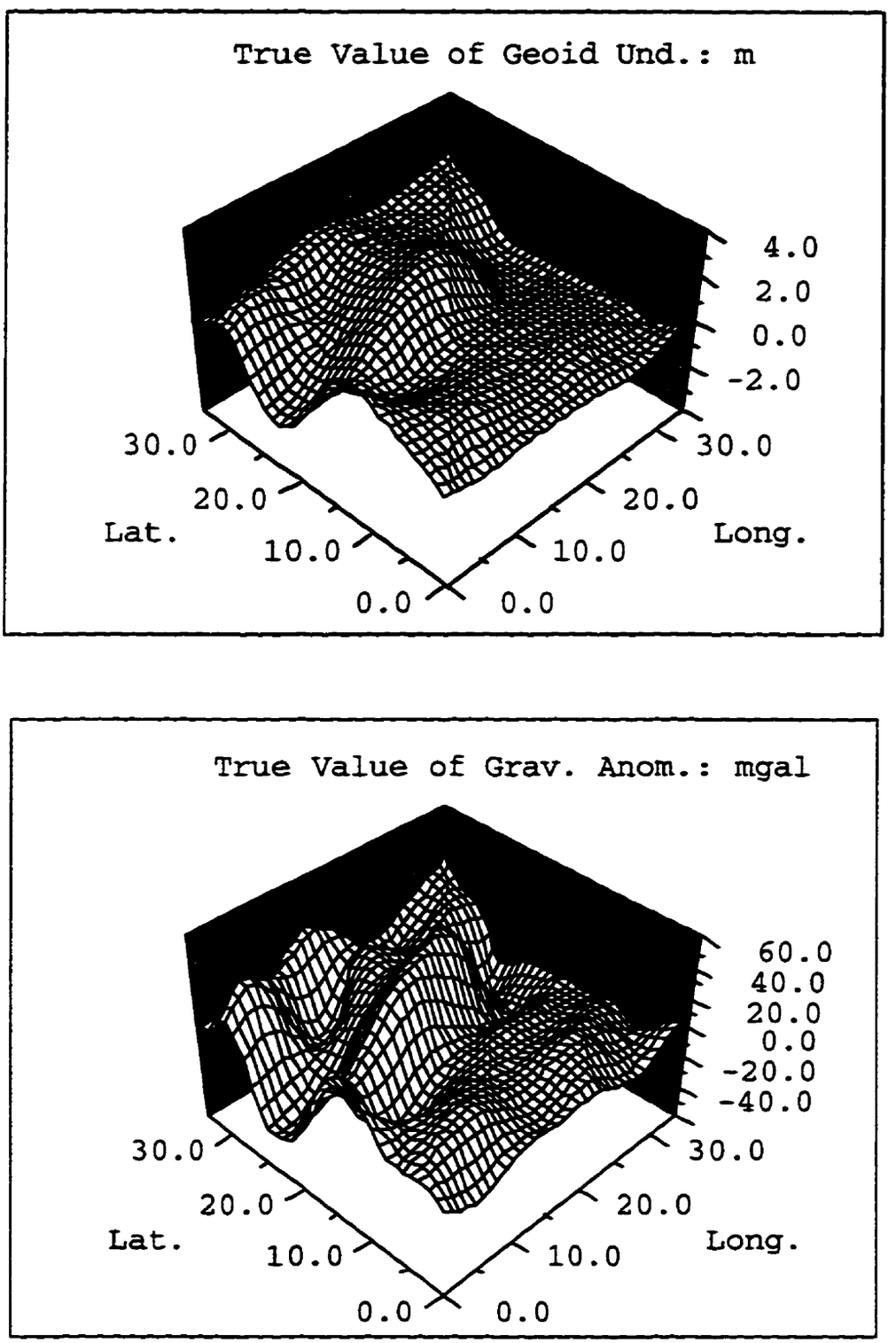

Fig. 5-1: Simulated rue values of geoid heights and gravity anomalies

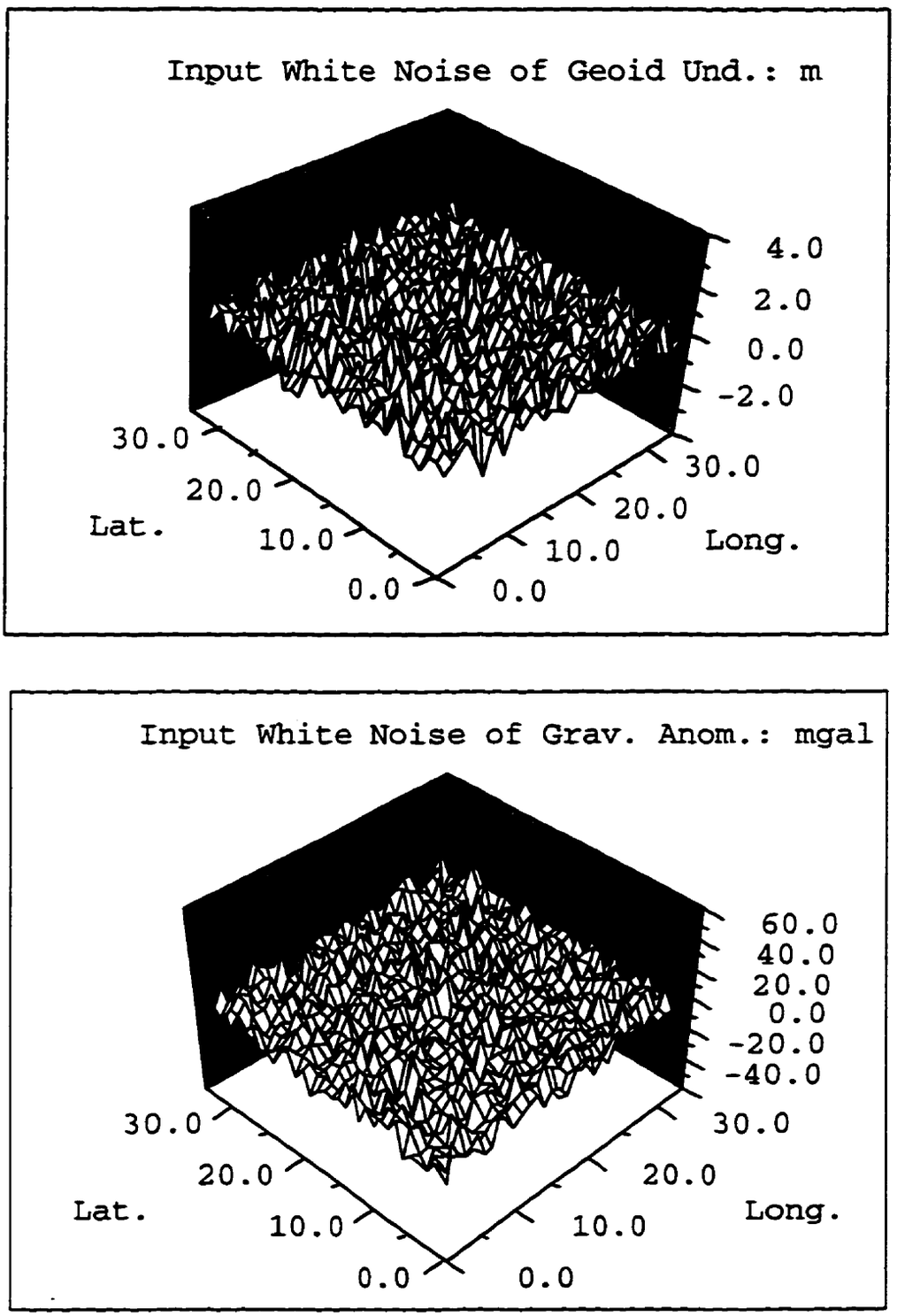

Fig. 5-2: Uniform disttributed input noises for geoid undulation and gravity anomaly, respectively

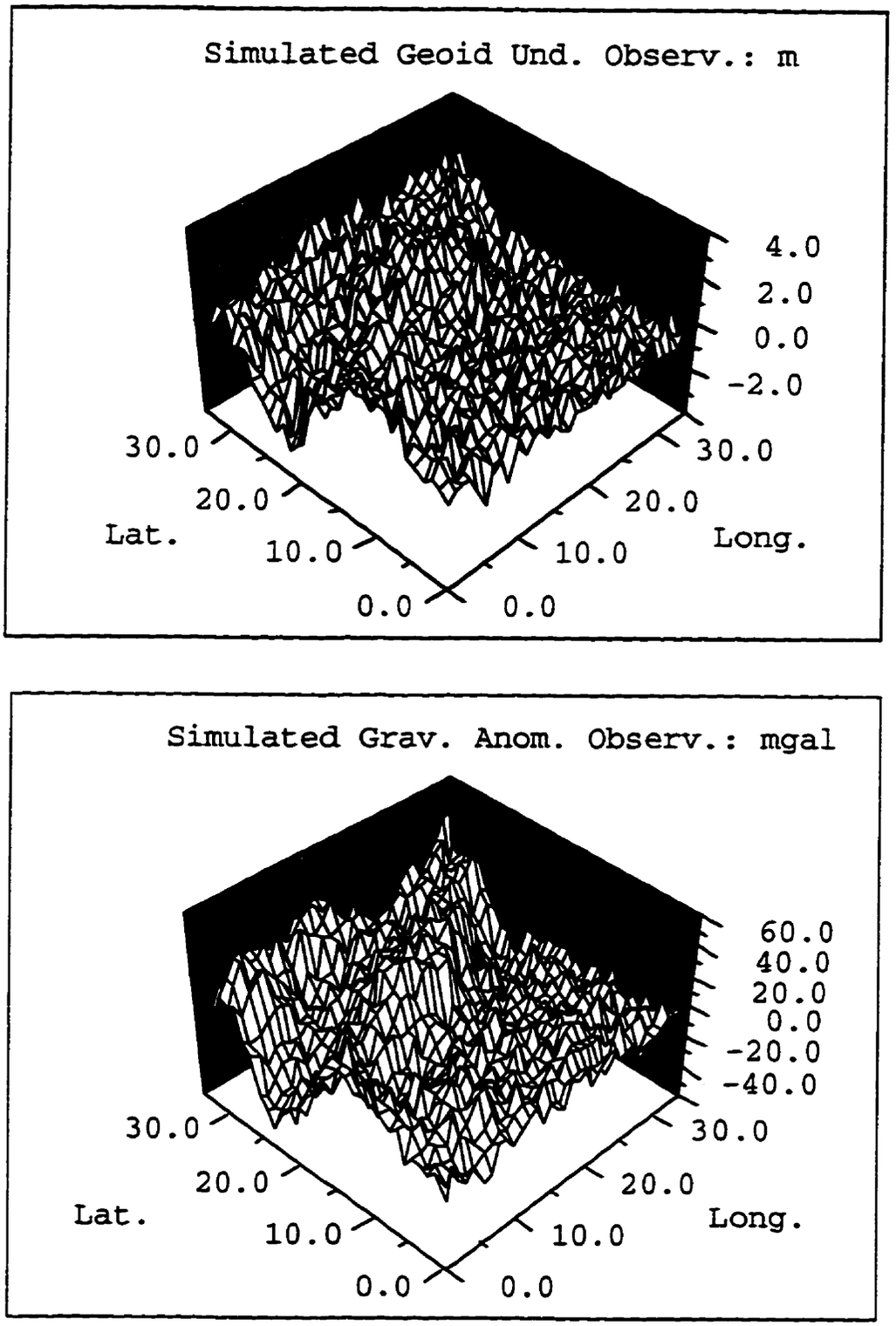

Fig. 5-3: Simulated geoid height and gravity anomaly observations

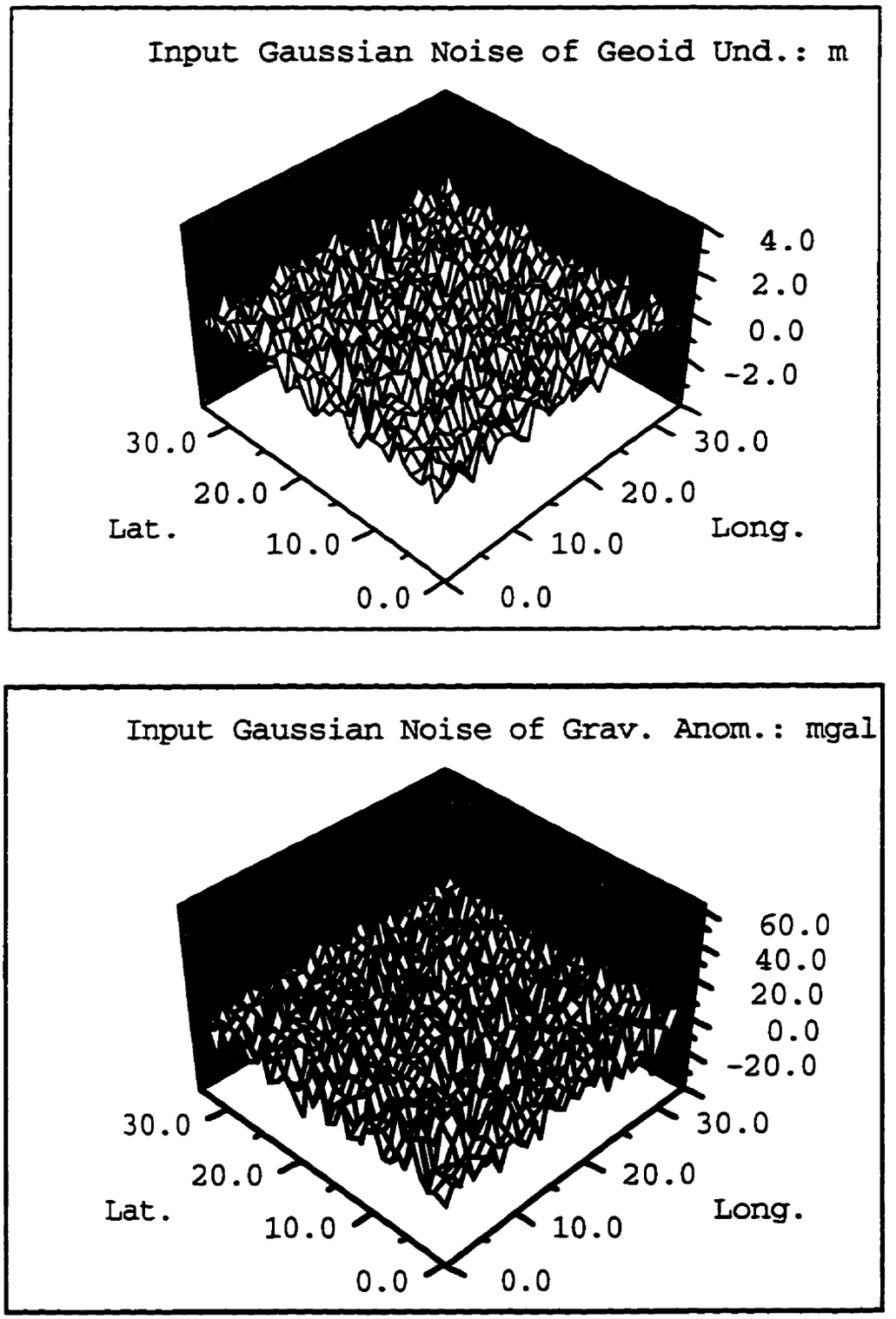

Fig. 5-4: Gaussian distributed input noises for geoid undulation and gravity anomaly, respectively

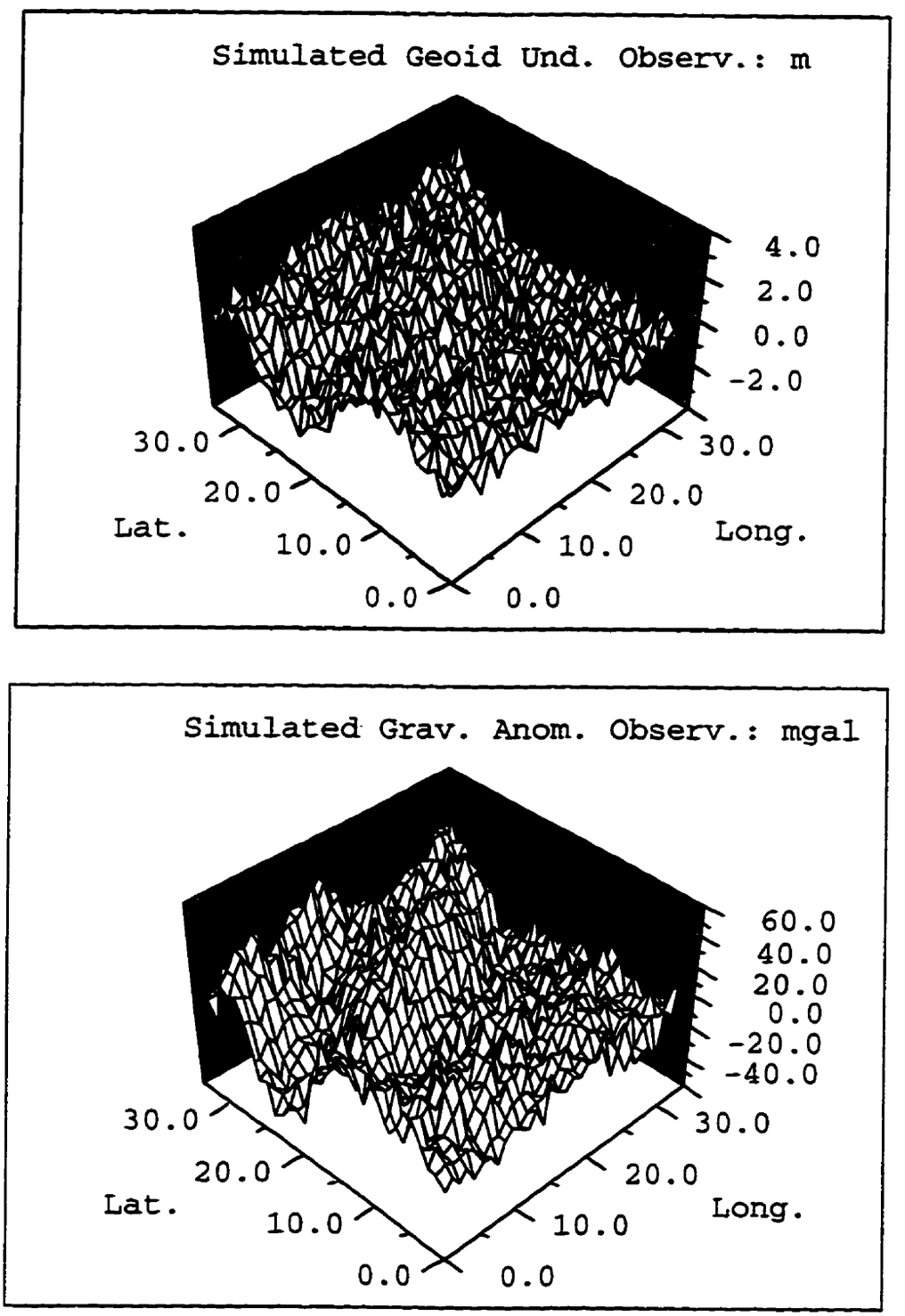

Fig. 5-5: Simulated geoid height and gravity anomaly observations with Gaussian distributted noises

5.2 Results From Simulated Observations Corrupted by Uniform Distributed Noise

Gridded geoid heights and gravity anomalies on 66 x 66 points were predicted employing the techniques of LSAFD, LSC and IOST with these simulated data. To avoid edge effects, the predicted results were compared with the simulated true values only in the inner 34 x 34 points.

Tables 5.2 and 5.3 give the statistics of standard deviations (S.D.), RMS errors, minimum errors and maximum errors of predicted geoid heights and gravity anomalies using LSC, IOST and LSAFD under different input white noise levels. These statistics are based on external prediction errors of the estimates, which are obtained by taking differences between estimates and true values. For easier visualization purposes, the RMS errors are also plotted in Figures 5-6 and 5-7. In Figure 5-6, the vertical axis represents geoid RMS errors and the horizontal one represents input anomaly RMS noise. In Figure 5-7, the vertical axis represents gravity anomaly RMS errors and the horizontal one represents input geoid RMS noise. We did not plot the S.D. results because these values are very close to the corresponding RMS errors, as shown in Tables 5.2 and 5.3. This similarity implies that there is no bias in the predicted geoid heights and gravity anomalies for all the cases. We observe from Tables 5.2 and 5.3 that all three methods have performed smoothing of geoid height and gravity anomaly observations. This observation can be seen more easily in Figures 5-6 and 5-7.

Plotted in Figures 5-8 through 5-13 are 3D graphs of geoid height and gravity anomaly prediction errors (predicted values minus true values) for different methods. The corresponding input data are those plotted in Figures 5-1 through 5-3. These figures enable

Table 5.2: Statistics of Geoid Height External Estimation Error for Different Input Noise Levels (Input Noises Are Assumed of Uniform Distribution)

RMS of Input Noise		External Prediction Error (m)											
Δg (mgal)	N (m)	LSC				IOST				LSAFD			
		S.D.	RMS	Min	Max	S.D.	RMS	Min	Max	S.D.	RMS	Min	Max
3.0	0.1	0.02	0.02	-0.08	0.09	0.02	0.02	-0.04	0.05	0.02	0.02	-0.06	0.06
6.0	0.1	0.02	0.03	-0.07	0.09	0.02	0.03	-0.08	0.07	0.03	0.04	-0.19	0.13
10.0	0.1	0.02	0.03	-0.07	0.09	0.02	0.03	-0.08	0.07	0.05	0.05	-0.19	0.13
3.0	0.5	0.05	0.05	-0.13	0.17	0.03	0.02	-0.08	0.09	0.03	0.03	-0.09	0.09
6.0	0.5	0.05	0.05	-0.15	0.16	0.04	0.02	-0.17	0.14	0.06	0.06	-0.17	0.19
10.0	0.5	0.05	0.06	-0.14	0.18	0.05	0.03	-0.14	0.19	0.06	0.08	-0.27	0.22
3.0	1.0	0.05	0.05	-0.20	0.27	0.03	0.03	-0.10	0.08	0.02	0.04	-0.12	0.09
6.0	1.0	0.07	0.07	-0.20	0.27	0.05	0.06	-0.19	0.13	0.04	0.06	-0.24	0.16
10.0	1.0	0.07	0.08	-0.21	0.27	0.06	0.06	-0.16	0.19	0.07	0.08	-0.27	0.27

Table 5.3: Statistics of Gravity Anomaly External Estimation Error for Different Input Noise Levels (Input Noises Are Assumed of Uniform Distribution)

RMS of Input Noise		External Prediction Error (mgal)											
Δg (mgal)	N (m)	LSC				IOST				LSAFD			
		S.D.	RMS	Min	Max	S.D.	RMS	Min	Max	S.D.	RMS	Min	Max
3.0	0.1	1.6	1.6	-4.9	4.4	1.1	1.2	-3.4	3.7	2.9	2.9	-8.9	10.8
3.0	0.5	1.6	1.7	-5.2	5.3	1.2	1.3	-3.9	5.1	2.9	2.9	-8.5	10.2
3.0	1.0	1.6	1.7	-5.4	5.2	1.3	1.3	-4.2	5.0	3.0	3.0	-8.8	10.2
6.0	0.1	1.9	2.1	-7.3	6.5	1.7	1.7	-5.6	5.1	5.4	5.6	-19.0	16.3
6.0	0.5	2.3	2.4	-7.6	6.4	2.1	2.2	-7.4	7.0	5.8	5.9	-17.3	21.8
6.0	1.0	2.4	2.4	-7.9	7.0	2.2	2.2	-7.7	6.6	5.9	5.9	-19.0	20.8
10.0	0.1	2.4	2.5	-9.2	6.0	1.7	1.8	-5.6	6.0	7.9	8.1	-31.2	24.3
10.0	0.5	2.4	2.6	-7.2	8.6	2.4	2.5	-7.0	8.3	9.0	9.1	-32.0	28.1
10.0	1.0	2.5	2.6	-6.9	8.9	2.5	2.6	-7.5	9.0	9.4	9.5	-34.6	32.0

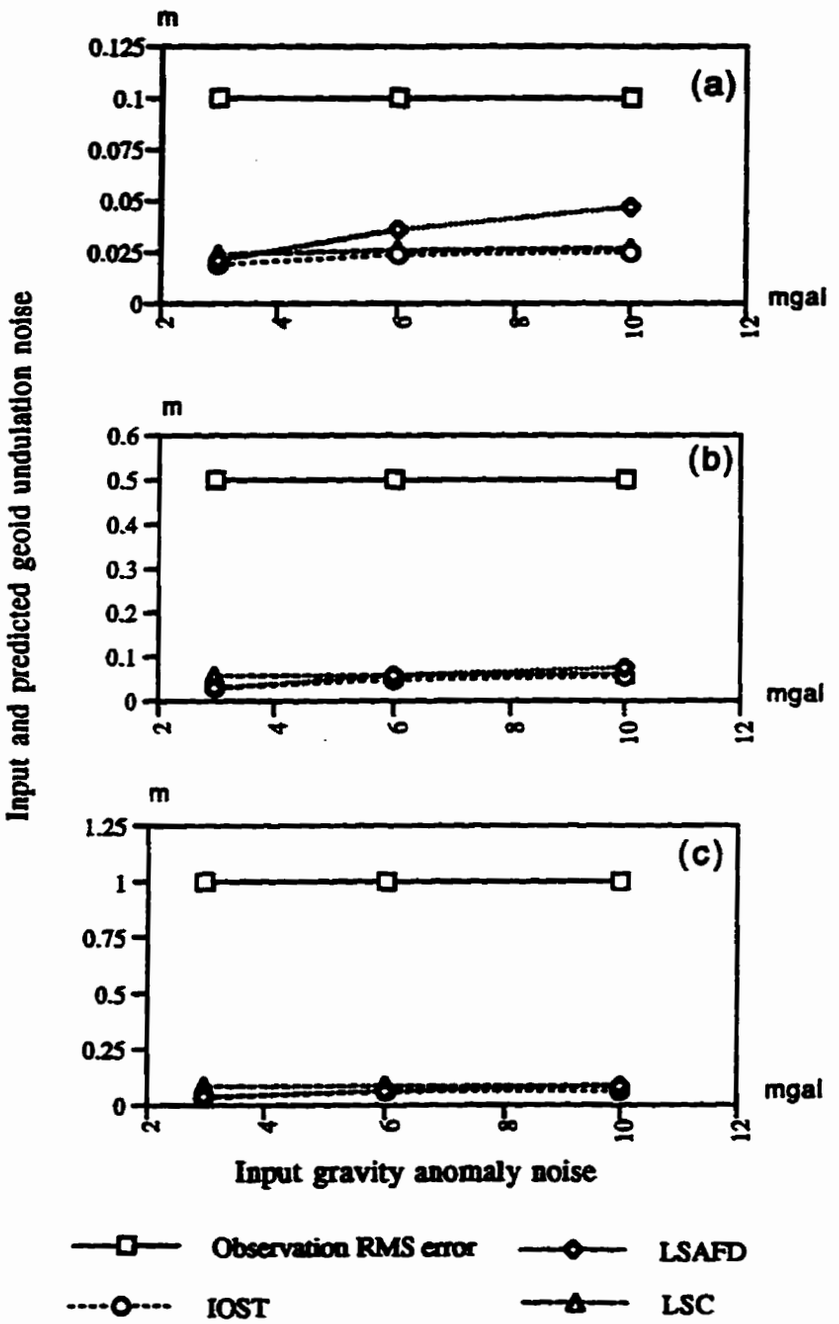

Fig. 5-6: Comparison of RMS errors of predicted geoid heights using different methods and different values of input undulation noise and input gravity noise

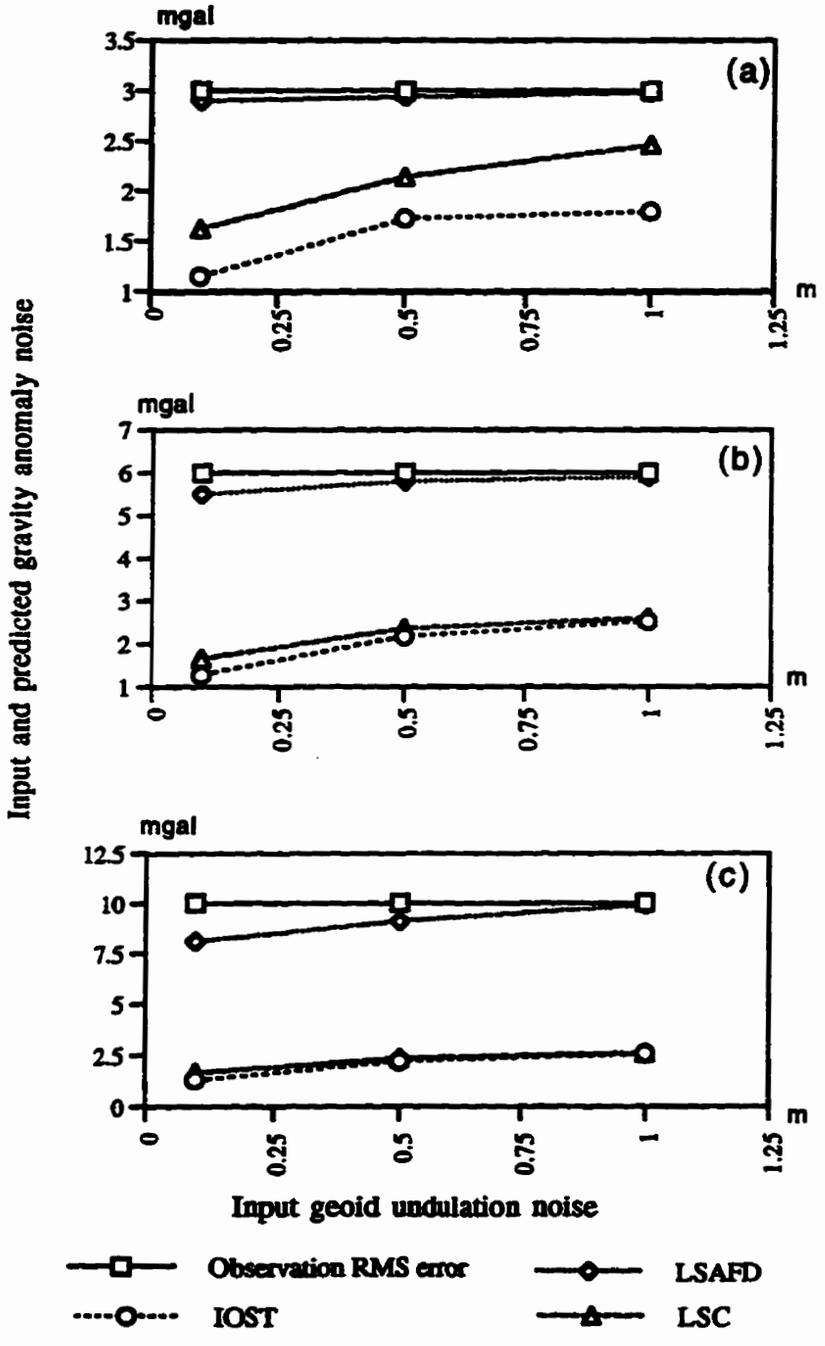

Fig. 5-7: Comparison of RMS errors of predicted gravity anomalies using different methods and different values of input undulation noise and input gravity noise

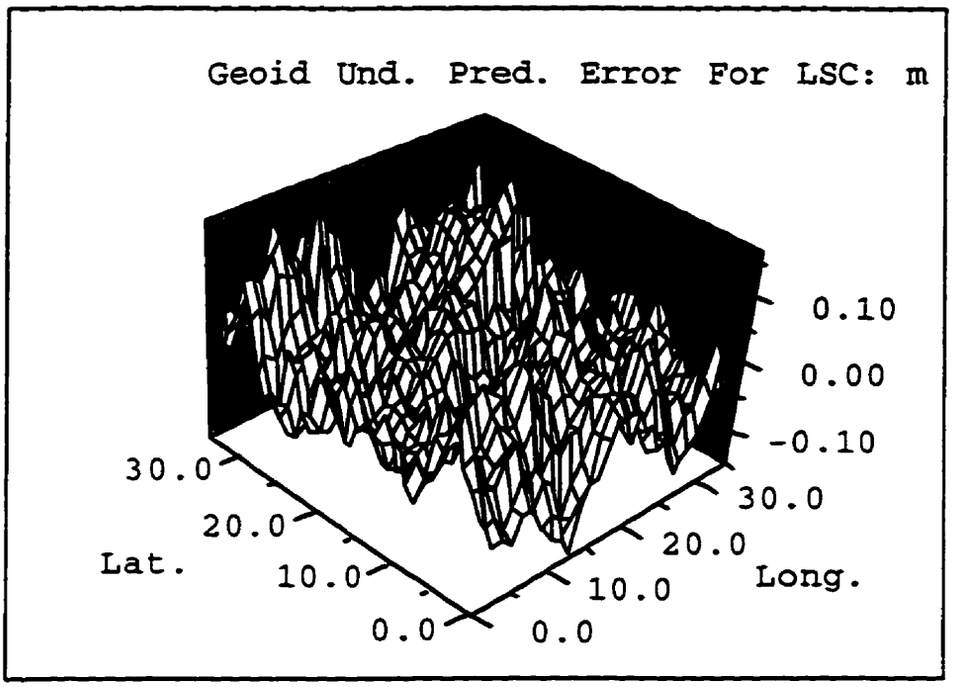

Fig. 5-8: External geoid height prediction errors for LSC (input data are those plotted in the Figures 5-1 through 5-3)

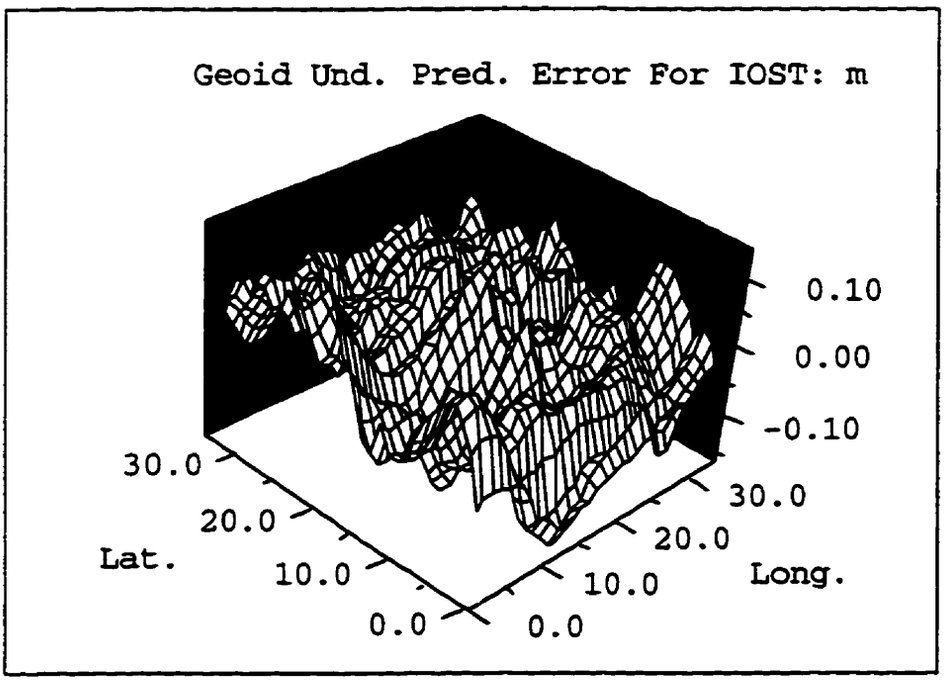

Fig. 5-9: External geoid height prediction errors for IOST (input data are those plotted in the Figures 5-1 through 5-3)

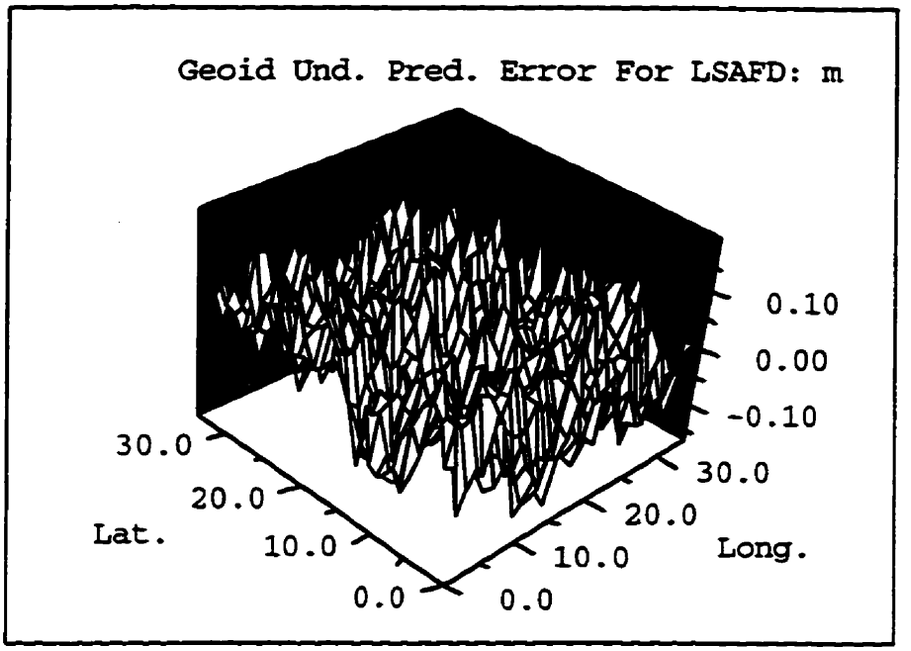

Fig. 5-10: External geoid height prediction errors for LSAFD (input data are those plotted in the Figures 5-1 through 5-3)

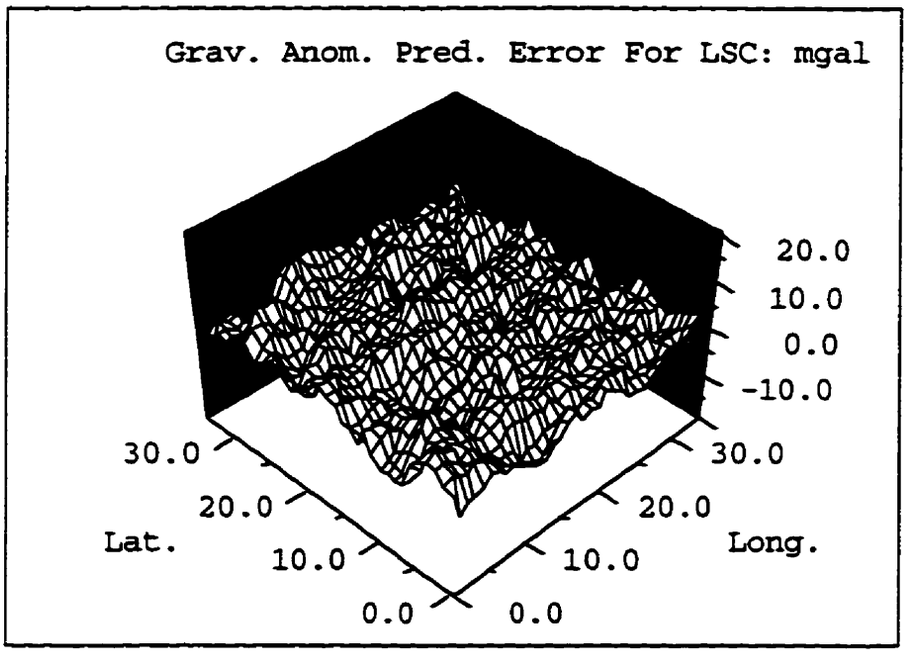

Fig. 5-11: External gravity anomaly prediction errors for LSC (input data are those plotted in the Figures 5-1 through 5-3)

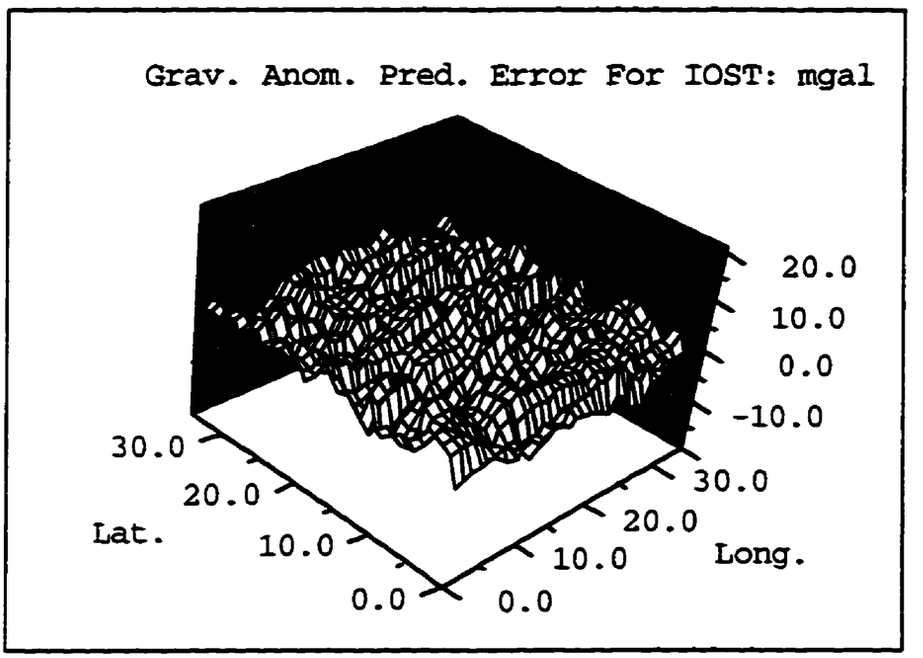

Fig. 5-12: External gravity anomaly prediction errors for IOST (input data are those plotted in the Figures 5-1 through 5-3)

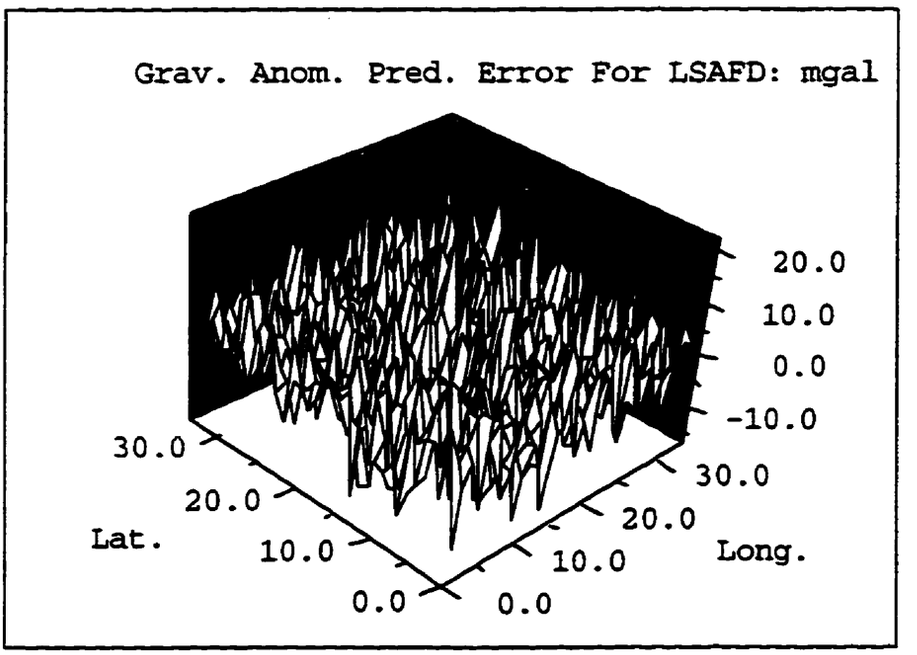

Fig. 5-13: External gravity anomaly prediction errors for LSAFD (input data are those plotted in the Figures 5-1 through 5-3)

us to see in detail the behavior of the prediction errors.

By observing Figures 5-6 and 5-7, we see that gravity anomaly estimates obtained using the LSAFD method show only a weak improvement over the observations, while geoid height estimates show a significant improvement over the observations. This is simply because the noise level of gravity anomaly observations is much lower than that of geoid height observations in our simulated data. This also would imply that if noise levels between geoid undulation and gravity anomaly do not match each other, the accuracies of the estimation obtained for the data type with higher input noise level, after combination with the data type of lower input noise by using the LSAFD method, can have significant improvement over its observation. The combination using the LSAFD will not give much improved estimation to the data type with lower input noise level.

Comparing the external RMS errors of the estimates associated with different input noise levels, we observe that with the significant increase of the noise level of input data, the RMS errors of the geoid height and gravity anomaly estimates obtained using LSC and IOST methods increased only slightly. That is, the LSC and IOST methods are not very sensitive to input noise levels. Yet, the LSAFD method is more sensitive to noise levels. Therefore, we may conclude that the LSC and IOST methods are preferable to the LSAFD method in the sense that they better suppress input errors.

When we compare the results obtained using the IOST and the LSC, we see from Figures 5-6 and 5-7 that in all cases with different input noise levels, the IOST method always produces a little better results (less RMS error) than the LSC technique. This is understandable because the IOST employs detailed signal PSD information (non-isotropic PSD functions), while the LSC uses only approximate signal PSD information by having the covariance function

isotropicaly structured (see Sections 4.2 and 4.3). This observation leads to the conclusion that the IOST method slightly outperforms the LSC technique as far as accuracy is concerned. In addition, the IOST method is based on spectral techniques, thus, its use has the well-known advantage of saving computer time over the conventional LSC technique. Our experiments show that the LSC method takes about 2 days for the computation of the gravity anomaly and geoid height on 66 x 66 points. The IOST and LSAFD methods take only several minutes to complete the same task.

If we observe the behavior of the external RMS prediction errors vs. input noise levels in Tables 5.2 and 5.3, we see that the ratios of prediction error to input noise for the IOST method are 40% ~ 43%, 28% ~ 37% and 17% ~ 25% for gravity anomaly and 20% ~30%, 6% ~ 10% and 3% ~ 6% for geoid undulation. We conclude from these ratios that the input noise of the gravity anomaly and geoid undulation are significantly suppressed by the optimal combination (IOST) of two types of data. This optimal combination is especially useful for suppressing high-level input noise. For example, when the RMS value of the input noise of the geoid undulation was 0.1 m, we obtained estimation of geoid height with noise level suppressed by 70% to 80%. But when the RMS value of the input noise of the geoid undulation was 1.0 m (which is considered to be a considerably high noise level for altimetry-derived geoid undulation), the noise level of the estimation of the geoid undulation obtained by IOST method was suppressed by 94% to 97% as compared to its input noise level. This behavior is particularly interesting when the high noise level altimetry data from the earlier missions are to be combined with the new lower noise data.

Internal and external accuracies are two important indices for evaluation of the reliability of the estimation results. In practice, only internal prediction error will be available. The internal estimation errors for the LSC can be computed using eqs. (3.38) and (3.39). The internal

estimation errors for IOST and LSAFD can be obtained by first computing the error PSDs using equations (3.26) and (3.45), respectively, and then transforming the error PSDs to covariances using FFT. Tables 5.4 and 5.5 present some test comparisons between internal and external prediction errors for the case of uniform-distributed input noises.

Table 5.4: Comparison of External and Internal RMS Error for Geoid Height Estimation (Input Noises Are Assumed of Uniform Distribution)

RMS of Input Noise		Prediction Error (m)					
Δg (mgal)	N (m)	LSC		IOST		LSAFD	
		Ext..	Int.	Ext.	Int.	Ext.	Int.
3.0	0.1	0.02	0.02	0.02	0.01	0.02	0.03
6.0	0.1	0.03	0.02	0.03	0.02	0.04	0.04
10.0	0.1	0.03	0.03	0.03	0.03	0.05	0.05
3.0	0.5	0.05	0.05	0.02	0.03	0.03	0.03
6.0	0.5	0.05	0.06	0.02	0.04	0.06	0.06
10.0	0.5	0.06	0.05	0.03	0.05	0.08	0.07
3.0	1.0	0.05	0.07	0.03	0.03	0.04	0.04
6.0	1.0	0.07	0.07	0.06	0.05	0.06	0.06
10.0	1.0	0.08	0.08	0.06	0.07	0.08	0.09

Table 5.5: Comparison of External and Internal RMS Error for Gravity Anomaly Estimation (Input Noises Are Assumed of Uniform Distribution)

RMS of Input Noise		Prediction Error (mgal)					
Δg (mgal)	N (m)	LSC		IOST		LSAFD	
		Ext..	Int.	Ext.	Int.	Ext.	Int.
3.0	0.1	1.6	2.0	1.2	1.3	2.9	2.8
6.0	0.1	2.1	2.2	1.7	2.0	5.6	5.2
10.0	0.1	2.5	2.1	1.8	2.1	8.1	8.1
3.0	0.5	1.7	2.1	1.3	1.4	2.9	3.0
6.0	0.5	2.4	2.7	2.2	2.1	5.9	5.9
10.0	0.5	2.6	2.4	2.5	2.3	9.1	9.7
3.0	1.0	1.7	1.9	1.3	1.6	3.0	3.0
6.0	1.0	2.4	2.5	2.2	2.2	5.9	6.0
10.0	1.0	2.6	2.9	2.6	2.8	9.5	9.8

From Tables 5-4 and 5-5 we see that in many cases both the internal and external errors are the same, though there are cases where internal and external errors differ a little. This observation along with the fact that in Figures 5-8 through 5-13, no bias and systematic errors existed in the estimate, would imply that in the real world applications where the true values are not known, and thus the external estimation error can not be computed, the internal accuracy can give a reliable picture of the estimation errors.

5.3 Results From Simulated Observations Corrupted by Gaussian Distributed Noise

To investigate the effects of different noise characteristics on the prediction errors, Gaussian noise with the same noise levels as the uniform distributed noises used previously are also used to generate the simulated observations for both geoid and gravity anomaly at the same grids. Simulated data with Gaussian distribution input noises are shown in Figures 5-4 and 5-5.

Using the Gaussian noise corrupted data, geoid heights and gravity anomalies were estimated using the three methods. Tables 5.6 and 5.7 show the statistics of the external errors of the estimates. Figures 5-14 through 5-19 show the detailed prediction errors for geoid height and gravity anomaly, respectively. Tables 5.8 and 5.9 present some test comparisons between internal and external prediction errors.

From Tables 5-8 and 5-9 we see that in many cases both the internal and external errors are the same, though there are cases where internal and external errors differ a little. These facts have already been observed in Section 5.2 where uniform distribution data noise were used. Thus, we may conclude that in real data processing where input noise can be modeled by

white noise models (this is almost always true for geodetic data) the internal accuracy can give a reliable picture of the estimation errors.

By comparing the results obtained for the uniform distribution noise corrupted data with those obtained for the Gaussian noise corrupted data, we see that the external prediction errors are almost the same when the input noise levels are the same in both cases. There are only little differences for the internal prediction errors in both cases.

Similar observations as in Section 5.2 can be seen from the results for the Gaussian noise data. Because the similarities between the results obtained for both uniform distribution noise and Gaussian noise corrupted data, we will not discuss in more detail the results obtained from the Gaussian noise corrupted data. Similar conclusions can be drawn here as in the previous section.

Table 5.6: Statistics of Geoid Height External Estimation Error for Different Input Noise Levels (Input Noises Are Assumed of Gaussian Distribution)

RMS of Input Noise		External Prediction Error (m)											
Δg (mgal)	N (m)	LSC				IOST				LSAFD			
		S.D.	RMS	Min	Max	S.D.	RMS	Min	Max	S.D.	RMS	Min	Max
3.0	0.1	0.01	0.02	-0.10	0.09	0.01	0.01	-0.04	0.05	0.02	0.02	-0.06	0.07
6.0	0.1	0.01	0.02	-0.09	0.09	0.02	0.02	-0.07	0.08	0.04	0.04	-0.11	0.12
10.0	0.1	0.02	0.03	-0.08	0.10	0.03	0.02	-0.06	0.07	0.05	0.05	-0.14	0.16
3.0	0.5	0.05	0.05	-0.15	0.13	0.02	0.03	-0.08	0.12	0.03	0.04	-0.11	0.12
6.0	0.5	0.05	0.06	-0.14	0.13	0.04	0.04	-0.09	0.13	0.05	0.05	-0.17	0.16
10.0	0.5	0.05	0.06	-0.14	0.13	0.05	0.05	-0.14	0.17	0.08	0.08	-0.22	0.25
3.0	1.0	0.08	0.08	-0.20	0.25	0.03	0.03	-0.08	0.07	0.03	0.03	-0.10	0.07
6.0	1.0	0.09	0.08	-0.20	0.26	0.04	0.05	-0.13	0.09	0.06	0.06	-0.21	0.14
10.0	1.0	0.09	0.08	-0.20	0.25	0.06	0.06	-0.17	0.15	0.09	0.09	-0.27	0.27

Table 5.7: Statistics of Gravity Anomaly External Estimation Error for Different Input Noise Levels (Input Noises Are Assumed of Gaussian Distribution)

RMS of Input Noise		External Prediction Error (m)											
Δg (mgal)	N (m)	LSC				IOST				LSAFD			
		S.D.	RMS	Min	Max	S.D.	RMS	Min	Max	S.D.	RMS	Min	Max
3.0	0.1	1.6	2.0	-5.8	5.2	1.1	1.3	-3.2	3.8	2.8	2.8	-9.2	10.5
3.0	0.5	1.7	2.1	-6.4	5.0	1.4	1.4	-4.4	4.2	3.0	3.1	-11.5	9.5
3.0	1.0	1.6	2.1	-6.3	4.8	1.4	1.3	4.2	3.7	3.0	3.0	-10.6	9.4
6.0	0.1	2.1	2.7	-6.5	5.8	1.5	1.7	-4.7	5.0	5.2	5.4	-15.3	18.6
6.0	0.5	2.3	2.9	-7.9	8.2	1.9	2.1	-6.0	6.6	5.9	6.1	-19.5	19.3
6.0	1.0	2.3	3.0	-8.3	8.0	2.0	2.2	-6.2	5.7	6.0	6.1	-20.0	18.9
10.0	0.1	2.8	3.3	-8.5	8.0	1.7	2.0	-4.9	5.5	8.1	9.2	-32.9	27.7
10.0	0.5	3.3	3.7	-10.7	9.2	2.5	2.8	-7.9	8.0	9.9	10.0	-31.1	29.5
10.0	1.0	3.3	3.7	-10.2	9.3	2.9	3.1	-9.3	7.9	10.1	10.1	-38.3	28.7

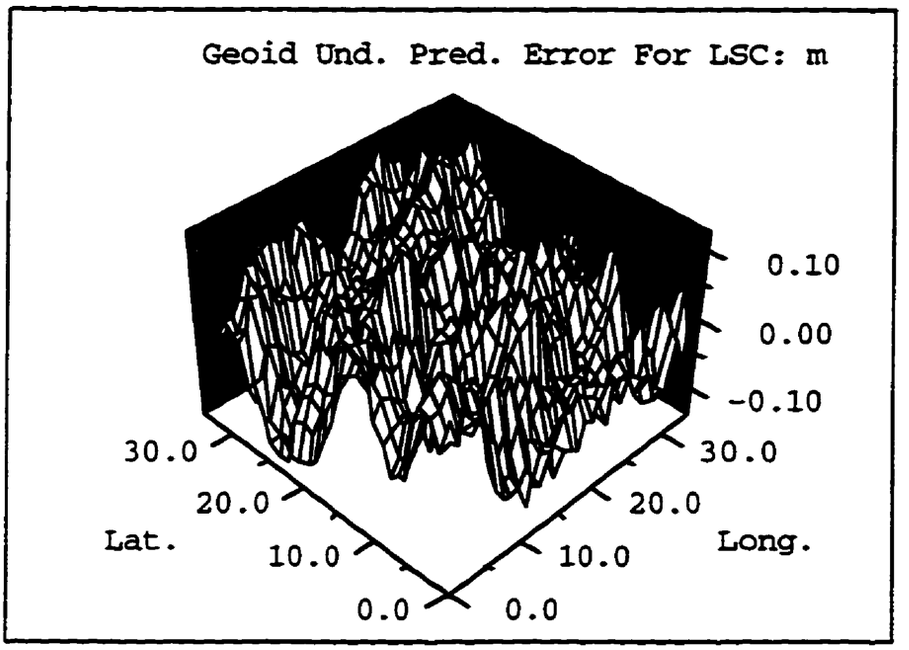

Fig. 5-14: External geoid height prediction errors for LSC (input data are those plotted in the Figures 5-4 and 5-5)

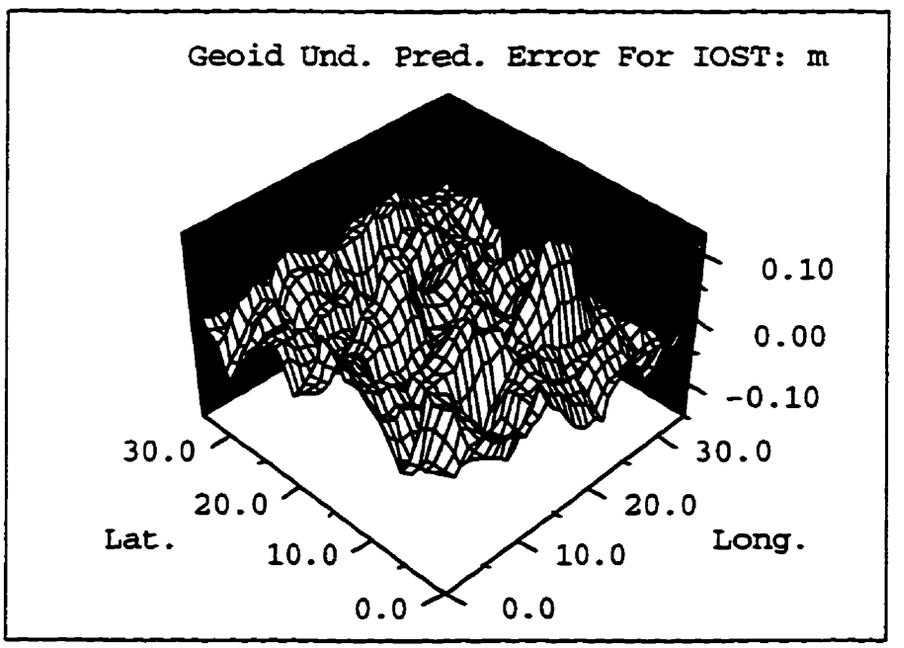

Fig. 5-15: External geoid height prediction errors for IOST (input data are those plotted in the Figures 5-4 and 5-5)

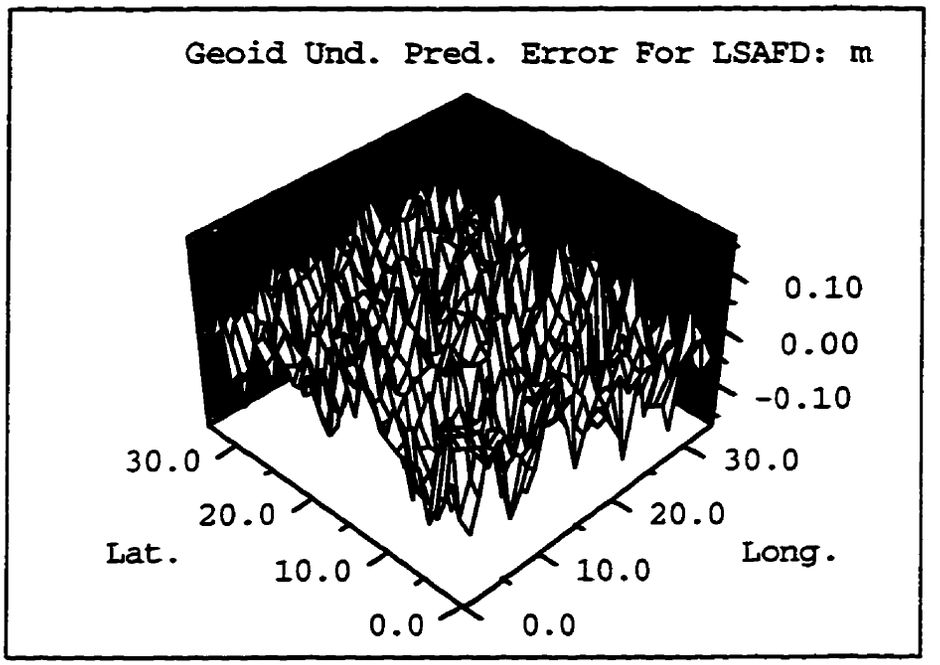

Fig. 5-16: External geoid height prediction errors for LSAFD (input data are those plotted in the Figures 5-4 and 5-5)

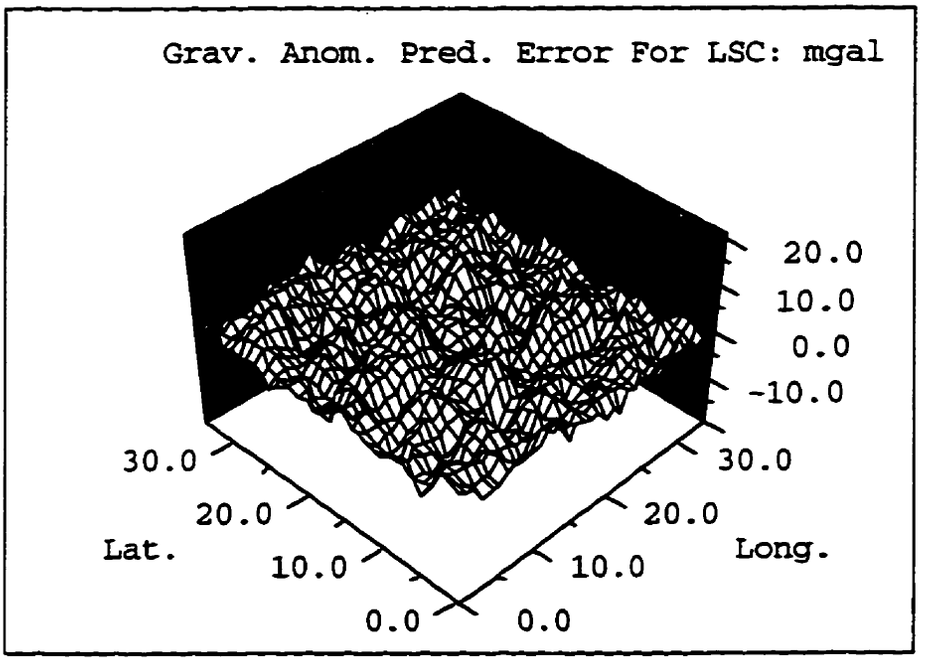

Fig. 5-17: External gravity anomaly prediction errors for LSC (input data are those plotted in the Figures 5-4 and 5-5)

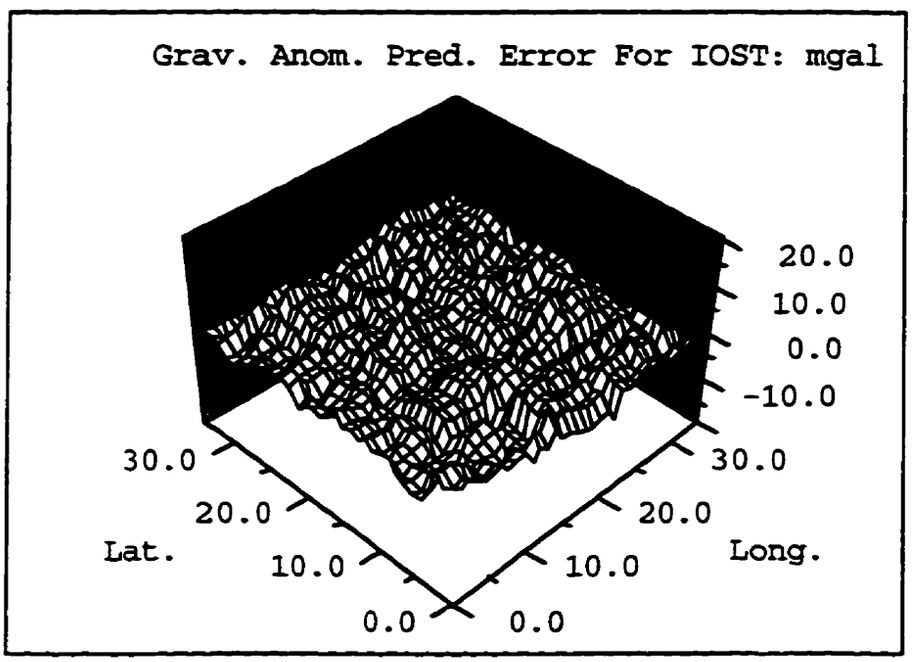

Fig. 5-18: External gravity anomaly prediction errors for IOST (input data are those plotted in the Figures 5-4 and 5-5)

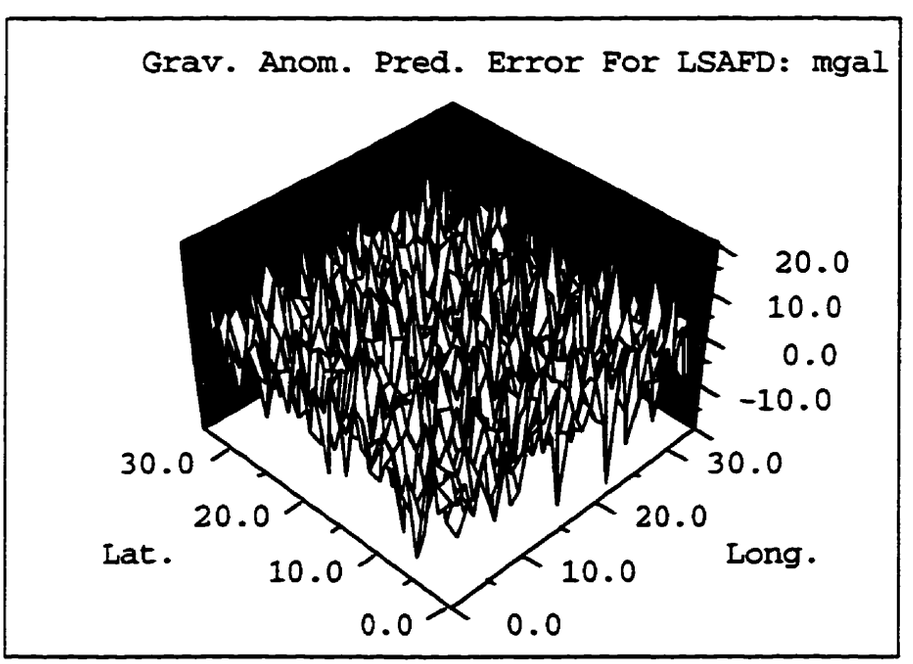

Fig. 5-19: External gravity anomaly prediction errors for LSAFD (input data are those plotted in the Figures 5-4 and 5-5)

Table 5.8: Comparison of External and Internal RMS Error for Geoid Height Estimation (Input Noises Are Assumed of Gaussian Distribution)

RMS of Input Noise		Prediction Error (m)					
Δg (mgal)	N (m)	LSC		IOST		LSAFD	
		Ext..	Int.	Ext.	Int.	Ext.	Int.
3.0	0.1	0.02	0.01	0.01	0.01	0.02	0.02
6.0	0.1	0.02	0.01	0.02	0.02	0.04	0.04
10.0	0.1	0.03	0.02	0.02	0.03	0.05	0.05
3.0	0.5	0.05	0.05	0.03	0.02	0.04	0.03
6.0	0.5	0.06	0.05	0.04	0.04	0.05	0.05
10.0	0.5	0.06	0.05	0.05	0.05	0.08	0.08
3.0	1.0	0.08	0.08	0.03	0.03	0.03	0.03
6.0	1.0	0.08	0.08	0.05	0.04	0.06	0.06
10.0	1.0	0.08	0.09	0.06	0.07	0.09	0.09

Table 5.9: Comparison of External and Internal RMS Error for Gravity Anomaly Estimation (Input Noises Are Assumed of Gaussian Distribution)

RMS of Input Noise		Prediction Error (mgal)					
Δg (mgal)	N (m)	LSC		IOST		LSAFD	
		Ext..	Int.	Ext.	Int.	Ext.	Int.
3.0	0.1	2.0	2.0	1.3	1.4	2.8	2.8
6.0	0.1	2.7	2.5	1.7	1.7	5.4	5.3
10.0	0.1	3.3	3.1	2.0	2.1	9.2	8.7
3.0	0.5	2.1	1.9	1.4	1.4	3.1	3.1
6.0	0.5	2.9	3.0	2.1	1.9	6.1	5.9
10.0	0.5	3.7	3.4	2.8	2.9	10.0	9.9
3.0	1.0	2.1	2.1	1.3	1.4	3.0	2.9
6.0	1.0	3.0	3.2	2.2	2.2	6.1	6.0
10.0	1.0	3.7	3.5	3.1	3.0	10.1	10.0

CHAPTER SIX

PROCESSING OF REAL DATA

This chapter presents test results obtained using real data in the Central Mediterranean area and the Labrador Sea area. Results obtained by different methods are compared. Results corresponding to using different a priori input information will also be presented and compared.

6.1 Data and a Priori Information

The altimeter data used for the Central Mediterranean area (33.08° to 38.0° of latitude and 16.0° to 20.92° of longitude) are from the ERS-1 Geodetic Mission (GM). We employed 60 x 60 points with a spacing of 5' x 5' in the computations. The altimeter and marine gravity data used in this area have been provided by Professor I. N. Tziavos of the University of Thessaloniki, Greece, in gridded form; see also Tziavos et al. (1996).

The shipborne data used for the Labrador Sea are have been provided by Dr. J. A. R. Blais. The altimeter data used for the Labrador Sea area are from GEOSAT ERMs. The altimeter data were first edited according to the criteria given in Table 2.1. All the 62 exact repeat tracks available were stacked. Crossover adjustments were carried out by employing bias/tilt radial orbital error model. Gridded data for geoid height and gravity anomaly on 30 x 30 points with spacing of 10' x 10' were obtained by least squares collocation produce. We chose the least-squares collocation method for data gridding, because it has the advantage of taking into account data accuracy estimates and providing theoretically accuracy estimates of the predicted values (Cruz, 1983). The covariances used in the least squares collocation gridding procedure were derived by linear interpolation from a table of covariances that was

computed empirically from the real irregular data. These covariance functions are shown in Figures 2-1 and 2-2. Only neighboring data around the prediction grid were used in the gridding process.

The OSU91A geopotential model field is removed from the data. The SST effect is computed using the spherical coefficients model of Denker and Rapp (1990) and is subtracted from the data. The mean value of the data for the area is subtracted to obtain a centred field. Figure 6-1 shows the altimeter and shipborne data for the Central Mediterranean area. Shown in Figure 6-2 are the altimeter and shipborne data for the Labrador Sea area.

For the Central Mediterranean area, the empirical signal covariances are first computed from the gridded data, and then fitted to the Tscherning/Rapp model described in 4.2 to obtain self-consistent local covariance functions. In doing so, covariance functions are isotropicaly structured. These covariance functions have been shown in Figures 4-4 to 4-6. Two methods, i.e., the direct method and the indirect method, which have been described in 4.3, are used in computing the signal PSDs that are required by the IOST method. Using the indirect method, we get isotropic signal PSDs from the isotropic covariance functions. Using the direct method, we have non-isotopic signal PSDs. Gravity filed quantities determined by IOST using the PSDs computed by these two methods are compared.

The signal covariance functions for the Labrador sea area are computed using the indirect method. That is, we first computed the signal PSDs from the data spectra using the direct PSD estimation technique, then transformed the PSDs to covariance functions. In order to obtain isotropic covariance functions, the FFT-derived PSDs have been averaged over all azimuths before transforming them to covariance functions. The PSDs used in IOST are these non-isotropic ones.

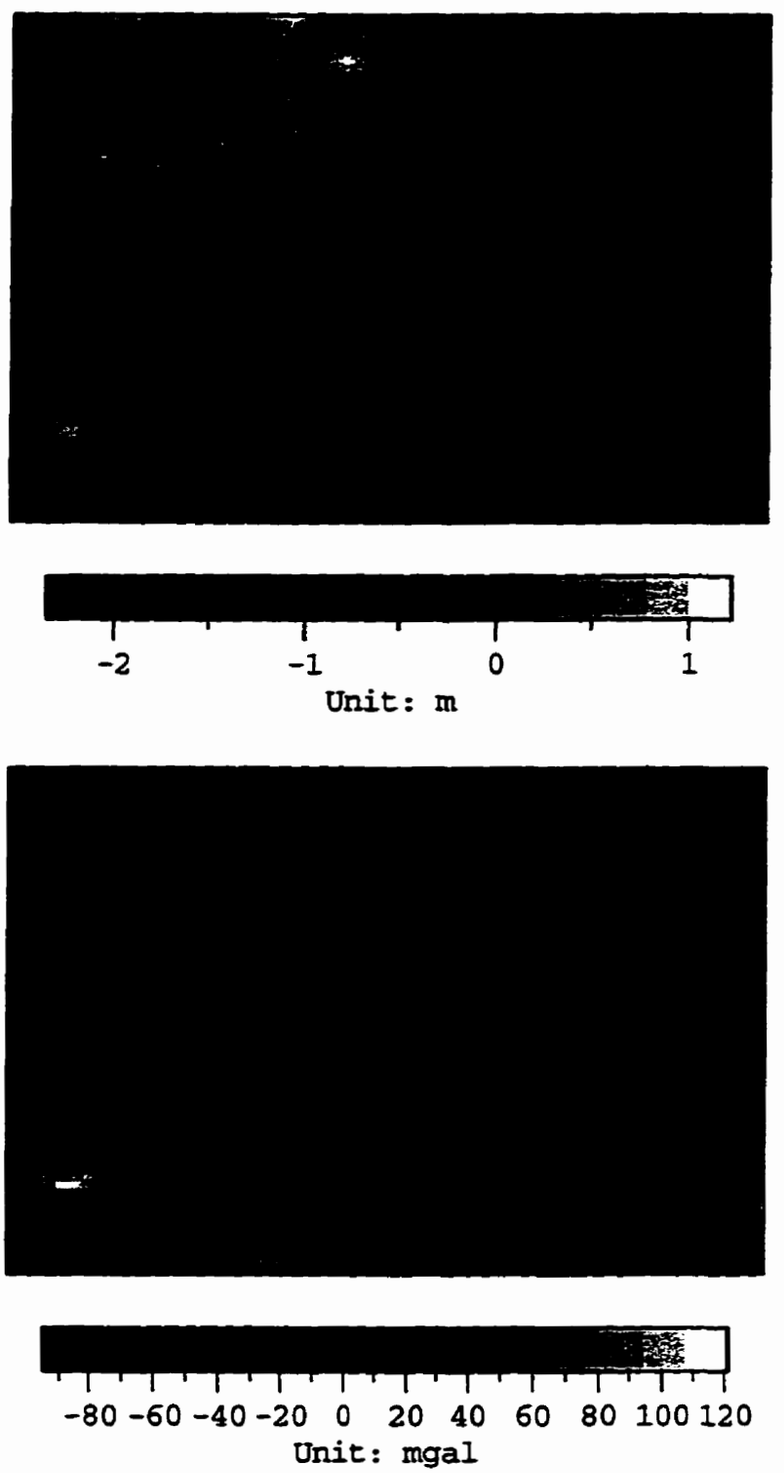

Fig. 6-1: Altimeter geoid height and shipborne gravity anomaly in the Central Mediterranean area

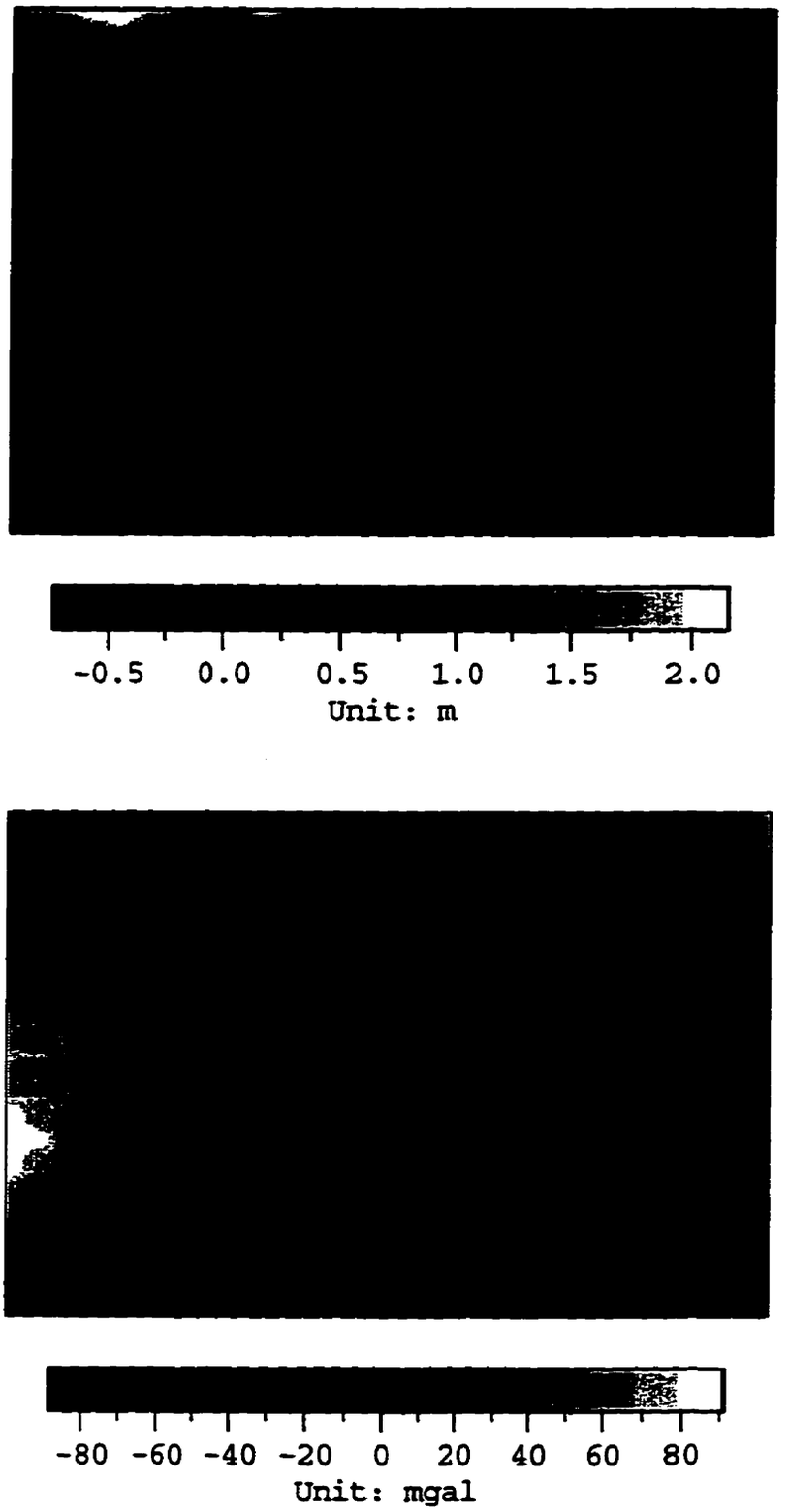

Fig. 6-2: Altimeter geoid height and shipborne gravity anomaly in the Labrador Sea area

We assumed the input noise of the altimeter and shipborne data is white noise.

6.2 Results From the Central Mediterranean Area

This section presents and discusses the estimation of the marine geoid and gravity anomaly in the area of Central Mediterranean. The LSC predictions for both geoid heights and gravity anomalies have been provided by Professor Tziavos of the University of Thessaloniki, Greece. The job of predicting geoid height using gravity only as input using Fast Collocation (FC) and One Dimensional FFT (1DFFT) have also been carried out by Professor Tziavos (Tziavos et al., 1996).

The high efficiency of the IOST and LSAFD over the LSC is indicated by the fact that for processing the 60 x 60 points using LSC requires about 36 hours for geoid height and gravity anomaly computations, while using the spectral methods (i.e., IOST and LSAFD) requires only several minutes.

6.2.1 Comparison of Internal Error Estimates for Different Methods

Table 6.1 shows some test results of the error estimates of the predictions for geoid height and gravity anomaly using IOST, LSAFD and LSC. White noise is assumed here for the input data. In the Central Mediterranean area, the noise level of about 10 mgal for the gravity data is considered reasonable based on some previous studies (Tziavos et al., 1996). So we first used 100 $mgal^2$ as the input noise variance for the shipborne data. To investigate the effects of using incorrect input noise variance on the results, we then used 25 $mgal^2$ as the input noise variance. For the altimeter data, we used only 100 cm^2 as the input noise variance. This value is based on the preprocessing of the results.

The spectral methods give a single error estimate for the whole prediction area because of the use of stationary error covariance functions. That is, all the points are predicted with the same error estimate. In using the space domain method (LSC), however, different error estimates for each point are obtained because LSC can handle non-stationary data noise, i.e., having different error variance at different points. For this reason, Table 6.1 gives the ranges of the error estimates for geoid height and gravity anomaly predictions obtained by LSC. The meaning of some abbreviations appearing in the tables and figures below are as follows:

OBS: Observation;
LSC - OBS: LSC prediction minus Observation;
IOST - OBS: IOST prediction minus observation;
LSAFD - OBS: LSAFD prediction minus observation;
IOST - LSC: IOST prediction minus LSC prediction;
IOST - LSAFD: IOST prediction minus LSAFD prediction;
LSC - FC: LSC prediction minus FC prediction;
LSC - 1DFFT: LSC prediction minus 1DFFT prediction;
FC - IOST: FC prediction minus IOST prediction;
IOST - 1DFFT: IOST prediction minus 1DFFT prediction;
FC - LSAFD: FC prediction minus LSAFD prediction;
LSAFD - 1DFFT: LSAFD prediction minus 1DFFT prediction;
OBS - FC: Observation minus FC prediction;
OBS - 1DFFT: Observation minus 1DFFT prediction;

From Tables 6.1 through 6.4 we observed that the prediction errors by IOST and LSC are close and much smaller than the corresponding input noise levels. This means that these two

methods filtered the observations to the same extent, and predictions with approximately the same accuracies have been obtained by the two methods. The error estimates for geoid height predictions using LSAFD are smaller, especially for the case when 5 mgal noise level is assumed for the shipborne data, than those using IOST and LSC. This is resulted from unrealistic weighting the two data sets by using unrealistic noise PSDs. As being pointed out previously, LSAFD depends completely on the noise PSDs to weight data. When a lower but unrealistic noise level is assumed for the shipborne data, it means that we trusted the shipborne data too much and gave an unrealistic weight to the data. Consequently, a false accuracy estimate has been obtained for LSAFD.

Table 6.1: Internal prediction accuracies for IOST, LSAFD and LSC for the Central Mediterranean area

	Input noise		Prediction accuracy	
Method	Geoid (m)	Gravity (mgal)	Geoid (m)	Gravity (mgal)
IOST	0.10	10.0	0.057	4.46
	0.10	5.0	0.054	2.90
LSAFD	0.10	10.0	0.040	9.38
	0.10	5.0	0.024	4.89
LSC	0.10	10.0	0.030 -- 0.060	4.43 -- 5.78
	0.10	5.0	0.020 -- 0.050	2.51 -- 3.99

When we compare the gravity prediction errors by different methods we see from Table 6.1 that the error estimates by LSAFD are much bigger than those by IOST and LSC, and very close to the input noise levels of the gravity observations. This would imply that almost no improvement has been obtained for the gravity anomaly predictions in using LSAFD. The

reason of this behavior relies again in the fact that the LSAFD method depends completely on the input noise levels of the two data types to weight their contributions to the adjusted results. Because the assumed noise level for shipborne data is much lower that that of the altimeter data, the shipborne data are more trusted that the altimeter data. Therefore, the accuracies of the shipborne data should have no obvious changes after applying LSAFD adjustment. The IOST and LSC methods have both filtering and adjustment functions. Therefore, always better predictions can be obtained by them.

6.2.2 Comparison of Geoid Height and Gravity Anomaly Predictions Obtained by Different Methods

Tables 6.2 through 6.4 give some statistics for differences of geoid height predictions employing different methods, while Tables 6.5 through 6.7 show statistics for the differences of gravity anomaly predictions.

From Tables 6.2 through 6.4 we see clearly that the geoid height predictions by combination of two types of data (i.e., altimeter and shipborne data) using IOST, LSC and LSAFD are significantly different from those obtained using only shipborne data as input. The differences between the results obtained using the same input data type(s) but employing different methods are small. Comparing the root-mean-square (RMS) difference values with the standard deviation (S.D.) values, we see that there is no significant bias between the results obtained using IOST, LSC and LSAFD. The RMS and S.D. values show that a significant bias occurred between predictions obtained by combinations of two types of data and those obtained by use of only a single input data type. By comparing the RMS differences between results of IOST, LSC and LSAFD (Tables 6.2 - 6.4) with the internal prediction errors shown in Table 6.1, we see that the RMS difference values are smaller than

the internal prediction errors in all cases, which would mean all the three combination methods give, to some extent, consistent and reliable results. Therefore, either method can be employed for the task of prediction of geoid height by combination of two types of data.

Table 6.2 Differences of geoid height estimates from LSC and other methods (input noises are n_h=0.10 m and $n_{\Delta g}$=10.0 mgal, respectively)

	Max diff. (m)	Min diff. (m)	RMS diff. (m)	S.D. (m)
LSC - IOST	0.113	-0.123	0.029	0.029
LSC - LSAFD	0.087	-0.105	0.014	0.014
LSC - 1DFFT	0.562	-0.750	1.008	0.222
LSC - FC	0.537	-0.708	0.922	0.236
LSC - OBS	0.374	-0.426	0.075	0.075

Table 6.3 Differences of geoid height estimates from IOST and other methods (input noises are n_h=0.10 m and $n_{\Delta g}$=10.0 mgal, respectively)

	Max diff. (m)	Min diff. (m)	RMS diff. (m)	S.D. (m)
IOST - LSC	0.123	-0.113	0.029	0.029
IOST - LSAFD	0.125	-0.188	0.030	0.030
IOST - 1DFFT	0.667	-0.832	1.012	0.231
IOST - FC	0.642	-0.804	0.926	0.244
IOST - OBS	0.314	-0.302	0.057	0.057

From Tables 6.5 through 6.7 we see that the RMS differences between the gravity anomaly predictions obtained by IOST and LSC are close, while the RMS differences between the results obtained by LSAFD and IOST, and those between the results obtained by LSAFD and

LSC are much bigger. This observation indicates that the gravity anomaly predictions produced by LSAFD significantly deviate from the results obtained by IOST and those by LSC. The IOST and LSC methods give close result because they use the same or similar information (the PSD functions used by IOST are the frequency domain equivalents of the covariance functions used by LSC). The deviations between the results obtained by LSAFD method and those by IOST and LSC methods can be explained by that IOST and LSC have both filtering and adjustment functions, but LSAFD has only one function, that is the function of adjustment. The RMS and S.D. values are close which means that no bias occurred between the results obtained by different methods. These results are consistent with those obtained through internal prediction errors and can also explained by the same reasons as given in the above section. We did not compute gravity anomalies using a single data type (i.e., altimeter data), because it is known that the expected prediction accuracies are generally not as good (about 8 mgal RMS, as shown in Zhang and Sideris, 1996).

Table 6.4 Differences of geoid height estimates from LSAFD and other methods (input noises are n_h=0.10 m and $n_{\Delta g}$=10.0 mgal, respectively)

	Max diff. (m)	Min diff. (m)	RMS diff. (m)	S.D. (m)
LSAFD - LSC	0.105	-0.087	0.014	0.014
LSAFD - IOST	0.188	-0.125	0.030	0.030
LSAFD - 1DFFT	0.550	-0.709	1.011	0.222
LSAFD - FC	0.518	-0.680	0.924	0.236
LSAFD - OBS	0.378	-0.394	0.070	0.070

Table 6.5 Differences of gravity anomaly estimates from LSC and other methods (input noises are n_h=0.10 m and $n_{\Delta g}$=10.0 mgal, respectively)

	Max diff. (mgal)	Min diff. (mgal)	RMS diff. (mgal)	S.D. (mgal)
LSC - IOST	10.64	-10.04	2.99	2.83
LSC - LSAFD	25.51	-30.86	4.17	4.04
LSC - OBS	18.81	-43.38	4.29	4.18

Table 6.6 Differences of gravity anomaly estimates from IOST and other methods (input noises are n_h=0.10 m and $n_{\Delta g}$=10.0 mgal, respectively)

	Max diff. (mgal)	Min diff. (mgal)	RMS diff. (mgal)	S.D. (mgal)
IOST - LSC	10.04	-10.64	2.99	2.83
IOST - LSAFD	32.85	-36.74	5.13	5.13
IOST - OBS	26.15	-41.27	3.71	3.71

Table 6.7 Difference of gravity anomaly estimates from LSAFD and other methods (input noises are n_h=0.10 m and $n_{\Delta g}$=10.0 mgal, respectively)

	Max diff. (mgal)	Min diff. (mgal)	RMS diff. (mgal)	S.D. (mgal)
LSAFD - LSC	30.86	-25.51	4.17	4.04
LSAFD - IOST	36.74	-32.85	5.13	5.13
LSAFD - OBS	18.14	-19.36	3.87	3.87

6.2.3 Effect of Signal-to-Noise levels

To test the effects of the input noise levels on the predictions, input noise levels with RMS values of 10.0 mgal and 5.0 mgal for gravity anomalies are assumed. As have been pointed out before, the noise level of 10 mgal is a reasonable value for the gravity data in the Central Mediterranean area. The dependency of the internal prediction errors on the signal-to-noise levels can be observed from Tables 6.1 and 6.10. These tables show that the internal prediction errors depend on the input signal-to-noise levels of the gravity anomaly. This observation is consistent with those made in the simulation studies.

Tables 6.8 and 6.9 show some statistics of the predictions with different input noise levels. We see from Table 6.8 that the RMS differences for geoid height predictions obtained between different methods increased when input noise levels of the gravity anomaly are changed from 10 mgal to 5 mgal. A 5 mgal noise level for gravity anomaly does not match the real situation in the Central Mediterranean area (Tziavos et al., 1996). The above observation would then imply that the consistency between the results by IOST, LSC and LSAFD depends on to what extent the input noise variance used in computation matches reality. A smaller discrepancy between the results obtained by different methods also means that better accuracy has been obtained for the results. Therefore, we conclude from the above observation that better results can be obtained for the geoid height estimates by the three methods when correct error variance information is used. This conclusion has also been obtained in the Labrador Sea area tests (see Section 6.3 below). From Table 6.9, however, we see that the consistency between the gravity predictions obtained by IOST, LSC and LSAFD is better for the case of using 5 mgal input noise than for the case of using 10 mgal input noise level for the input gravity anomaly.

Table 6.8: Differences of geoid height estimates for different input noise levels of gravity anomaly

	Input noise		Max diff.	Min diff.	RMS diff.	S.D.
	Geoid (m)	Gravity (mgal)	(m)	(m)	(m)	(m)
LSC -IOST	0.10	10.0	0.113	-0.123	0.029	0.029
	0.10	5.0	0.197	-0.253	0.058	0.058
LSC - LSAFD	0.10	10.0	0.087	-0.105	0.014	0.014
	0.10	5.0	0.123	-0.193	0.027	0.027
IOST - LSAFD	0.10	10.0	0.125	-0.188	0.030	0.030
	0.10	5.0	0.268	-0.306	0.063	0.063

Table 6.9: Differences of gravity anomaly estimates for different input noise levels of gravity anomaly

	Input noise		Max diff.	Min diff.	RMS diff.	S.D.
	Geoid (m)	Gravity (mgal)	(mgal)	(mgal)	(mgal)	(mgal)
LSC -IOST	0.10	10.0	10.64	-10.04	2.99	2.83
	0.10	5.0	7.21	-8.00	2.34	2.29
LSC - LSAFD	0.10	10.0	25.51	-30.86	4.17	4.04
	0.10	5.0	21.56	-20.67	3.21	3.16
IOST - LSAFD	0.10	10.0	32.85	-36.74	5.13	5.13
	0.10	5.0	26.41	-26.83	3.52	3.52

6.2.4 Comparison of Predictions Obtained Using PSDs Computed by Direct and Indirect Methods

As it has been discussed in chapter 4, the signal PSDs can be computed through two methods (the direct method and the indirect method). Table 6.10 gives the internal prediction errors for geoid height and gravity anomaly using different PSDs in IOST and Table 6.11 gives statistics of the differences of the predictions obtained by using these two types of PSDs.

Tables 6.10 and 6.11 enable us to compare the differences of the predictions when using two types of signal PSDs in IOST. From Table 6.10 we see that the internal accuracies associated with using signal PSDs derived by the direct method are better than those associated with using the indirect method. This observation is very interesting. Theoretically, on the one hand, the indirectly computed signal PSDs are preferable, because the covariance functions for different quantities, which were used as the input of the indirect method, have been adjusted to fit the Tscherning/Rapp model so that they are self-consistent. Thus the indirect method derived PSDs also satisfy these relationships while the PSD functions for different quantities computed by the direct method may not. On the other hand, however, signal PSDs computed by the direct method are non-isotropic. The unadjusted PSDs (i.e., the non-isotropic PSDs) are surely more close to reality because the real gravity field is a non-isotropic field. The non-isotropic PSDs can be handled in IOST just as easy as the isotropic ones. The second aspect may explain the fact that higher accuracies for the predictions have been obtained by using PSDs computed by the direct method.

Comparing Table 6.10 and Table 6.11 we see that the RMS differences of the predictions obtained using two types of PSDs are smaller than the estimation errors of the results, which

would mean that, especially for geoid computations, we could use signal PSDs computed by either method.

Table 6.10 Comparison of internal prediction accuracies for IOST using covariance derived PSDs and observation spectra derived PSDs

IOST		PSDs are derived from covariances		PSDs are derived from observation spectra	
Input noise		Internal accuracy		Internal accuracy	
Geoid (m)	Gravity (mgal)	Geoid (m)	Gravity (mgal)	Geoid (m)	Gravity (mgal)
0.10	10.0	0.057	4.46	0.045	2.85
0.10	5.0	0.057	2.90	0.040	2.26

Table 6.11 Statistics of the differences (estimates obtained using covariance derived PSD minus estimates obtained using data spectra derived PSD) of the estimates obtained using different PSD information in IOST (input noises are as the same as stated in Table 6.3)

	Max diff.	Min diff.	RMS diff.	S.D.
Geoid (m)	0.094	-0.112	0.028	0.028
Gravity (mgal)	7.34	-10.64	1.10	1.10

6.2.5 Examining the Details of the Differences of Predictions Obtained Using Different Methods

To investigate in more detail the behavior of the differences between the results obtained by different methods, Figures 6-3 through 6-9 were plotted to illustrate these differences.

Figure 6-3 shows the differences between geoid estimates obtained by LSC, IOST and LSAFD and the altimeter geoid observations. From this figure we see that all the graphs show some common diagonal stripes. These stripes are obviously altimeter track related.

Figure 6-4 shows detailed differences between geoid predictions obtained by different combination methods. We observed from this figure that these differences are smoother than those shown in Figure 6-3, which means that all three methods yield comparable results. No diagonal stripes appeared in Figure 6-4, which indicates that after the combinations, the adjusted field are free from track-related errors. There is some weak dependency on the behavior of the observed field for the differences of predictions obtained by different methods.

Figure 6-5 shows the differences between gravity estimates and gravity observations. Figure 6-6 gives the differences between gravity estimates obtained by different methods. We see from Figure 6-5 that graphs (a) and (b) are very similar but they are quite different from graph (c). This means that the adjustments to the gravity observations done by the IOST and LSC are almost the same. The reason for this similarity between the results obtained by the IOST and LSC relies on the fact that they used the same a-priori information. Because LSAFD did not use a-priori information, the difference show in graph (c) of Figure 6-5 is therefore quite different from those shown in (a) and (b). There are some patterns, which are obviously related to the observed field, in graphs (a) and (b). But these patterns do not appear in graph (c). The reason is that the covariance (or PSD) functions used by LSC (or IOST) methods have been fitted to the Tscherning/Rapp model. This fitting process adjusted the a-priori information and thus the method was not be able to reproduce the observed field

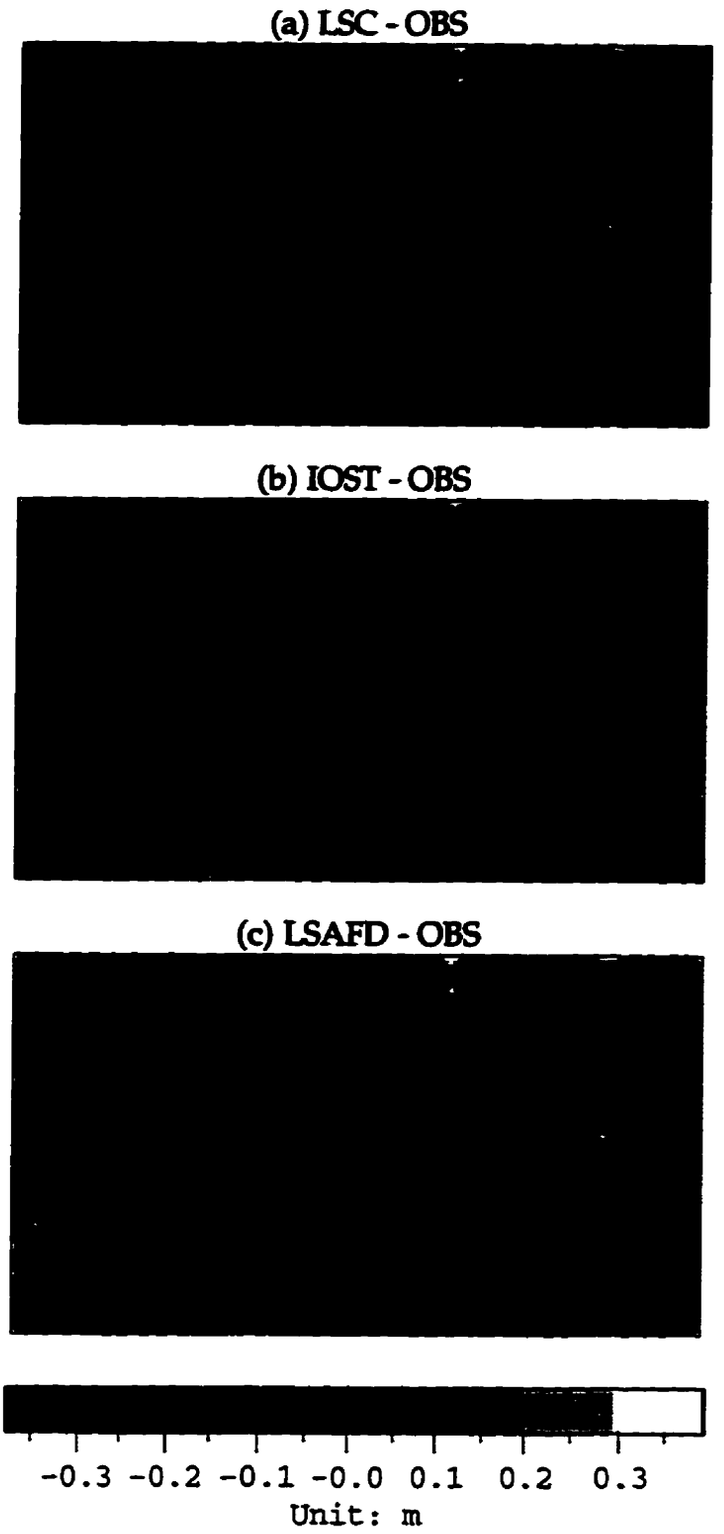

Fig. 6-3: Differences between geoid estimates and geoid observations

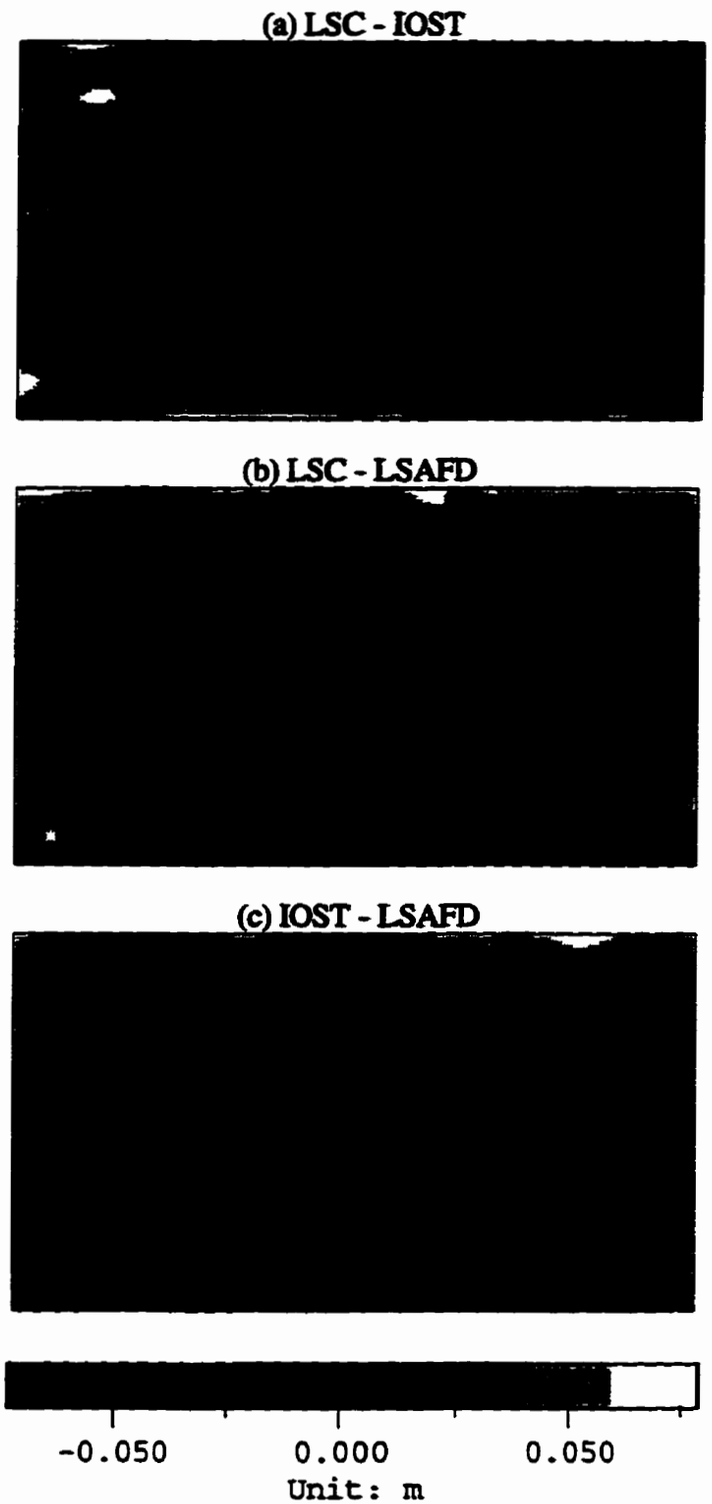

Fig. 6-4: Differences between geoid predictions obtained by LSC, IOST and LSAFD methods

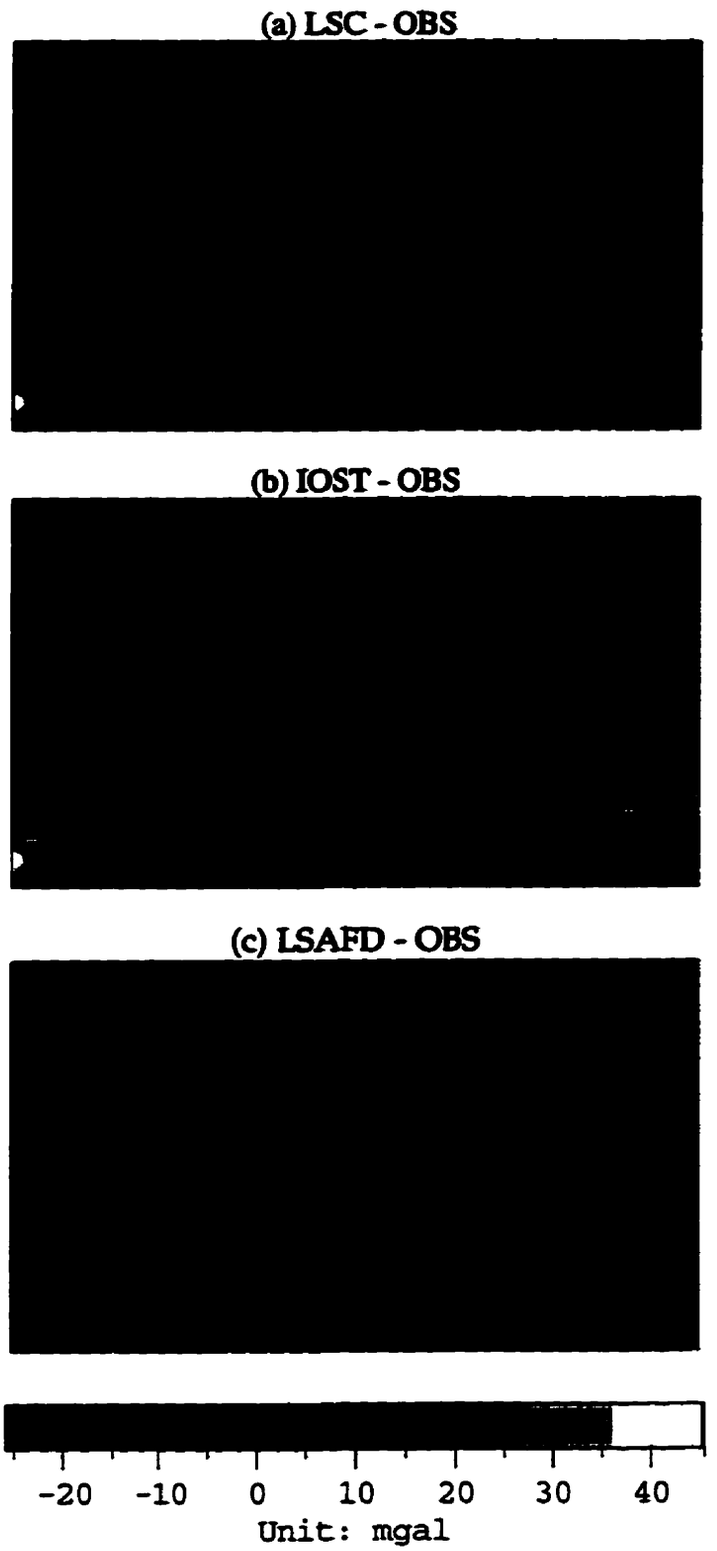

Fig. 6-5: Differences between gravity anomaly estimates and gravity anomaly observations

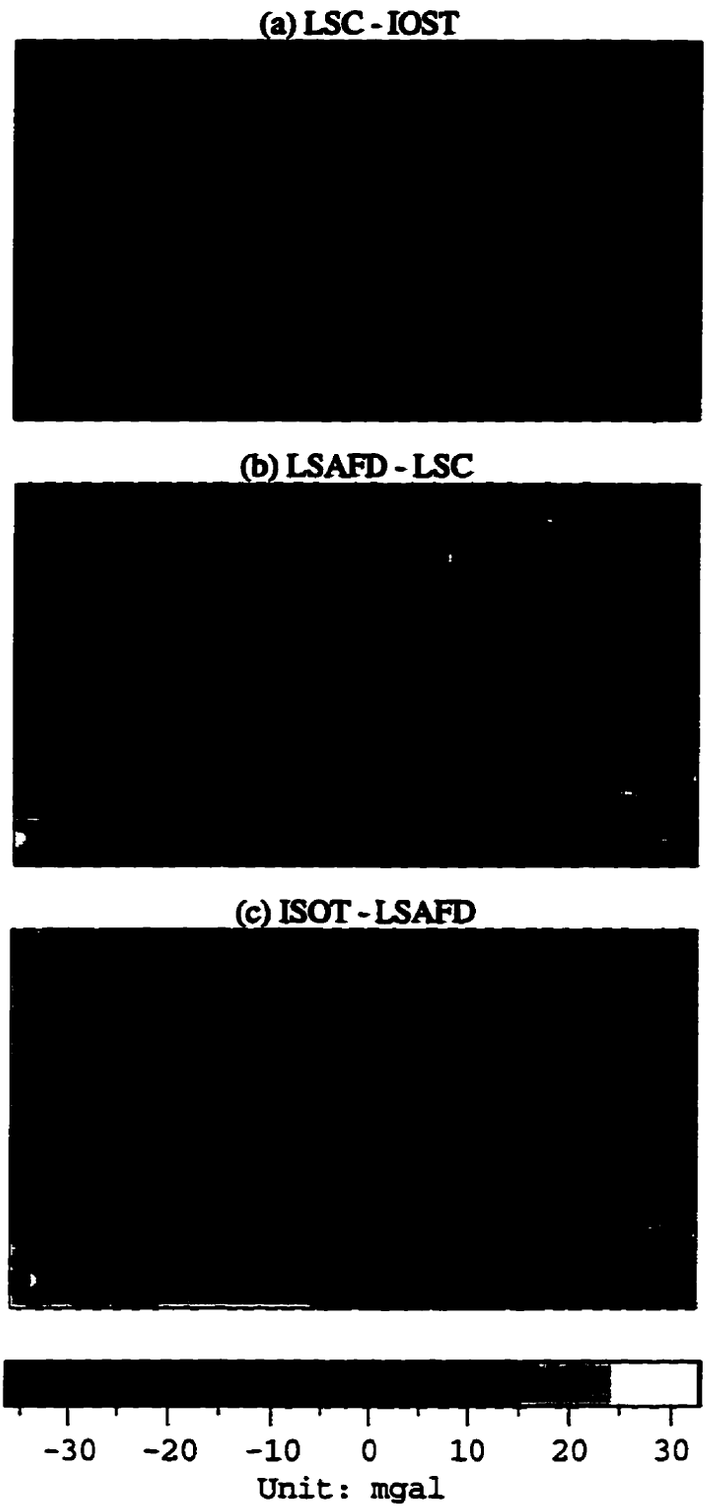

Fig. 6-6: Differences between gravity predictions obtained by LSC, IOST and LSAFD methods

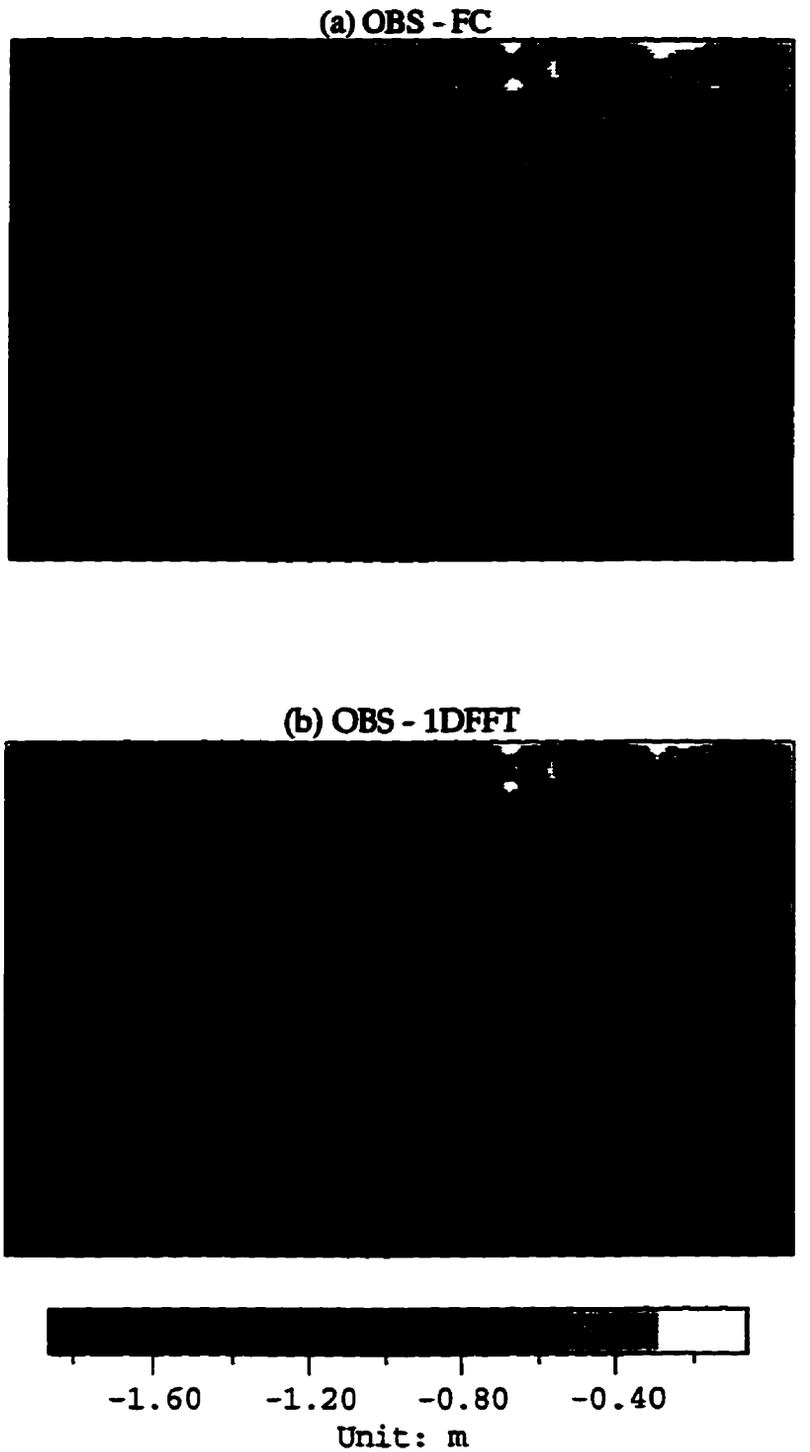

Fig. 6-7: Differences between geoid observations and geoid estimates obtained using only shipborne data

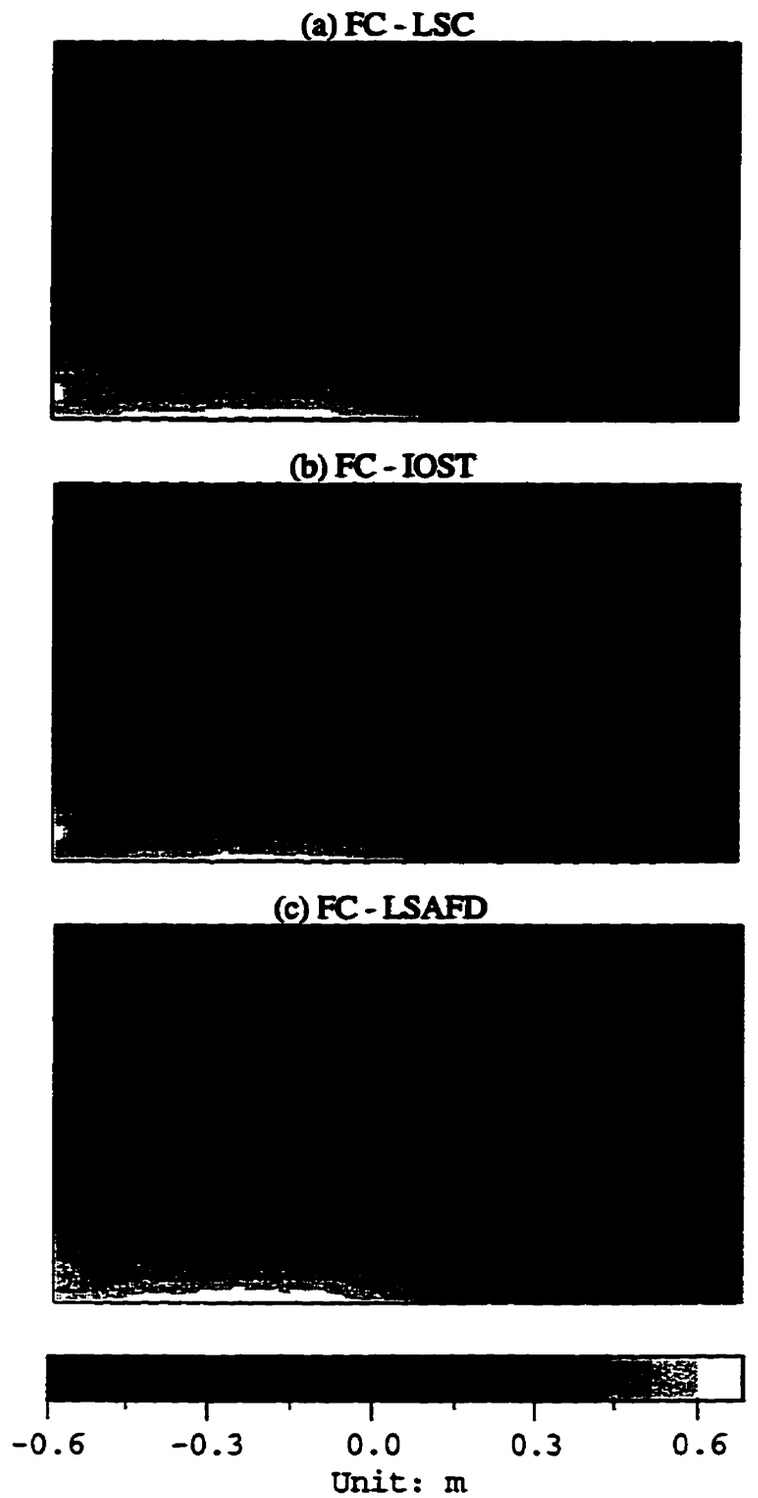

Fig. 6-8: Differences between geoid estimates obtained by FC and those obtained by LSC, IOST and LSAFD

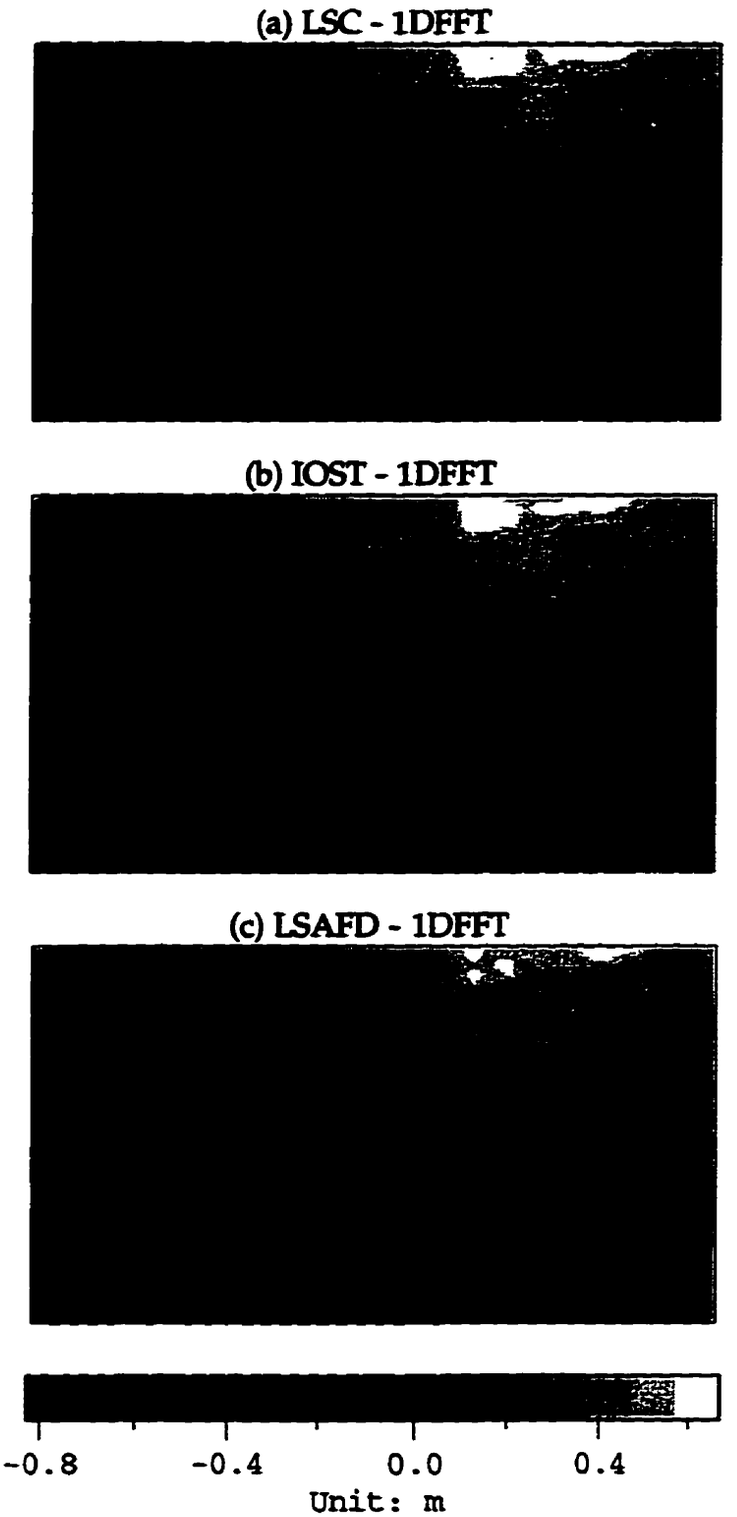

Fig. 6-9: Differences between geoid estimates obtained by 1DFFT and those by LSC, IOST and LSAFD

using these new a-priori information.

Graphs (b) and (c) in Figure 6-6 show also some patterns that are related to the observed field. We do not see these patterns in graph (c). The same reason given above can also be used here to explain these observations.

Figure 6-7 shows the difference between altimeter geoid observation and the geoid estimates obtained using a single input data type only, that is shipborne data. Plotted in Figures 6-8 and 6-9 are the differences between the geoid predictions obtained by combination of two types of data and those obtained by using single input data type (gravity anomaly). We see from the latter two figures that there are significant differences between the geoid predictions obtained using two types of data and those obtained using single data type only. The magnitudes of the differences shown in Figures 6-8 and 6-9 are much bigger than those shown in Figures 6-3 through 6-6. Another observation we can get from Figures 6-8 and 6-9 is that these differences are not of random characteristic. This observation indicates that using gridded gravity anomaly alone in the local area for geoid height prediction on the same grid may produce significantly biased predictions. The reason lies on that the gravity anomaly data contains only short wave length contributions of the field, while geoid height should contain longer wavelength contributions of the field. Using gridded gravity data only for geoid computation on the same grids causes the resulting loss of geoid height long wavelength information.

6.3 Results From the Labrador Sea Area

This section describes the test results from the Labrador Sea area. IOST, LSAFD and LSC are used in this area. No single input prediction has been done for this area. The data used in

this area have been discussed before in this thesis. The input noise levels are assumed 0.15 m for GEOSAT data and 10 mgal for the shipborne data, respectively, based on our preprocessing results.

Table 6.12 gives the error estimates of the results. From this table we see that the internal prediction errors for geoid height by the three methods are close and much smaller that the corresponding input noise levels. This would mean that these three methods filtered and/or smoothed the observations to approximately the same extent, and that the prediction of geoid height with approximately the same accuracies has been obtained in this area by the three methods. The error estimates for gravity anomaly predictions obtained by LSAFD are much bigger than those by IOST and LSC, and very close to the input noise levels of the gravity observations. We have already observed this behavior in the error estimates for LSAFD in Table 6.1. This would imply that hardly any improvement has been obtained for the gravity anomaly predictions by using LSAFD.

Tables 6.13 and 6.14 show the differences of geoid height and gravity predictions obtained employing IOST, LSAFD and LSC. From Table 6.13 we can see that some significant deviations exist between the geoid predictions obtained by LSAFD and those obtained by IOST and IOST. The reason is the same, as explained in the previous section. The same observations made in Tables 6.2 through 6.4 can still be made here for IOST and LSC; the IOST and LSC give close results and the RMS difference values between IOST results and LSC results are smaller than the internal prediction errors in all cases. From Table 6.14 we see that the RMS differences between the gravity anomaly predictions by IOST and LSC are close, while the RMS differences between the results obtained by LSAFD and IOST, and those between the gravity results obtained by LSAFD and LSC are much bigger. This observation has been already observed in the Central Mediterranean area.

To investigate the effects of using different input noise levels on the results, we assumed incorrect noise levels of 0.10 m for the altimeter data and of 5 mgal for the gravity data, respectively, and the repeated the computations. Tables 6.15 and 6.16 show some statistics on the predictions for different input noise levels. Observing these two tables, we see that the RMS differences between geoid height predictions obtained by different methods increased when the input noise levels deviated from the correct values, even though the incorrect values are smaller than the correct values. This fact would still indicate that the consistency between the results by IOST, LSC and LSAFD depends on what extent the input noise levels are estimated and used correctly, as stated in section 6.2.3. Only noise levels that match the real situation will give consistent results between different methods. Therefore, the closer the estimated input noise levels to their correct values, the better the results can be expected.

Table 6.12: Internal prediction accuracies for IOST, LSAFD and LSC for the Labrador Sea area

	Input noise		Prediction error	
Method	Geoid (m)	Gravity (mgal)	Geoid (m)	Gravity (mgal)
IOST	0.15	10.0	0.065	3.56
	0.10	5.0	0.069	4.84
LSAFD	0.15	10.0	0.064	9.30
	0.10	5.0	0.054	8.83
LSC	0.15	10.0	0.051 -- 0.078	3.16 -- 5.07
	0.10	5.0	0.059 -- 0.083	4.00 -- 6.24

Table 6.13 Comparison of geoid height estimates for LSC, IOST and LSAFD (input noises are n_h=0.15 m and $n_{\Delta g}$=10 mgal)

	Max diff. (m)	Min diff. (m)	RMS diff. (m)	S.D. (m)
LSC - IOST	0.210	-0.174	0.032	0.032
IOST - LSAFD	0.380	-0.447	0.105	0.105
LSC - LSAFD	0.412	-0.488	0.111	0.110
LSC - OBS	0.161	-0.144	0.030	0.030
IOST - OBS	0.129	-0.159	0.029	0.029
LSAFD - OBS	0.511	-0.343	0.112	0.112

Table 6.14 Comparison of gravity anomaly estimates for LSC, IOST and LSAFD (input noises are as the same as stated in Table 6.13)

	Max diff. (mgal)	Min diff. (mgal)	RMS diff. (mgal)	S.D. (mgal)
LSC - IOST	14.10	-10.174	3.43	3.43
IOST - LSAFD	23.81	-27.34	9.24	9.24
LSC - LSAFD	18.93	-23.10	8.86	8.86
LSC - OBS	12.79	-13.63	3.51	3.51
IOST - OBS	12.95	-15.10	3.25	3.25
LSAFD - OBS	25.69	-22.31	9.12	9.12

Table 6.15: Differences of geoid height estimates for different input noise levels

	Input noise		Max diff.	Min diff.	RMS diff.	S.D.
	Geoid (m)	Gravity (mgal)	(m)	(m)	(m)	(m)
LSC -IOST	0.15	10.0	0.210	-0.174	0.032	0.032
	0.10	5.0	0.337	-0.303	0.050	0.50
LSC - LSAFD	0.15	10.0	0.412	-0.488	0.111	0.110
	0.10	5.0	0.576	-0.593	0.146	0.146
IOST - LSAFD	0.15	10.0	0.380	-0.447	0.105	0.105
	0.10	5.0	0.519	-0.621	0.153	0.153

Table 6.16: Differences of gravity anomaly estimates for different input noise levels

	Input noise		Max diff.	Min diff.	RMS diff.	S.D.
	Geoid (m)	Gravity (mgal)	(mgal)	(mgal)	(mgal)	(mgal)
LSC -IOST	0.15	10.0	14.10	-10.174	3.43	3.43
	0.10	5.0	15.61	-14.44	3.72	3.72
LSC - LSAFD	0.15	10.0	18.93	-23.10	8.86	8.86
	0.10	5.0	18.25	-30.28	9.00	9.00
IOST - LSAFD	0.15	10.0	23.81	-27.34	9.24	9.24
	0.10	5.0	18.67	-23.10	8.25	8.25

From Table 6.16, we see that the consistency between the gravity predictions obtained by IOST, LSC and LSAFD because, in most cases, slightly worse when we change the variance values of both input noises from their correct values to incorrect values. The internal prediction errors shown in table 6.12 show no clear dependency on the input signal-to-noise levels.

CHAPTER SEVEN
CONCLUSIONS AND RECOMMENDATIONS

7.1 Conclusions

1) Optimal estimates of gravity field quantities can be obtained by optimal combination of multiple data types using either space or spectral techniques. Comparisons of the geoid height predictions obtained using two data types and those obtained by using a single data type (gravity anomaly only) show that significant deviations existed. The combination of two types of data gives much better results than the use of only one data type. This suggests that for a local area, if multiple data types are available, all the data types should be incorporated into the solution.

2) Previous computations of gravity field quantities using spectral methods usually provided no error estimates of the results. This has been considered, in fact, as a disadvantage of the spectral methods. The numerical computations carried out in this study suggest, however, that reliable error estimates of the results using spectral methods can be obtained. The space domain method (LSC) provides different error estimates for each grid point. In using spectral methods, however, a single error estimate is obtained for all the grid points because stationarity has to be assumed for the input errors.

3) When using LSC, isotropic signal covariance functions are assumed. The use of isotropic signal functions in LSC makes the computations much simpler than using non-isotropic ones. When using the IOST method, non-isotropic PSDs can be used without increasing the difficulty and the complexity of the computations. Numerical testing carried out in this

study shows that using non-isotropic signal PSDs (derived by the direct method) in IOST gives better results than using isotropic ones (derived by the indirect method), according to the internal prediction errors. This can be explained by the fact that the real gravity field is actually non-isotropic. Since IOST can easily handle non-isotropic PSDs, which are more close to reality than isotropic ones, and better results have been obtained by using non-isotropic PSDs than using isotropic ones, we suggest that the non-isotropic PSDs should be used along with IOST. Note also that the dimensions of the matrices of the a priori information used by LSC and IOST are different. The dimension of the covariance matrix used in LSC are much bigger than the corresponding PSD matrix used by IOST. This is one reason why the LSC takes longer to compute.

4) Among the three methods, IOST and LSC give close results for both geoid height and gravity anomaly predictions, which can be explained by the fact that they use the same a priori information. LSAFD gives, to some extent, different results than IOST and LSC, which can be explained by that the LSAFD method has only one role, that is to carry out a combination adjustment employing input noise PSDs, while IOST and LSC have both filtering and adjustment functions. These two characteristics of IOST and LSC ensure that always more reliable results can be expected from IOST and LSC than LSAFD.

5) Numerical tests show that the prediction errors of the results depend on the reliability of the a priori information and also slightly on the signal to noise ratios.

7.2 Recommendations and Future Plans

1) Geoid heights obtained by a combination of data from different altimeter missions could be further combined with shipborne gravity anomalies using the methods investigated

herein to improve the accuracies of geoid height and gravity anomaly predictions. The use of LSC for the combination of altimeter data from different missions has the advantage that it can use all the available data with varying resolutions. Yet, the use of LSAFD and IOST for the combination of different altimeter missions requires that all the data be reduced to the same resolution. This problem can be overcome by employing the hybrid FFT/integration technique proposed in Sideris (1995b) or the wavelet multiresolution analyzing techniques studied in Li (1996).

2) The LSC, IOST and LSAFD can be used for gravity field recovery by a combination of any number of data types that are related to the gravity field. We tested only with two commonly available data types (geoid height and gravity anomaly) in this study. Numerical experiments and comparisons of these three methods for the optimal combination of data from different altimeter missions as well as from airborne gravimetry are also planned for the near future.

3) As it has been pointed out in Chapter 1, the use of geoid gradient instead of geoid height as input offers us many advantages when dealing with altimeter data. The derivative operation (to obtain geoid gradients from sea surface height observations) acts as a high-pass filter. This operation suppresses the long-wavelength radial orbit errors and other long-wavelength errors in the SSH, and also enhances the short-wavelength signals of the gravity field. No crossover adjustment is needed for the altimeter data if geoid gradients are used. Further studies on the combination of geoid gradients with other types of data using LSC, IOST and LSAFD should be done.

4) The noise PSDs of the altimeter-derived geoid height should be obtainable by using the method described in section 4.4. We used gridded data for such computations in the

Labrador Sea area, and unfortunately, were not able to obtain reasonable noise PSDs. We think that this failing is due to the use of gridded data. The gridding procedure smoothed the observed field (suppressed the noise) and produced non-random noises for the gridded observations. The method used for computing the noise PSDs, however, requires that the noises present in the observations be random noises. Therefore, we should consider using the observations directly in the computation of the noise PSDs. An extensive study on noise PSD estimations using real data should be carried out.

5) Numerical experiments and comparisons of these three methods and other methods such as the wavelet transform for the optimal combination of data from different altimeter missions are also planned for the near future.

References

Anderson, O. B., P. Knudsen, and C. C. Tscherning (1995). Investigation of methods for global gravity field recovery from the dense ERS-1 Geodetic Mission Altimetry. Paper presented at the XXI IUGG General Assembly, July 2-14, Boulder, Colorado.

Arabelos, D. and I. N. Tziavos (1995). Gravity and geoid in the Mediterranean from a common adjustment of ERS-1 and TOPEX altimeter data. International Association of Geodesy 113, convened and edited by Sünkel H. and I. Marson, Springer, 376-385.

Arabelos, D., and I. N. Tziavos (1990a). Estimation of the gravity field and sea surface heights from heterogeneous data in the central Mediterranean. International Association of Geodesy Symposia, 106, edited by R. H. Rapp and F. Sansò, Springer-Verlag, 63-74.

Arabelos, D., and I. N. Tziavos (1990b). Sea surface heights in the Mediterranean Sea from GEOSAT altimeter data. J. Geophys. Res., Vol. 95, C10, 17947-17956.

Arabelos, D., P. Knudsen, and C. C. Tscherning (1987). Covariance and bias treatment when combining gravimetry, altimetry, and gradiometer data by collocation. Proceedings of the IAG Symposia, International Association of Geodesy, Paris, 443-454.

AVISO (1994). Aviso user handbook: merged Topex/Poseidon products. AVI-NT-02-101-CN, Edition 2.1.

Balmino, G (1992). Orbit choice and the theory of radial orbit error for altimetry. Satellite Altimetry in Geodesy and Oceanography, R. Rummel and F. Sanso (Eds), Springer-Verlag, 243-315.

Balmino, G., B. Moynot, M. Sarrailh, N. Vales (1987). Free air gravity anomalies over the oceans from SEASAT and GEOS-3 altimetry data. EOS Trans. AGU, 68, 17-19.

Barzaghi, R., M. Brovelli, and P. Knudsen (1992). Different cross-over analysis applied in the Mediterranean area. Bolletino di Geofisica Teorica ed Applicata.

Barzaghi, R., M. Brovelli, F. Sacerdote (1989). Altimetry-gravimetry problem: An example. International Association of Geodesy Symposia, 104, Edited by H. Sünkel and T. Baker, Springer-Verlag, 87-94.

Barzaghi, R., A. Fermi, S. Tarantola and F. Sansò (1993). Spectral techniques in inverse Stokes and overdetermined problems. Surveys in Geophysics 14, 461-475.

Basic, T., R. H. Rapp (1992). Ocean wide prediction of gravity anomalies and sea surface heights using GEOS-3, SEASAT and GEOSAT altimeter data, and ETOPO5U

bathematric data. Report No. 416, Department of Geodetic Science and Surveying, The Ohio State University, Columbus, Ohio.

Battric, B. (1993). ERS User Handbook. esa sp-1148.

Bendat, J. S. and A. G. Piersol (1986). Random data: Analysis and measurement procedures. Second edition, John Wiley and Sons, New York.

Bendat, J. S. and A. G. Piersol (1980). Engineering applications of correlation and spectral analysis. John Wiley and Sons, New York.

Blanc, F., S. Houry, P. Mazzega, and J. F. Minster (1990). A high-resolution, high-accuracy altimeter derived mean sea surface in the Norwegian Sea. Marine Geodesy, Vol. 14, No. 1, 57-76.

Bosh, W., Th. Gruber (1990). Altimetry based geoid determination at the German Processing and Archiving Facility within the ERS-1 project. International Association of Geodesy Symposia, 106, Edited by R. H. Rapp and F. Sanso, Springer-Verlag, 75-85.

Bottoni, G. P. and R. Barzaghi (1993). Fast collocation. Bulletin Geodesique, Vol. 67, 119-126.

Brammer, R. F., and R. V. Sailor (1980). Preliminary estimates of the resolution capability of the SEASAT radar altimeter. Geophys. Res. Lett., 7. 193-96.

Caporali, A. C. (1993). Combined regional geoid determination for ERS-1 radar altimeter calibration. Bulletin Geodesique, Vol. 67, 139-147.

Cazenave, A., S. Houry, B. Lago, and K. Dominh (1992). Geosat-derived geoid anomalies at medium wavelength. J. of Geophys. Res., Vol. 97, B5, 7081-7096.

Cheney, R., N. S. Doyle, B. C. Douglas, R. W. Agreen, L. Miller, E. L. Timmerman, D. C. McAdoo (1991). The complete Geosat Altimeter GDR Handbook. U. S. Department of Commerce, National Oceanic and Atmospheric Administration, National Ocean Service, Rockville, MD.

Cruz, J. (1983) Experiences with altimeter data gridding, Report No. 347, Department of Geodetic Science and Surveying, The Ohio State University, Columbus, Ohio.

Demmou, M.C., J.P. Dumont and J. Stum (1995). Quality assessment of CERSAT altimeter OPR products. CLS Argos, CLS.OC/NT/93.005, edition 19-43.

Denker, H.and R. H. Rapp (1990). Geodetic and oceanographic results from the analysis of 1 year of Geosat data. J. Geophys. Res., Vol. 95, C8, 13151-13168.

Dumont, J. P. and J. Stum (1993). Altimeter Products User Manual.

Engelis, T. (1987). Radial orbit error reduction and sea surface topography determination

using satellite altimetry. Report No. 377, Department of Geodetic Science and Surveying, The Ohio State University, Columbus, Ohio.

Engelis, T., and P. Knudsen (1989). Orbit improvement and determination of the oceanic geoid and topography from 17 days of SEASAT data. Manuscripta Geodaetica, Vol. 14, No. 3, 193-201.

Eren, K. (1980). Spectral analysis of Geos-3 altimetry data and frequency domain collocation. Report No. 297, Department of Geodetic Science and Surveying, The Ohio State University, Columbus, Ohio.

Farelly, B. (1991). The geodetic approximation in the conversion of geoid height to gravity anomaly by Fourier transform. Bulletin Geodesique, Vol. 65, 92-101.

Fukuda, Y. (1990). Precise determination of local gravity field using both the satellite altimeter data and the surface gravity data. Bulletin of the Oceanic Research Institute, University of Tokyo, No. 28.

Goad, C. C., C. C. Tscherning and M. M. Chin (1984). Gravity empirical covariance values for the continental United States. J. Geophys. Res., Vol. 89, B9, 7962-7968.

Hayling, K. L. (1994). The geoid and geophysical prospecting. Geoid and its Geophysical Interpretations, Edited by Petr Vaniceck and Nikolaos T. Christou, CRC Press, 299-319.

Heiskanen, W. A., and Moritz, H. (1967). Physical Geodesy. W. H. Freeman, San Francisco.

Houry,S., J. F. Minster, C. Brossier, K. Dominh, M. C. Gennero, A. Gazenave and P. Vincent (1994). Radial orbit error reduction and mean sea surface computation from the Geosat altimeter data. J. Geophys. Res., Vol.99, B3, 4519-4531.

Hwang, C. (1989). High precision gravity anomaly and sea surface height estimation from Geos-3/Seasat altimetry data. Report No. 399, Department of Geodetic Science and Surveying, The Ohio State University, Columbus, Ohio.

Hwang, C. and B. Parsons (1995). Gravity anomalies derived from Seasat, Geosat, ERS-1 and TOPEX/POSEIDON altimetry data and ship gravity: A case study over the Reykjanes Ridge. Geophys. J. Int., 122, 551-568.

Jekeli, C. (1989). Using line averages in least squares collocation. Bulletin Geodesique, Vol. 63, No. 2, 203-212.

Jekeli, C. (1979) Global accuracy estimates of point and mean undulation differences obtained from gravity disturbances, gravity anomalies and potential coefficients. Report No. 288, Department of Geodetic Science and Surveying, The Ohio State University, Columbus, Ohio.

Jordan, S. K. (1972). Self-consistent statistical models for the gravity anomaly, vertical deflections, and undulation of the geoid. J. Geophys. Res., Vol. 77, No. 20, 3660-3670.

Kaln and Bryan (1972). Use of a spacecraft Borne altimetry for determining the mean surface and geopotential. Document No. X-550-72-19, Goddard Space Flight Center, Greenbelt, Maryland.

Klokocnik, J., and C. A. Wagner (1993). A test of GEM T2 from GEOSAT crossovers using latitude lumped coefficients. Bullétin Géodésique, 100-108.

Knudsen, P. (1994). Seperation of residual ocean tide signals in a collinear analysis of Geosat altimetry. Bulliten Geodesique, Vol. 68, 7-18.

Knudsen, P. (1993). Integration of gravity and altimeter data by optimal estimation techniques. Lecture Notes in Earth Sciences, 50, edited by R. Rummel and F. Sansò, Springer-Verlag, 453-466.

Knudsen, P. (1992). Altimetry for geodesy and oceanography. Publication No. 115 of the Finnish Geodetic Institute, Edited by J. Kakkuri, 87-129.

Knudsen, P. (1991). Simultaneous estimation of the gravity field and sea surface topography from satellite altimeter data by least squares collocation. Geophys. J. Int., Vol. 104, No. 2, 307-317.

Knudsen, P. (1988). Determination of local empirical covariance functions from residual terrain reduced altimeter data. Report No. 395, Department of Geodetic Science and Surveying, The Ohio State University, Columbus, Ohio.

Knudsen, P. (1987a). Estimation and modeling of the local empirical covariance function using gravity and satellite altimeter data. Bulletin Géodésique, Vol. 61, 145-160.

Knudsen, P. (1987b). Adjustment of satellite altimeter data from cross-over differences using covariance relations for the time varying components represented by Gaussian Functions. Proceedings IAG Symposia, International Association of Geodesy, Paris, 617-628.

Knudsen, P., and M. Brovelli (1991). Collinear and cross-over adjustment of GEOSAT ERM and SEASAT altimeter data in the Mediterranean Sea. Surveys in Geophysics.

Knudsen, P., O. B. Andersen, and C. C. Tscherning (1992). Altimetric gravity anomalies in the Norwegian-Greenland Sea - Preliminary results from the ERS-1 35 days repeat mission, Geophys. Res. Lett., Vol. 19, No. 17, 1795-1789.

Koch, K. R. (1970). Gravity anomalies for ocean areas from satellite altimetry. Proceedings of the Second Marine Geodesy Symposium, Marine Technology Society, Washington, D. C..

Lenk, U., K. Seitz and B. Heck (1995). A datum defect and spectral analysis in regional cross-over adjustments of satellite altimeter data. International Association of Geodesy Symposia 113, convened and edited by Sunkel, H. and I. Marson, Springer, 357-365.

LeSchack, A. R. and R. V. Sailor (1988). A preliminary model for GEOSAT altimeter data errors. Geophys. Res. Lett., 15, 1203-1206.

Li, J. and M. G. Sideris (1995). Marine gravity and geoid determination by optimal combination of satellite altimetry and shipborne gravimetry data. Paper presented at the XXI IUGG General Assembly, July 2-14, Boulder, Colorado.

Li, Y. C. (1993). Optimized spectral geoid determination. UCGE Report No. 20050, Department of Geomatics Engineering, The University of Calgary, Calgary, Alberta.

Li, Z. (1996) A framwork for multiresolution approximation and its application to physical geodesy. Ph.D. Dissertation Submitted to the Department of Geomatics Engineering, The University of Calgary, Calgary, Alberta.

Marks, K. M., and R. V. Sailor (1986). Comparison of GEOS 3 and SEASAT altimeter resolutions. Geophys. Res. Lett., 13, 697-700.

Marple, S. Lawrence, Jr. (1987) Digital spectral analysis with applications. Prentice-Hall Signal Processing Seriers, USA.

Marsh, J. G., F. J. Lerch, S. M. Klosko, T. L. Engelis, G. B. Patel, J. W. Robbins, R. G. Williamson (1989). Geoid determination over basin-wide scales using a combination of satellite tracking, surface gravity and altimeter observations. International Association of Geodesy Symposia, 104, Edited by H. Sunkel and T. Baker, Springer-Verlag, 1-10.

McAdoo, D. C. and K. M. Marks (1992). Gravity field of the Southern Ocean from GEOSAT data. J. Geophys. Res., Vol. 97, B3, 3247-3260.

McAdoo, D. C. (1990) Gravity field of the Southeast Central Pacific from GEOSAT exact repeat mission data. J. Geophys. Res., Vol. 95, C3, 3041-3047.

Min, E. de (1995). A comparison of Stokes' numerical integration and collocation, and a new combination technique. Bulletin Geodesique, Vol. 69, 223-232.

Moore, P. and S. Ehlers (1993). Orbital refinement of ERS1 using dual crossover arc techniques with Topex/Poseidon. Manuscripta Geodaetica, Vol.18, 249-262.

Moritz, H. (1980). Advanced physical geodesy. H. Wichmann Verlag, Karlsruhe, Germany.

Nash, R. A. and Jordan, S. K. (1978). Statistical geodesy --An engineering perspective. Proceeding of the IEEE, Vol. 66, No.5, 532-550.

Nerem, R. S., C. Jekeli, and W. M. Kaula (1995). Gravity field determination and characteristics: Retrospective and prospective. J. Geophys. Res., Vol. 100, B8, 15053-15074.

Neyman, Y.M. (1985) Improperly posed problems in geodesy and methods of their solution, Proceedings of Local Gravity Field Approximation, Edited by K. P. Schwarz, 499-566.

Olgiati, A., G. Balmino, M. Sarrailh, and C. M. Green (1995). Gravity anomalies from satellite altimetry: comparison between computation via geoid heights and via deflections of the vertical. Bulletin Geodesique, Vol. 69, 252-260.

Rapp, R. H. (1985). Detailed gravity anomalies and sea surface height derived from Geos-3/Seasat altimeter data. Report No. 365, Department of Geodetic Science and Surveying, The Ohio State University, Columbus, Ohio.

Rauhut, R. V. (1992) Regularization methods for solution of the inverse problem. UCGE Report No. 20045, Depart. of Geomatics Engineering, The University of Calgary.

Rummel, R., L. Sjoberg, and R. H. Rapp (1977). The determination of gravity anomalies from geoid heights. Report No. 269, Department of Geodetic Science and Surveying, The Ohio State University, Columbus, Ohio.

Sailor, R. V. (1994). Signal processing techniques. Geoid and its Geophysical Interpretations, Edited by Petr Vaniceck and Nikolaos T. Christou, CRC Press, 148-185.

Sandwell, D. T. (1992). Antarctic marine gravity field from high-density satellite altimetry. Geophys. J. Int., 109, 437-448.

Sandwell, D. T. (1984). A detailed view of the south pacific geoid from satellite altimetry. J. Geophys. Res., Vol. 89, B2, 1089-1104.

Sandwell, D. T. and D. C. McAdoo (1990). High-accuracy, high-resolution gravity profiles from 2 years of the GEOSAT exact repeat mission. J. Geophys. Res., Vol. 95, No. C3, 3049-3060.

Sandwell, D. T., and D. C. McAdoo (1988). Marine gravity of the southern ocean and Antarctic margin from GEOSAT. J. Geophys. Res., Vol. 93, 10389-10396.

Sandwell, D. T., E. L. Winterer, J. Mammerickx, R. A. Duncan, M.A.Lynch, D. A. Levitt and C. L. Johnson (1995). Evidence for diffuse extension of the pacific plate from Pukapuka ridges and cross-grain gravity lineations. J. of Geophys. Res., Vol. 100, B8, 15087-15099.

Sansò, F. and M. G. Sideris (1995). On the similarities and differences between systems

theory and least-squares collocation in physical geodesy. Paper presented at the XXI IUGG General Assembly, July 2-14, Boulder, Colorado.

Schrama, E. J. O. (1989). The role of orbit errors in processing of satellite altimeter data. Report No. 33, Netherlands Geodetic Commission. Publications on geodesy, New series, Delft.

Schwarz, K. P. and G. Lachapelle (1980). Local characteristic of the gravity anomaly covariance function, Bulletin Geodesique, Vol. 54, 21-36.

Schwarz, K. P., M. G. Sideris and R. Forsberg (1990). The use of FFT techniques in physical geodesy. Geophysical Journal International, Vol. 100, 485-514.

Seeber, G. (1993) Satellite Geodesy. Walter de Gruyter, Berlin, New York.

Sideris, M. G. (1996). On the use of heterogeneous noise data in spectral gravity field modeling methods. Journal of Geodesy, 70/8, 470-479

Sideris, M. G. (1995). Fourier geoid determination with irregular data. Journal of Geodesy, 70, 2-12.

Sideris, M. G. (1987). On the application of spectral techniques to gravimetric problem. Proceedings of the XIX IUGG General Assembly, Tome II, Vancouver, B. C., August 9-22, 428-442.

Sideris, M. G. (1984) Computation of gravimetric terrain corrections using Fourier transform techniques, UCSE Report No. 20007, Department of Surveying Engineering, The University of Calgary.

Sideris, M. G. and Y. C. Li (1993). Gravity field convolutions without windowing and edge effects. Bulletin Geodesique, Vol. 67, 107-118.

Stewart, M. P. and R. G. Hipkin (1989). A high resolution, high precision geoid for the British Isles. International Association of Geodesy Symposia, 104, Edited by H. Sunkel and T. Baker, Springer-Verlag, 39-46.

Strang van Hees, G. (1990). Stokes formula using fast Fourier techniques. Manuscripta Geodaetica, 15, 235-239.

Svensson, S. L. (1994). Spectral Decomposition of the geoid. Geoid and its Geophysical Interpretations, Edited by Petr Vaniceck and Nikolaos T. Christou, CRC Press, 114-124.

Tai, C. K. (1988) Geosat crossover analysis in the tropical Pacific, 1, constrained sinusoidal crossover adjustment, J. Geophys. Res., 93, 10621 - 10629.

Tapley, B. D., G. H. Born, and M. E. Parke (1982). The SEASAT altimeter data and its accuracy assessment. J. Geophys. Res., Vol. 87, No. C5, 3179-3188.

Tscherning, C.C. (1990). A strategy for gross-error detection in satellite altimetry data applied in the Baltic-Sea area for enhanced geoid and gravity determination. International Association of Geodesy Symposia, 106, Edited by R. H. Rapp and F. Sanso, Springer-Verlag, 95-107.

Tscherning, C. C. (1976). Covariance expressions for second and lower order derivatives of the anomalous potential. Report No. 225, Department of Geodetic Science and Surveying, The Ohio State University, Columbus, Ohio.

Tscherning, C. C. (1974). A FORTRAN IV program for the determination of the anomalous potential using stepwise least squares collocation. Report No. 212, Department of Geodetic Science and Surveying, The Ohio State University, Columbus, Ohio.

Tscherning, C. C., and P. Knudsen (1986). Determination of bias parameters for satellite altimetry by least squares collocation. Proceedings of the International Associations of Geodesy, Hotine-Marussi Symposium on Mathematical Geodesy, Rome, June 3-6, 833-853.

Tscherning, C. C. and R. H. Rapp (1974). Closed covariance expressions for gravity anomalies, geoid undulations, and deflections of the vertical implied by anomaly degree variances. Report No. 208, Department of Geodetic Science and Surveying, The Ohio State University, Columbus, Ohio.

Tziavos, I. N., M. G. Sideris and J. Li (1996). Optimal spectral combination of satellite altimetry and marine gravity data. Presented at EGS XII General Assembly, The Hague, May 6-10.

Vassiliou, A. A. (1986). Numerical techniques for processing airborne gradiometer data. UCSE Report #20017, Department of Surveying Engineering, The University of Calgary

Vermeer, M. (1993). First crossover adjustment experience with ERS-1 data in the Mediterranean. Mare Nostrum III - Geomed Rep. 3, Milano.

Wagner, C. A. (1986). Accuracy estimates of geoid and ocean topography recovered jointly from satellite altimetry. J. Geophys. Res., Vol. 91, No. B1, 453-461.

Wagner, C. A. (1994). Accuracy of the GEM-T2 geopotential from Geosat and ERS 1 crossover altimetry. J. Geophys. Res., Vol. 99, B5, 9179-9201.

Wang, Y. M. (1993). On the optimal combination of potential coefficient model with terrestrial gravity data for FFT geoid computations. Manuscripta Geodaetica, Vol. 18, 406-416.

Wang, Y.M., R. H. Rapp (1992). The determination of a one year mean sea surface height track from GEOSAT altimeter data and ocean variability implications. Bulletin Geodesique, Vol. 66, 336-345.

Wu, L. and M. G. Sideris (1995). Using multiple input-output system relationships in post processing of airborne gravity vector data. Airborne Gravimetry, IAG Symposium G4, IUGG XXI General Assembly, July 2-14, Boulder, Colorado, 87-94.

Wunsch, C (1991). Global scale sea surface variability from combined altimetric and tide gauge measurements, J. Goephys. Res., 96, 15053-15082.

Wunsch, C., and V. Zlotnicki (1984). The accuracy of altimetry surfaces. Geophys. J. R. astr. Soc., 78, 795-808.

Yale, M. M., D. T. Sandwell, W. H. F. Smith (1995). Comparison of along-track resolution of stacked Geosat, ERS 1, and TOPEX satellite altimeters. J. Geophys. Res., Vol. 100, B8, 15117-15127.

Zhang, C. (1993). Recovery of gravity information from satellite altimetry data and associated forward geopotential models, UCGE Report No. 20058, Depart. of Geomatics Engineering, The University of Calgary.

Zhang, C., J. A. R. Blais (1995). Comparison of methods for marine gravity determination from satellite altimetry data in the Labrador Sea. Bulletin Geodesique, Vol. 69, 173-180.

Zhang, C., J. A. R. Blais (1993). Recovery of gravity disturbances from satellite altimetry and by FFT techniques: a synthetic study. Manuscripta Geodaetica, 18, 158-170.

Zhang, C., M. G. Sideris (1996). Oceanic gravity by analytical inversion of Hotine's formula. Marine Geodesy, Vol. 19, No. 2, 115-136.

Zhang, C., M. G. Sideris (1995). Gravity disturbances from GEOSAT data and forward geopotential models in the Labrador Sea. International Association of Geodesy Symposia 113, convened and edited by Sunkel, H. and I. Marson, Springer, 317-328.

Zlotnicki, V. (1994). The geoid from satellite altimetry. Geoid and its Geophysical Interpretations, Edited by Petr Vaniceck and Nikolaos T. Christou, CRC Press, 96-110.